Doctoral Dissertation (Shinshu University)

Carbon cycle and interactions of surface hydrosphere and deep-subsurface: key molecule and isotopic ratio approaches

March 2021

Atsushi Urai

Carbon cycle and interactions between surface hydrosphere and deep-subsurface: key molecule and isotopic ratio approaches

Abstract

Microorganisms play a role in the hydrosphere's carbon cycle by producing, decomposing, and recycling organic matter. Therefore, it is important to understand microorganisms' functions for solving environmental problems such as eutrophication and global warming. In this thesis, we firstly assessed microorganism’s functions on the carbon cycle in the surface and deep subsurface hydrosphere using microbial-specific compounds (biomarkers) and their isotopic ratios; i) origin and fate of dissolved organic matter in lake water, ii) foraging strategy of zooplankton in oligotrophic pond, iii) deep methanogenesis in an organic- and iodine-rich aquifer, iv) planktonic microbial methane production in a eutrophic lake. Although the carbon cycle in these hydrospheres has been studied independently, it is thought that there is an interaction between the surface and the deep subsurface hydrosphere. We elucidated the interaction of the carbon cycle between the surface and deep subsurface hydrosphere.

Dissolved organic matter (DOM), accounting for more than 95 % of the total organic carbon in the hydrosphere, plays an essential role in the surface hydrosphere's carbon cycle. However, the source and formation of high-molecular-weight dissolved organic matter (HMW-DOM) and its interaction

with other organic components such as particulate organic matter (POM) and low-molecular-weight DOM (LMW-DOM) have been poorly understood so far. To elucidate DOM's origin and interactions, we performed the sterol compositions and their isotopic ratio analyses for phytoplankton, POM, HMW-DOM, and total-DOM isolated from three lakes in different aquatic environments. 24-ethylcholesta-5,22-dien-3β-ol (stigmasterol) was dominant in HMW-DOM, which was the different trend in other components, suggesting that HMW-DOM has a different origin and interaction from other components. Moreover, from the carbon and hydrogen isotope analysis, we reveal autochthonous algae as a significant source of the abundant stigmasterol in the lakes. These results suggest that HMW-DOM in summer is derived from autochthonous phytoplankton rather than allochthonous terrestrial plants and that HMW-DOM likely has few interactions with POM and LMW-DOM in the lake water.

Phytoplankton and zooplankton, the primary source of DOM, are the most important primary producers and primary consumers in lake water ecosystems. The biomass of the primary consumers is limited to that of the primary producers, while it has been reported that many zooplankton are present in lakes where the biomass of phytoplankton is extremely low. In this study, trophic position (TP) of the daphnia *Daphnia longispina* and the copepod *Acanthodiaptomus pacificus* in an oligotrophic lake, Shirakoma-ike, was investigated via stable nitrogen isotope composition analysis of amino acids, to understand the foraging strategy of these two dominant freshwater zooplankton species in an oligotrophic lake. The surface water of this lake is frozen in winter, and the life cycle and trophic behavior are different between these two species: the daphnia is found only in spring-autumn, whereas

the copepod is found in a whole season. We found that the TP is 2.1±0.0 for the daphnia in spring-autumn and 2.3±0.3 for the copepod in a whole season. These results reveal strong herbivory for the daphnia compared to dietary plasticity and facultative omnivory for the copepod. The latter is suggested to feed on phytoplankton for spring and autumn (TP=2.1±0.0) and on both phytoplankton and heterotrophic microbes for summer and winter (TP=2.6±0.0). The foraging strategy is thus different between daphnia and copepods in this pond.

The surface hydrosphere is a eukaryotic-dominated ecosystem, while the deep subsurface hydrosphere is a prokaryotic-dominated ecosystem. Methanogenic archaea produce methane in an anaerobic environment, which is the final step in the decomposition of organic matter. Although insights into methanogenesis and the methane cycle in the deep subsurface are important for understanding early life development on Earth, the ecology of deep subsurface environments is still unclear because of a limited number of surveys utilizing culture-based approaches. We performed coenzyme factor 430 (F430) analysis and radiocarbon measurements to identify deep microorganisms, including methanogenic archaea, and assessed the origin of methane in a deep organic- and iodine-rich aquifer in a forearc basin at the Southern Kanto gas field, Boso Peninsula, Japan. Both lipid analysis and small-subunit rRNA gene sequencing indicated that the biomass of domain archaea was less than 10% of the total prokaryotes, while methanogenic archaea (e.g., *Methanomicrobia*) was detected in the gene sequencing. High concentrations of native F430 (1.67×10^4 femto mol/L) in the absence of the F430 epimer strongly suggested high active methanogenesis potential mediated by the subsurface

microbes. Radiocarbon measurements of methane and dissolved inorganic carbon (DIC) revealed ^{14}C-depleted (both $\Delta^{14}C_{methane}$ and $\Delta^{14}C_{DIC}$, <−997.4 ‰), suggesting that the entire deep habitat and methanogenesis represents an isolated subterranean microbial ecosystem.

Deep methane is potentially transported to the surface hydrosphere and affects the surface carbon cycle; however, it is poorly understood how deep methane affects the carbon cycle in the surface hydrosphere. We quantitatively evaluated the impacts of deep methane on the carbon cycle in a eutrophic lake's surface hydrosphere using the radiocarbon measurements. The $\Delta^{14}C$ of deep methane and carbon dioxide seeping from the bottom of the lake were depleted ($\Delta^{14}C_{methane}$, <−972.1 ‰), and DIC and cyanobacterial bloom (Aoko) collected from surface lake water contained ^{14}C-depleted carbon ($\Delta^{14}C_{DIC}$, −630.6 to −103.1 ‰ and $\Delta^{14}C_{aoko}$, −110.3 ‰), suggesting that 10−60% of DIC is affected by deep carbon, which is also propagated through phytoplankton into lake ecosystems. Also, we detected F430 in cyanobacterial bloom (6.8−35 × 10^2 femto mol/g-wet), suggesting the coexistence of methanogenic archaea with cyanobacterial bloom in the lake water under aerobic conditions. This result may provide insight into the methane paradox, in which the accumulation of methane under aerobic conditions has been reported in oceans and lakes.

Contents

List of Figures

collected by the water displacement method; the gas phase is >99 % methane. The bubbled scum and yellow brine-rich water are also visible.

Figure 15. Flowcharts of analysis. (a) Prokaryotic lipid and F430 analysis. (b) rRNA gene, total cell counts, ionic composition, and isotope analysis ($\delta^{13}C$ and $\Delta^{14}C$). AMS, accelerator mass spectrometry; EA/IRMS, elemental analysis/isotope ratio mass spectrometry; GC/FID, gas chromatography/flame ionization detection; GC/MS, gas chromatography/mass spectrometry; HPLC, high-performance liquid chromatography; IC, ion chromatography; PCR, polymerase chain reaction; SSU rRNA, small-subunit rRNA.

Figure 16. Chromatograms of brine-rich water samples analyzed by GC/MS. (a) Fatty-acid fraction showing bacterial lipid composition; (b) neutral ether lipid fraction showing archaeal lipid composition. Bacterial fatty acids were identified using the fatty acid methyl ester standard; archaeal phytane and biphytane were identified using the standard from *Methanobacterium* sp. Culture (Takano et al., 2009).

Figure 17. Proportions of prokaryotic archaea (red) and bacteria (blue) in brine-rich water and bubbled scum, cross-validated by (i) lipid-based analysis and (ii) SSU rRNA gene analysis. Membrane lipids of microorganisms are known to be the most representative biomarkers for characterizing prokaryotes. We calculated the proportions assuming that C_{16} and C_{18} fatty acids originated from bacterial cells and phytane and biphytane originated from archaeal cells.

List of Tables

Chapter 1: General Introduction

1.1 The purpose of this thesis

Microorganisms play a role in the hydrosphere's carbon cycle by producing, decomposing, and recycling organic matter (Figure 1). Therefore, it is important to understand microorganisms' functions for solving environmental problems such as eutrophication and global warming (e.g., Bolin et al., 1979). The research in the surface hydrosphere has focused on various forms of carbon, such as dissolved organic matter (DOM) and dissolved inorganic carbon (DIC), as well as the biological food web (e.g., Thurman, 1985; Tranvik et al., 2009; Steinberg et al., 2017; Brett et al., 2017). In contrast, the insights of the carbon cycle in the deep subsurface are becoming apparent with the recent progress of international ocean drilling research, such as the international ocean discovery program (IODP) and international continental scientific drilling program (ICDP) (e.g., Orcutt et al., 2013; Inagaki et al., 2015; Imachi et al., 2019). Although these researches on the global carbon cycle have been discussed individually into surface and deep sub-surface spheres, there can be an interaction between the surface and deep subsurface by geological function (e.g., active fault and forearc basin)(Figure 2).

In this thesis, we assessed the microorganism's function on the carbon cycle focused on lake ecosystems and deep aquifer, and elucidated the interaction of the carbon cycle between the surface and deep subsurface using the microbial specific compounds (biomarkers) and their isotopic ratios. In chapter 2, we evaluated the origin and fate of dissolved organic matter in lake water using sterols composition and its isotopic ratios. In chapter 3, we assessed the foraging strategy of zooplankton in oligotrophic pond by nitrogen isotopic ratios of amino acids. In chapter 4, we determined the biomass

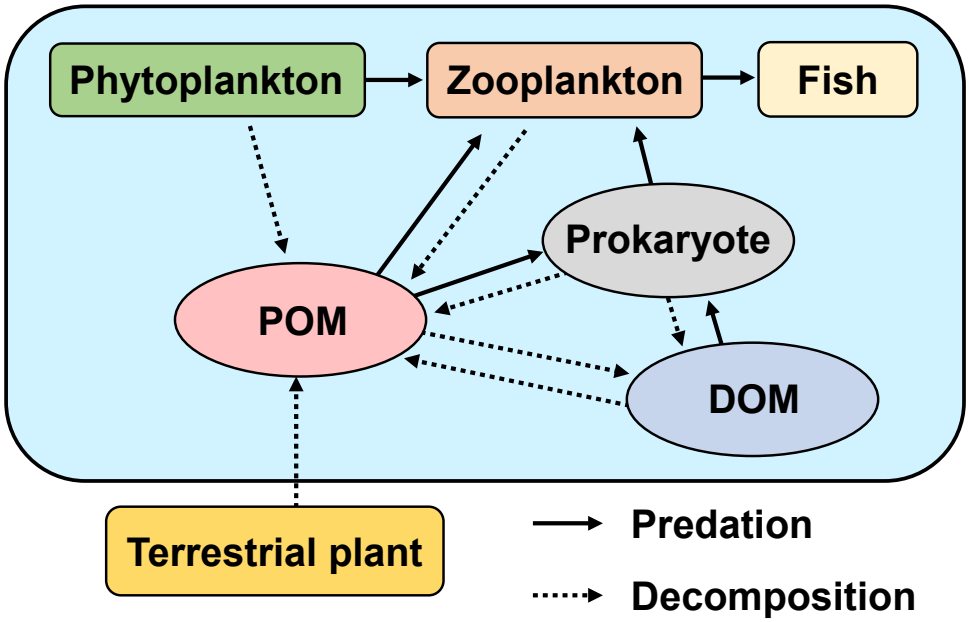

Figure 1. Interactions of carbon cycle in aquatic ecosystems. These interactions (i.e, production, decomposition, and recycling of organic compounds) are recorded in isotopic ratios.

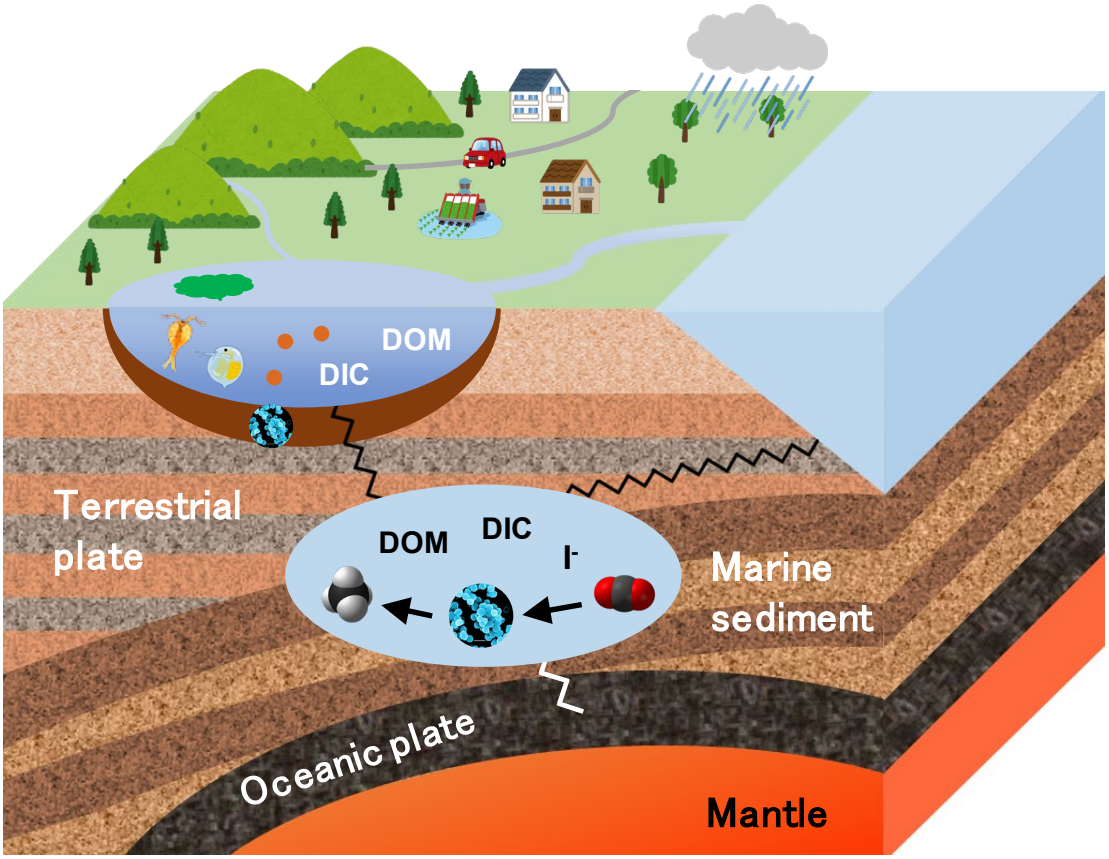

Figure 2. The conceptual map summarizing the contents of this thesis.

of prokaryote, including the methanogenic archaea, and deep carbon cycle using the coenzyme factor 430 (F430), a kye molecular of methanogenic archaea, and radiocarbon measurements. In chapter 5, we verified the planktonic microbial methane production in a eutrophic lake by F430 analysis. Finally, in chapter 6, we elucidated the interaction between the surface ecosystems and deep carbon, especially methane and dissolved inorganic carbon by radiocarbon measurements. This is the first data to describe in detail the impact of deep carbon, especially methane and carbon dioxide, on the surface hydrosphere and its ecosystems.

1.2 Membrane lipids as a biomarker for organic geochemistry

Biomarkers have been widely used as a tool to unravel microorganisms' functions in organic geochemistry (e.g, Killops and Killops, 2005). Membrane lipids contain a wide variety of compounds, and their compositions vary among species. Also, even the same species produces different composition of membrane lipids depending on its habitat.

Sterols are essential components of eukaryotic cell membranes as a role of membrane fluidity (e.g, Pearson et al., 2000; Volkman, 2003). It is empirically known that the sterol composition varies among species; cholest-5-en-3β-ol (cholesterol) is found in a wide species, mainly in animals and zooplankton, in contrast, 24-ethylcholest-5-en-3β-ol (β-sitosterol) and 24-ethylcholest-5,22-dien-3β-ol (stigmasterol) are mainly found in terrestrial plants (e.g., Volkman, 2003). These insights make it possible to estimate the contribution of eukaryotes to the carbon cycle from the environment's sterol

composition. Prokaryotic membrane lipids are formed by a double structure, whereas bacterial and archaeal membrane lipids composed of different compositions; bacterial membrane lipids are composed of fatty acids and glycerol bound by ester bonds, and archaeal membrane lipids are composed isoprenoid hydrocarbons and glycerol bound by ether bonds (e.g., Goldfine, 1982; Kate, 1993; Sohlenkamp and Geiger, 2015). Therefore, we can estimate the biomass ratio of prokaryotes using a quantitative analysis of membrane lipids in environmental samples, such as sediment core, water column, and soil. In addition, it has reported that some membrane lipids are only possessed by certain species; methanogenic archaea has a hydroxyarchaeol which is a type of diether lipid (e.g., Koga and Nakano, 2008).

1.3 Compound-specific isotopic ratio analysis

While biomarker-based environmental assessment has the advantage of directly converting compound concentrations into biological biomass, the effects of microbial degradation and reproduction can make accurate estimates difficult. Also, the rate of degradation of each compound in the environment is different, which means that even if we measure the concentration of fatty acids in a sediment core, there is always the question of whether the fatty acids originate from the time of sedimentation, are a byproduct of degradation, or were in situ produced by microorganisms.

The isotopic ratio analysis is an evaluation method that does not depend on the concentration in the environment. Significant elements of organisms (e.g., carbon, hydrogen, oxygen, nitrogen, and

sulfur) have some isotopes, and these isotopic ratios (e.g., $^{13}C/^{12}C$) change regularly in response to biosynthesis, predation, and decomposition (e.g., Blair et al., 1985; Peterson and Fry, 1987; Wada, 2009). Therefore, the isotopic ratio of biomarker can determine the transiti ons of biomarker; the isotopic ratio of sterol varies depending on the organism's origin, even if they are the same type of sterols (e.g., Chikaraishi et al., 2004; Chikaraishi, 2006).

It is empirically known that the food chain enriches the nitrogen isotope ratio ($\delta^{15}N$), and the trophic position (TP) can be determined from the $\delta^{15}N$ in all organisms (e.g., Minagawa and Wada, 1984; Takano et al., 2009; Ohkouchi et al., 2017). The carbon isotopic ratio ($\delta^{13}C$) also reflected the relationship between predator and predated. The TP of animals and planktons in the food chain can be estimated by combining $\delta^{15}N$ and $\delta^{13}C$. We note that isotope ratios within organisms are distributed unevenly; amino acids are the most important components of energy metabolism in animals, and some of them are affected by ^{15}N enrichment by the food chain (e.g., glutamic acid), while others are not (e.g., phenylalanine)(Wada, 2009). The combination of these two amino acids provides an estimate of TP in the organism without relying on the primary producer (e.g., Chikaraishi et al., 2007, 2014; Ohkouchi et al., 2017)(Figure 3).

1.4 Radiocarbon measurements

Radiocarbon (^{14}C) is produced by the reaction of nitrogen (^{14}N) with cosmic rays in the atmosphere, which half-life is 5730 years. While ^{14}C is rapidly oxidized and diffused as carbon dioxide

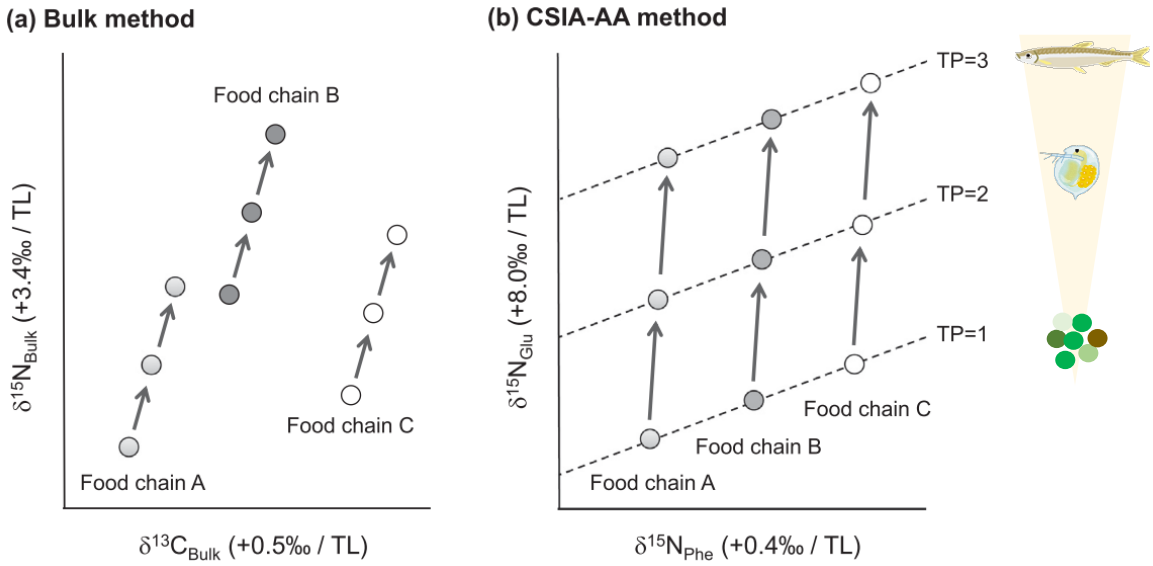

Figure 3. Schematic illustrations of the trophic position (TP) estimated by (a) bulk and (b) compound-specific isotope analysis of amino acids (CSIA-AA) methods (modified by Ohkouchi et al., 2017).

($^{14}CO_2$) into the atmosphere, atmosphere, hydrosphere, and biosphere, ^{14}C is reduced in the geosphere where there is no supply of atmospheric carbon (Larsen et al., 2018; Yokoyama et al., 2019, Figure 4). Therefore, ^{14}C is a critical indicator for evaluating the supply of atmospheric carbon. In the decade, the development of the radiocarbon measurement by an accelerator mass spectrometry (AMS) enables the measurement of ^{14}C in carbon on the order of 100 micrograms or less (e.g., Pearson et al., 1998; Yokoyama et al.,2010; Hirabayashi et al., 2017; Haghipour et al., 2019). As such, ^{14}C measurements by AMS has been utilized as a tracer to understanding biogeochemical carbon cycle (e.g., Larsen et al., 2018; Ishikawa et al., 2015, 2018, 2019; Wyatt et al., 2019; Nishida et al., 2020; Kelsey et al., 2020; Yamamoto et al., 2020). The compound-specific radiocarbon measurement provides insight into the biogeochemical carbon cycle and organic matter deposition processes in the environment. Ishikawa et al. (2013, 2015) conducted ^{14}C measurements on biological samples collected from the river, including aquatic insects and periphyton, to elucidate the river ecosystems' food web. The results clearly indicated the difference between autochthonous (periphyton) and allochthonous (terrestrial plants) organisms and the extent to which zooplankton and fish use allochthonous carbon as a food resource. Yamamoto et al. (2020) also performed ^{14}C measurements for elucidating the detailed deposition process of organic matter in the volcanic lake using the wood chips, plant litter, fatty acids, and chlorophylls collected from the lake sediments. These results suggest that the sediment's ^{14}C age is older than the original depositional age due to the large contribution of recirculated carbon in terrestrial ecosystems. Besides, the $\Delta^{14}C$ of chlorophyll *a* was different from that of pheophytin *a* which is the

degradation product of chlorophyll *a*, suggesting that the relationship between "compound" and "degradation product," which is considered to be of the same origin at first glance, is actually of different origin.

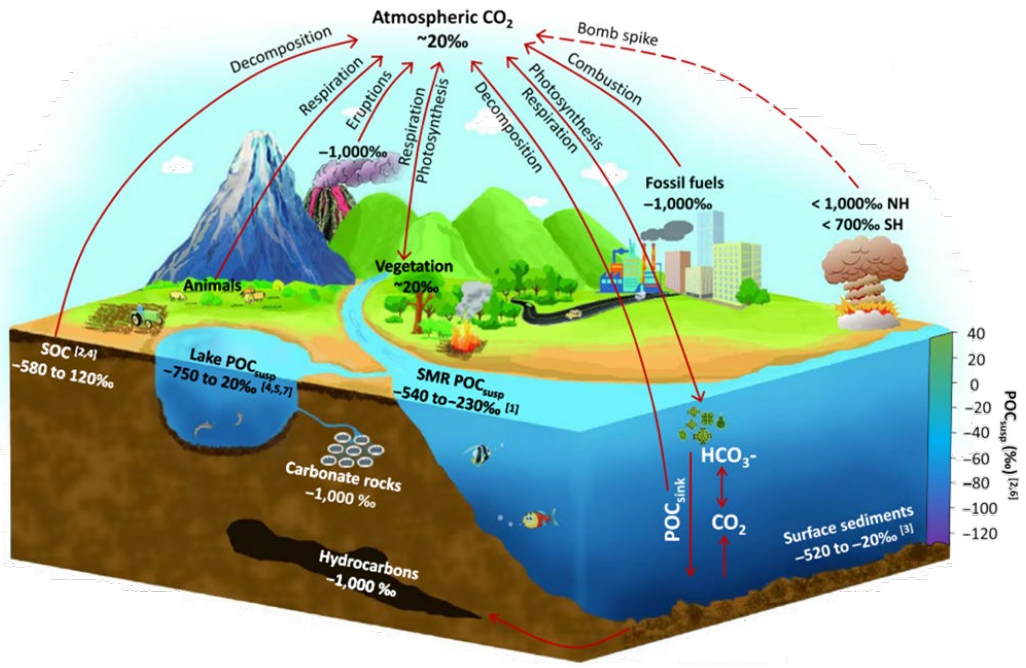

Figure 4. Radiocarbon distribution in the environment (Larsen et al., 2018).

Chapter 2: Chemical characterization of sterols dissolved in lake water

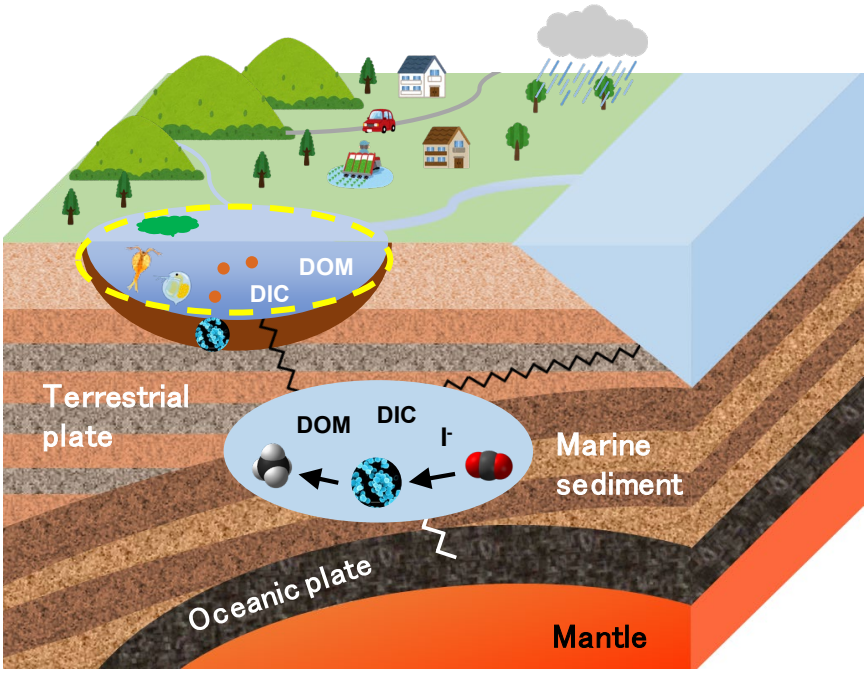

2.1 Aim of this study

Dissolved organic matter (DOM) represents a large reservoir of organic carbon in the hydrosphere and makes up a key component of the global carbon cycle (e.g., Mostofa et al., 2013; Nebbioso and Piccolo, 2013; Repeta, 2015; Hansell and Carlson, 2015). Moreover, DOM is generally derived from multiple sources and is affected by complicated transformation and degradation reactions in aquatic environments (e.g., Benner et al., 1992; McCarthy, 1998; McCallister et al. 2006a, 2006b). Therefore, the study of DOM, including the identification of the biological sources and evaluation of biogeochemical fates, is still challenging. Among size fractions of DOM, high-molecular-weight DOM (HMW-DOM; >1 kDa) mainly represents a unique organic carbon pool, which is accompanied by considerable difference in the molecular and stable isotopic compositions from other organic components such as particulate organic matter (POM) and low-molecular-weight DOM (LMW-DOM; <1 kDa) (e.g., Benner et al., 1997; Ziegler and Fogel, 2003; Yoshiyama et al., 2003; McCallister et al., 2006a, 2006b; Repeta, 2015). Source and formation of HMW-DOM and its interaction with POM and LMW-DOM (e.g., transfer and exchange of components, how to link with the other pools) thus have been particularly poorly understood so far.

Against this considerable difference in the molecular and stable isotopic compositions of HMW-DOM from the other pools, the molecular distribution of sterols, which are ubiquitous organic compounds and characteristically distributed in different taxa of eukaryotes (e.g., Volkman, 2003), have been used in the tracing biological sources and formation processes of HMW-DOM in aquatic

environments (e.g., Yoshiyama et al., 2003; McCallister et al., 2006b). For instance, Yoshiyama et al. (2003) found an unusually high concentration of 24-ethylcholesta-5,22-dien-3β-ol (stigmasterol) in HMW-DOM collected from the five lakes, Nakatsuna, Kizaki, Suwa, Misumaike, and Shirakomaike, in Japan. McCallister et al. (2006b) also found such abundant stigmasterol in HMW-DOM collected from York River estuary, in USA. Thus, it is assumed that the further analysis (e.g., of molar and molar-isotopic compositions) of sterols in HMW-DOM in freshwater environments will provide a key for better understanding of the biological source and formation of HMW-DOM and its interaction with other organic carbon pools in environments.

Here, we further investigated the molar composition of sterols (Figure 5) in the HMW-DOM throughout a year together with that of phytoplankton and sediments in three types of lakes: freshwater lakes Kizaki and Suwa and a brackish water lake Suigetsu, in Japan (Figure 6). Moreover, for the samples from Lake Kizaki, we determined stable carbon and hydrogen isotopic compositions of the sterols to identify the biological sources of sterols associated with the HMW-DOM in these lakes. Lake Kizaki was chosen as a representative lake, where has long been studied so far in diverse fields (e.g., Yoshioka et al., 1988; Park and Hayashi, 1993; Yoshiyama et al., 2003; Ito, 2013).

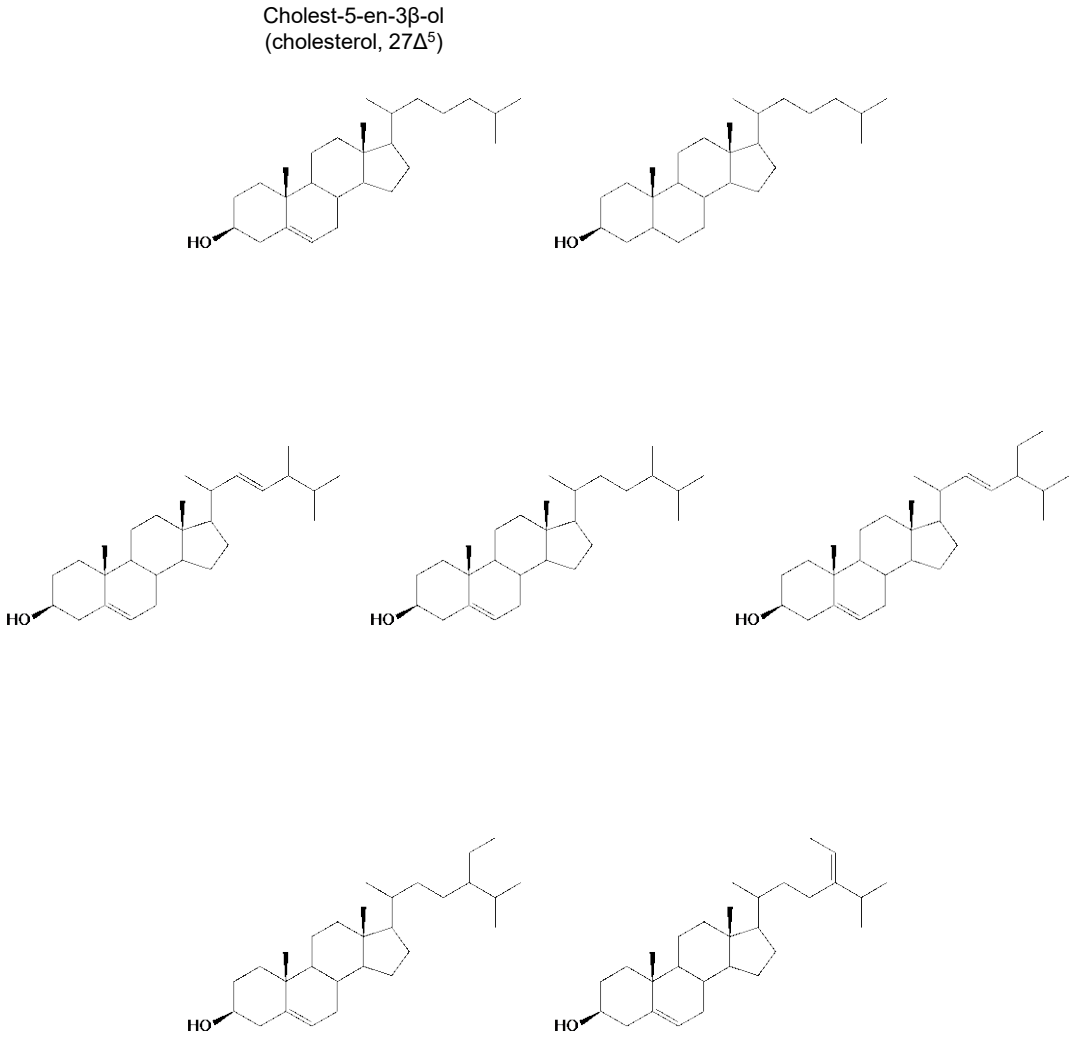

Figure 5. Molecular structure and systematic name (trivial name, abbreviation) of sterols discussed in this study.

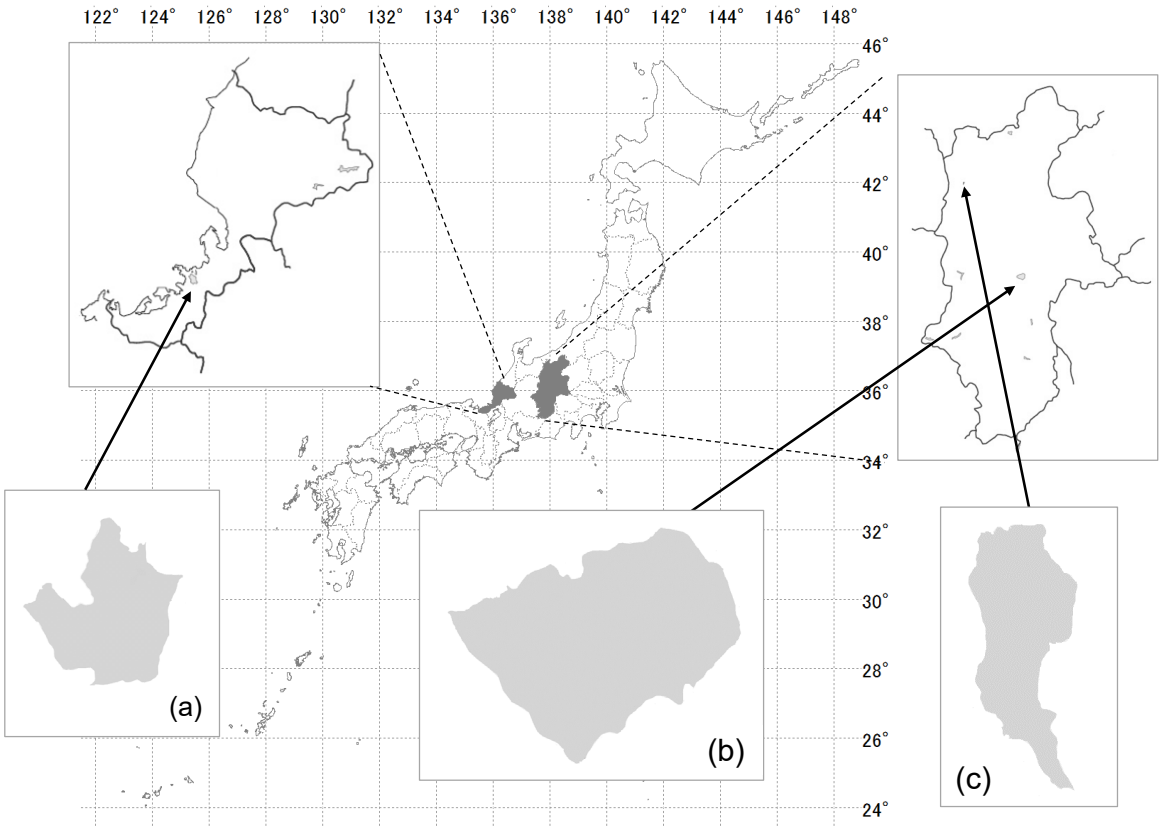

Figure 6. Geological location of sampling sites; (a) Lake Suigetsu, Fukui Pref. (eutrophic brackish water lake), (b) Lake Suwa, Nagano Pref. (eutrophic freshwater lake), and (c) Lake Kisaki, Nagano Pref. (mesotrophic subalpine freshwater lake).

2.2 Materials and Methods

2.2.1 Geological setting and sampling procedure

Samples were collected from Lake Kizaki (36º33’30”N, 137º50’15”E), a mesotrophic subalpine freshwater lake (altitude: 764 m, surface area: 1.4 km^2, maximum depth: 29.5 m), in April to December 2012, from Lake Suwa (36º2’57”N, 137º5’7”E), a eutrophic freshwater lake (759 m, 13.3 km^2, 7.2 m), in July 2013, and from Lake Suigetsu (35º35’15”N, 135º52’53”E), a eutrophic brackish water lake (0 m, 4.3 km^2, and 34 m), in August 2012 (cf. geological location in Figure 6). Lake water was taken from the center of lakes at the depth just below the thermocline to minimize the effects of biological activity in the surface layer and of contamination of resuspended particles from sediments, and immediately filtrated with two plankton-nets (100 and 40 μm mesh) and a glass fiber filter (GB100R, 30 cm × 30 cm, Toyo Co. Ltd., Japan) the filtered samples were thus defined as phytoplankton (100 μm >> 40 μm), POM (40 μm >> 0.6 μm), and DOM (<0.6 μm), and were lyophilized immediately. The HMW-DOM was isolated from the final filtrate by a tangential flow ultrafiltration (TFF) using a Pellicon Lab Casette (Millipore Co. Ltd., USA) equipped with a PLAC (Molecular Cut-off: MCO=1 kDa) filter. Principally 100 L of lake water was concentrated to 1 L by TFF and subsequently concentrated to about 200 mL by using a conventional stirring ultrafiltration. Apparatus used was a UHP-76 (Advantec Co. Ltd., Japan) equipped with Amicon YM1 (MCO=1 kDa, Millipore Co. Ltd., USA) filter. Finally, the concentrate was lyophilized. The HMW-DOM was obtained as a pale brown-colored puffy powder. Surface sediments (0-10 cm depth) were collected from the center of the lake

with a gravity core sampler in June 2008.

2.2.2 Lipid analysis

The phytoplankton, HMW-DOM and Lake Kizaki sediment were saponified with 1M KOH in methanol/water (95/5, w/w) in a sealed ampoule. The total DOM was obtained by 1L of filtered water saponified with the 0.1 M KOH under reflux. The neutral lipids were extracted from the alkaline medium with n-hexane/diethylether (9/1, v/v). The lipids in POM collected on the GF filter were extracted with dichloromethane/methanol (6/4, v/v) by sonication, dried, and then saponified with the 0.1 M KOH. The alcohol fraction was purified by a silica gel column chromatography according to the procedure in Fukusima et al. (2006), by eluting with n-hexane/diethyl ether (1/1, v/v) after elution of aliphatic and aromatic hydrocarbons with n-hexane/benzene (5/1, v/v), and subsequently trimethylsilylated with N,O-bistrimethylsilyltrifluoro acetamide (BSTFA). Sterols were identified by retention time and mass spectra recorded on a gas chromatograph-mass spectrometer (GC-MS: an HP 6970 GC coupled to an HP 5973 mass selective detector, Agilent Technologies, USA) (Figure 7). Quantification was performed on a GC-flame ionization detector (FID) using an HP 5890 series II GC (Agilent Technologies, USA), comparing the peak area with an internal standard, 16-hydroxyhexadecanoic acid methyl ester, spiked just before trimethylsilylation.

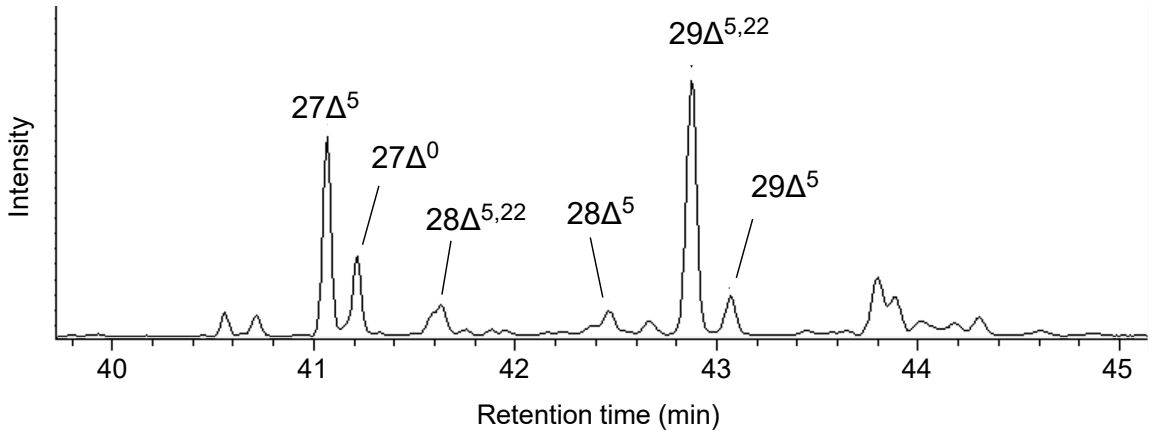

Figure 7. A representative total ion chromatogram (TIC) on GC/MS analysis (sterols in HMW-DOM fraction for August, Lake Kizaki). Abbreviations: cholest-5-en-3β-ol ($27\Delta^5$), cholestan-3β-ol ($27\Delta^0$), 24-methylcholest-5,22-dien-3β-ol ($28\Delta^{5,22}$), 24-methylcholest-5-en-3β-ol ($28\Delta^5$), 24-ethylcholest-5,22-dien-3β-ol ($29\Delta^{5,22}$), 24-ethylcholest-5-en-3β-ol ($29\Delta^5$).

2.2.3 Compound specific isotopic ratio analysis

In order to determine stable isotope ratios, the alcohol fraction isolated from the HMW-DOM in June, October, and December and surface sediment of Lake Kizaki were acetylated with acetic anhydride/pyridine (1/1, v/v). Purification of acetylated sterols was made by urea adduction. The sterols were further separated into three fractions: stanols, Δ^5 sterols, and other sterols (e.g., $\Delta^{5,22}$ and $\Delta^{5,24}$ sterols) using a silver nitrate (10 wt%) impregnated-silica gel column chromatography, according to the procedure described in Chikaraishi et al. (2005). The carbon and hydrogen isotopic compositions were determined by a GC-isotope ratio mass spectrometer (GC-IRMS) using an Agilent 6890N GC coupled to a Thermo Fisher Scientific Deltaplus XP IRMS. The contribution of carbon and hydrogen incorporated during derivatizations were corrected by an isotopic mass balance calculation described in Chikaraishi et al. (2004).

2.3 Results

2.3.1 Sterol compositions

In Lake Kizaki, cholest-5-en-3β-ol (cholesterol, $27\Delta^5$) is the most dominant sterol in the total-DOM, POM, and phytoplankton (45-85, 34-59, and 53-88 wt% of total sterols, respectively) fractions, whereas the sedimentary sterol is predominated by 24-ethylcholest-5-en-3β-ol (β-sitosterol, $29\Delta^5$) (31 wt% of total sterols) (Figure 8). On the contrary, HMW-DOM is uniquely characterized by a considerably high abundance and a large proportion of stigmasterol ($29\Delta^{5,22}$), particularly in May (0.58

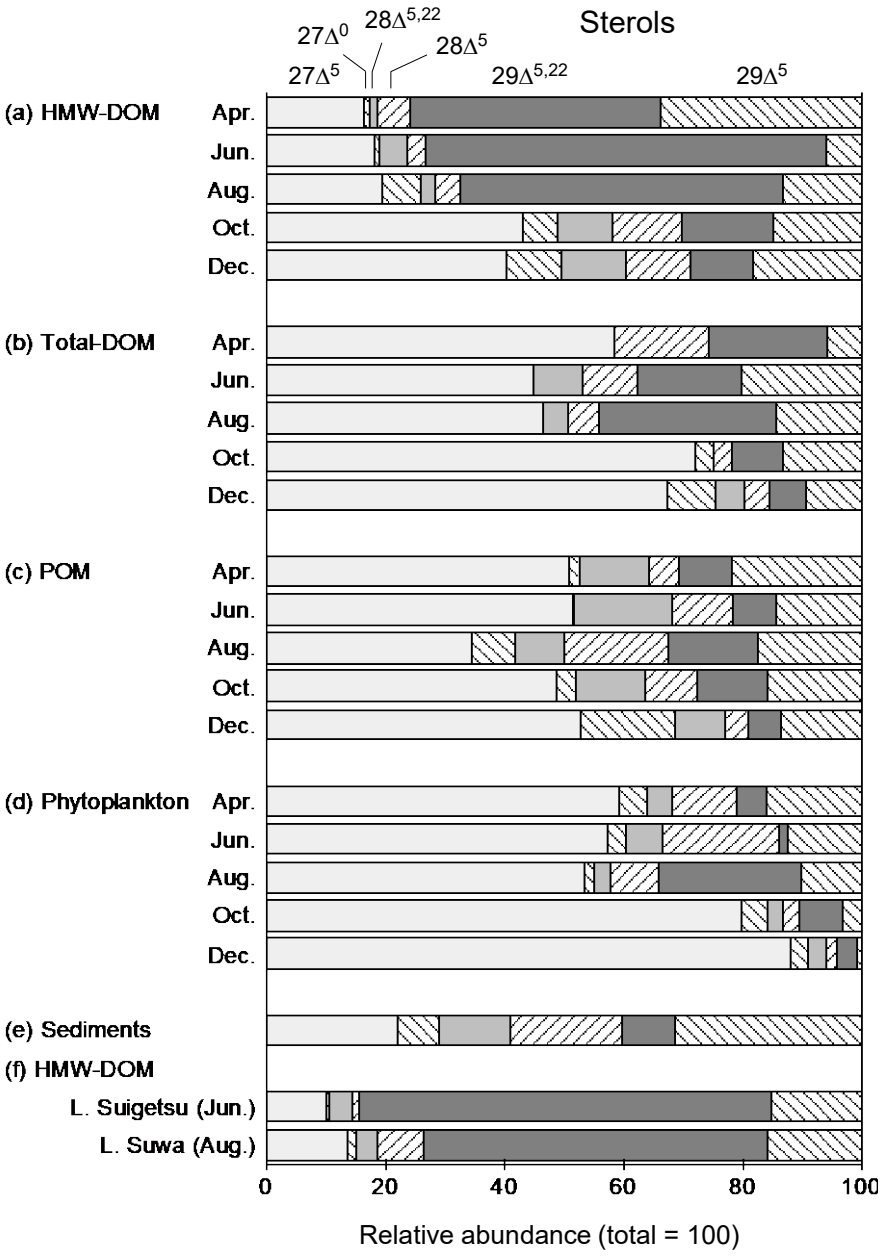

Figure 8. Relative abundance of sterols in (a) HMW-DOM, (b) total-DOM, (c) POM, (d) phytoplankton, and (e) sediments from Lake Kizaki, and in (f) HMW-DOM from lakes Suigetsu and Suwa (total = 100). Abbreviations are given in Figure 7.

μg/L, 65 wt% of total sterols), June (0.76 μg/L, 67 wt% of total sterols), and July (0.86 μg/L, 66 wt% of total sterols). Figure 8f also illustrates the predominance of stigmasterol in summer HMW-DOM isolated from Lakes Suwa (0.35 μg/L, 58 wt% of total sterols) and Suigetsu (0.24 μg/L, 69 wt% of total sterols). The predominance of stigmasterol in HMW-DOM fractions thus are commonly found in this and previous studies (e.g., Yoshiyama et al., 2003; McCallister et al., 2006b), which potentially implies that the high abundance of stigmasterol in HMW-DOM is universal, irrespective to the lake environments.

2.3.2 Stable carbon and hydrogen isotopic ratios for sterols

The stable isotopic ratio analysis reveals a large variation in the $\delta^{13}C$ value between −32.6 and −16.9‰ and in the δD value between −358 and −201‰ for these sterols (Figure 9). Among the great diversity in the isotopic compositions, cholesterol is scattered in the $\delta^{13}C$ and δD plot (from –32.6 to –26.2‰ for $\delta^{13}C$ and from −336 to –201‰ for δD). 24-ethylcholesta-5,22-dien-3β-ol (brassicasterol, $28\Delta^{5,22}$) and 24-ethylcholesta-5,24(28)E-dien-3β-ol (fucosterol, $29\Delta^{5,24(28)}$) fall within a relatively narrow region, where they are enriched in ^{13}C (between −22.9 and −16.9‰ for $\delta^{13}C$) and depleted in D (between −357 and −325‰ for δD). On the other hand, 24-ethylcholest-5-en-3β-ol (campesterol, $28\Delta^{5}$), stigmasterol, and β-sitosterol tend to be plotted on the mixing line between the ^{13}C -enriched with D-depleted zone and the ^{13}C-depleted with D-enriched zone. The plots of the three sterols thus shift on the line from the former zone in June toward the latter zone in December.

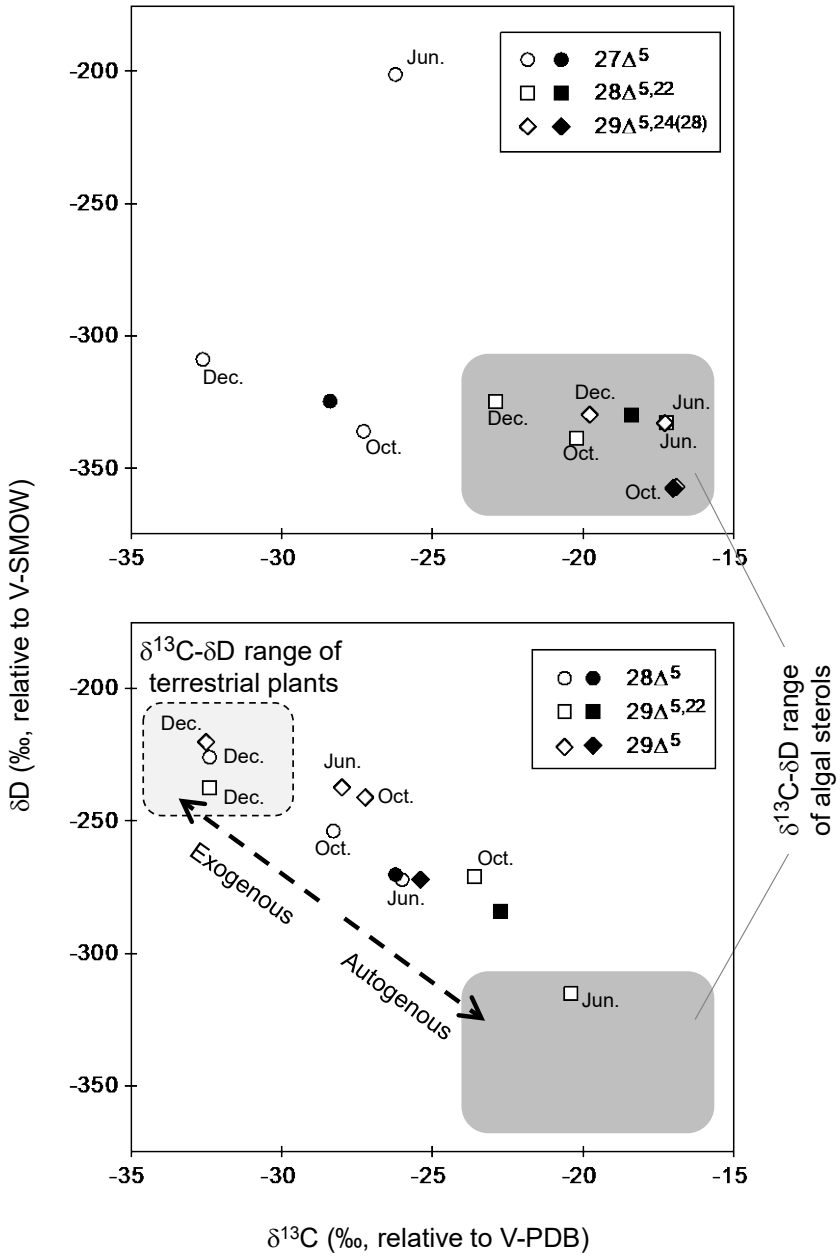

Figure 9. δ^{13}C-δD cross plots of sterols in HMW-DOM (open symbols) and surface sediments (closed symbols) from Lake Kizaki, with possible δ^{13}C-δD strange of sterols for the potential biological sources. Abbreviations are given in Figure 7.

2.4 Discussion

2.4.1 Sources of sterols

Sterols are widely distributed in eukaryotic cell membranes and the structure is variable depending on their biological sources (e.g., Volkman, 2003): among dominant sterols for HMW-DOM and sediments found in this study, it is thought that cholesterol is a widespread sterol found in many types of eukaryotes including algae and animals, but hardly found in terrestrial plants; brassicasterol and fucosterol are representative algae-derived sterols restricted sharply to algae including phytoplankton but not to terrestrial plants; and campesterol, stigmasterol, and β-sitosterol are dominantly found in terrestrial plants but also frequently found in phytoplankton (e.g., Volkman et al., 1998). These latter three sterols, however, show isotopic diversity depending on their biological sources: for instance, in the temperate regions, sterols in terrestrial C3 plants (approximately, from −35 to −30‰ for $\delta^{13}C$, from −250 to −200‰ for δD) are relatively depleted in ^{13}C and enriched in D compared to those in algae (approximately, from −15 to −25‰ for $\delta^{13}C$, from −300 to −350‰ for δD) (e.g., Chikaraishi et al., 2004; Chikaraishi, 2006). Thus, biological sources of these multi-source sterols (i.e., campesterol, stigmasterol, and β-sitosterol) can be identified by carbon ($\delta^{13}C$) and hydrogen (δD) isotopic analysis of them (Chikaraishi et al., 2005).

According to this knowledge, in this study, we used the two end-member mixing model with the following assumption to identify the biological sources of campesterol, stigmasterol, and β-sitosterol in HMW-DOM and sediments in this lake: (1) carbon and hydrogen isotopic compositions of algae-

derived sterols (the dark gray zone in Figure 7) are represented by those of brassicasterol and fucosterol; and (2) the isotopic compositions of terrestrial plant-derived sterols (the light gray zone in broken line in Figure 9) are available in the isotopic characterization described above. The two end-member models thus can be useful to evaluate biological sources of campesterol, stigmasterol, and β-sitosterol found in HMW-DOM and sediments in the lake, as these sterols are plotted in the mixing zone between the end-member sources, algae, and terrestrial plants, with its proportion likely varying among three sampling seasons (Figure 9).

As a common trend for the three sterols (i.e., campesterol, stigmasterol, and β-sitosterol), the plots for HMW-DOM are gradually moved on the mixing zones between algae- and terrestrial plant-derived sterols, from the former zone in June toward the latter zone in December, through intermediate in October. This trend is particularly remarkable for stigmasterol. A large quantity of stigmasterol in HMW-DOM is found from April to September, but not in October and December (Figure 8). The isotope signals of stigmasterol are found in the $\delta^{13}C$-δD region of algal sterols in June, but fall in the terrestrial plant region in December, and is intermediate between these two sources in October (Figure 9). These results suggest that (1) stigmasterol is principally the major sterol indicating terrestrial input of HMW-DOM throughout a year, but (2) an excess stigmasterol from spring to summer HMW-DOM is, however, derived from algal production.

In Lake Kizaki, although stigmasterol is also found in the phytoplankton fraction through seasons as well as in the surface sediments, the dominant sterol is cholesterol and β-sitosterol, respectively, in

these samples. These results imply that (1) some minor, specific phytoplankton is as a major source of stigmasterol found in the summer HMW-DOM in the lakes, (2) the stigmasterol from such specific phytoplankton can contribute much into the HMW-DOM, but little into the phytoplankton fraction and the surface sediments in this lake, and (3) major phytoplankton species rarely contribute to the stigmasterol in HMW-DOM fraction. Specific species responsible for the abundant stigmasterol observed in the HMW-DOM fraction cannot be identified in this study. However, we reveal at least a new finding that autochthonous algae (perhaps some minor phytoplankton) is a significant source of the abundant stigmasterol in the HMW-DOM fraction in the lakes.

2.4.2 Sources of HMW-DOM

Source and formation of HMW-DOM and its interaction with POM and LMW-DOM have been poorly understood so far because molecular and stable isotopic compositions of HMW-DOM are generally far different from those of POM and LMW-DOM (e.g., Benner et al., 1997; Ziegler and Fogel, 2003; Yoshiyama et al., 2003; McCallister et al., 2006a, 2006b; Repeta, 2015). Based on the $\delta^{13}C$ and δD values of sterols found in this study, we suggest that the source of HMW-DOM varies in season, as HMW-DOM in summer is mainly derived from autochthonous phytoplankton whereas that in winter is mainly derived from allochthonous terrestrial plants at least in Lake Kizaki. Moreover, as similar to the observation in previous studies (e.g., Benner et al., 1997; Repeta, 2015; McCallister et al., 2006a, 2006b), the relative proportion of sterols in HMW-DOM is far different from that in POM

and phytoplankton as well as sediments, meaning that organic components of HMW-DOM have only minor compatibility or transformability between HMW-DOM and POM and/or between HMW- and LMW-DOM in the lakes, and that HMW-DOM therefore plays a unique carbon cycle apparently independent of the carbon cycle composed of POM, LMW-DOM, and sediments.

Chapter 3: Difference in the foraging strategy between daphnia and copepods in oligotrophic pond: Evidence from $^{15}N/^{14}N$ amino acids

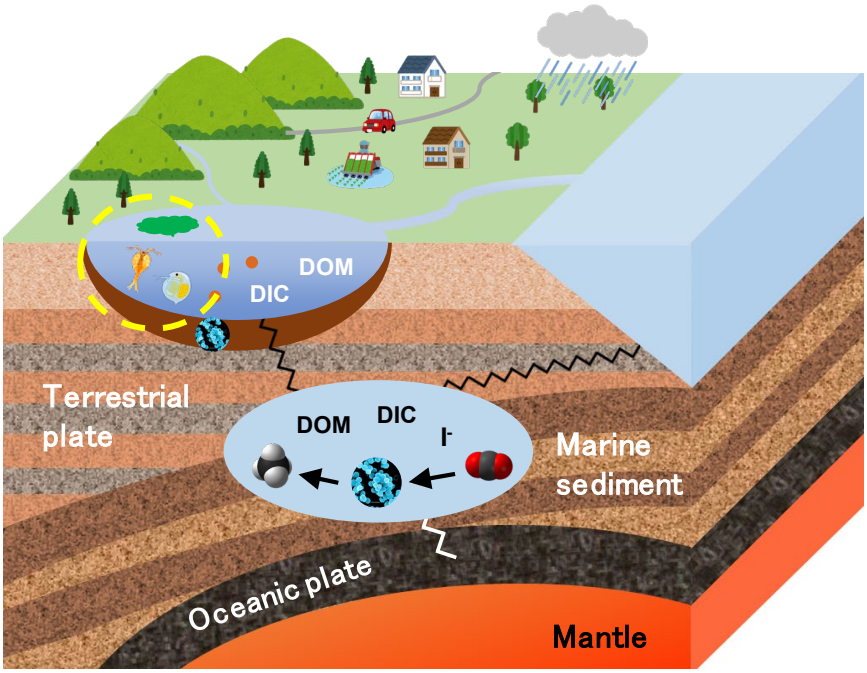

3.1 Aim of this study

Daphnia and copepods are two of the most dominant zooplankton species in freshwater environments such as ponds and lakes (e.g., Wetzel, 2001; Williamson, 1983, 1986; Ebert, 2005). They play a fundamental role in freshwater ecosystems, as a primary carrier of the solar energy fixed by phytoplankton into food webs (e.g., Sarvala and Halsinaho, 1990). However, it is well known that the biomass of zooplankton frequently exceeds that of phytoplankton even after spring and autumn blooms of phytoplankton in lakes, particularly for temperate and sub-polar regions, although the production should be exponentially decreased along the food chain (e.g., Sommer, 1989; Hairston et al., 1960). Moreover, it has been reported that such zooplankton biomass/density dynamics are species-specific and are independent of phytoplankton biomass in the environments (e.g., Sommer et al., 2003). Allochthonous materials (e.g., plant leaves and their detritus) thus have also been suggested as a potential food source for zooplankton in oligotrophic lakes (e.g., Janson et al., 2000; Karlsson et al., 2003; Cole et al., 2011).

Shirakoma-ike is a representative oligotrophic lake where such significant unbalance of plankton community was reported, as (1) daphnia and copepods are the dominant zooplankton species that have appeared more biomass than phytoplankton, and (2) the daphnia is found only in spring-autumn, whereas the copepod is found in whole season (e.g., Kadota, 1960; Lee et al., 2002). A number of previous studies have investigated potential food sources of this zooplankton in this lake, to solve the paradox on the plankton community in freshwater environments (e.g., Kadota, 1960; Lee et al., 2002).

For instance, based on gut content analysis, Kadota (1960) first identified attached-algae, bacteria, and detritus as potential food sources for the zooplankton species. More recently, Lee et al. (2002) suggested a large difference in the food sources between daphnia and copepods, based on the stable carbon and nitrogen isotopic compositions of bulk tissues for daphnia ($\delta^{13}C = -29.6 \pm 0.9$ ‰ and $\delta^{15}N = +1.3 \pm 0.4$ ‰, respectively) and copepods ($\delta^{13}C = -34.9 \pm 1.2$ ‰ and $\delta^{15}N = -0.4 \pm 0.9$ ‰, respectively). However, the identification of food sources and their contribution to the zooplankton species have been poorly understood so far.

Food web studies, particularly for the estimation of trophic position (TP) of organisms in food webs, has advanced remarkably during the last decade by the use of stable nitrogen isotopic composition analysis of amino acids (e.g., Chikaraishi et al., 2007; McCarthy et al., 2007; Popp et al., 2007). This methodology has been successfully applied in marine and freshwater environments (e.g., Kruse et al., 2015; Hirahara et al., 2015; Ohkouchi et al., 2015; Kruger et al., 2016). The TP has been simply calculated using the $\delta^{15}N$ values of glutamic acid ($\delta^{15}N_{Glu}$) and phenylalanine ($\delta^{15}N_{Phe}$), with the following equation (1) (Chikaraishi et al., 2009, 2014, Figure 8):

$$TP = [\ (\delta^{15}N_{Glu} - \delta^{15}N_{Phe} + \beta) / 7.6\ ] + 1$$

where β represents the difference between $\delta^{15}N_{Glu}$ and $\delta^{15}N_{Phe}$ values in primary producers (−3.4 ‰ for algae and cyanobacteria, +8.4 ‰ for plant leaves). It is known that the error of TP estimates (within

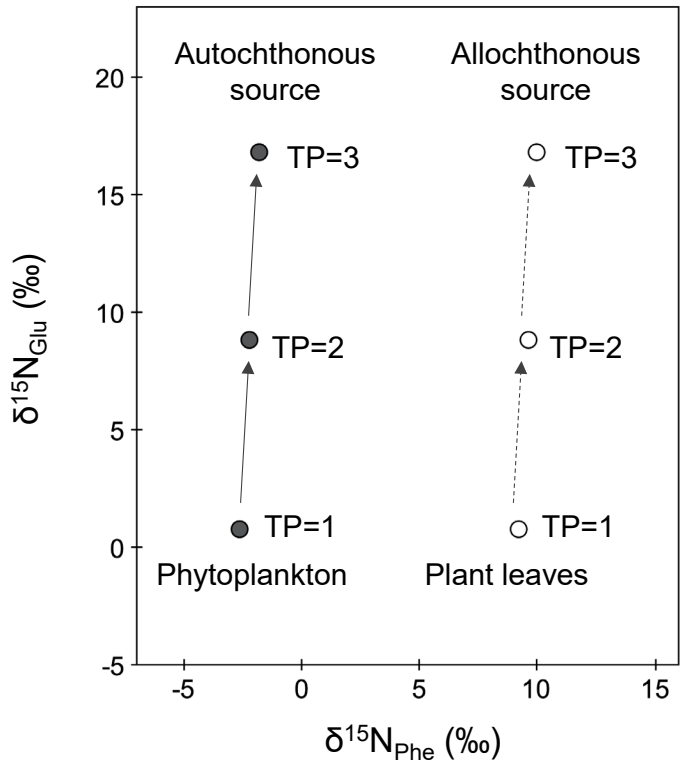

Figure 10. Schematic illustrations of the trophic position (TP) of autochthonous and allochthonous sources based on $\delta^{15}N$ values of Phenylalanine and Glutamic acid.

0.2 unit, Chikaraishi et al., 2009) is better than that in the traditional ones (e.g., gut content analysis, $\delta^{13}C$ and $\delta^{15}N$ analysis of bulk tissues, etc.), although major factors controlling for the $\delta^{15}N$ values of amino acids and the potential uncertainty of this methodology have still been debated (e.g., McMahon and McCarthy, 2016; Ohkouchi et al., 2017; Takizawa et al., 2017; Choi et al., 2018). Moreover, the contribution from aquatic and terrestrial primary producers (e.g., algae vs. plant) to food webs has been evaluated by applying mixing models with the $\delta^{15}N_{Phe}$ value (e.g., Naito et al., 2010, 2016).

In this study, we apply this methodology ($\delta^{15}N$ of amino acids) to estimate the TP and the potential food sources (and its seasonal variation) of the Daphnia *Daphnia longispina* and the copepod *Acanthodiaptomus pacificus* in Shirakoma-ike. We further evaluate the foraging strategy of these two dominant freshwater zooplankton species in the oligotrophic lake.

3.2 Materials and Methods

3.2.1 Geological setting and sampling Procedure

Shirakoma-ike is a subalpine oligotrophic-dystrophic lake, located in Nagano prefecture, Japan (36°03'5.1N, 138°21'43.2E, Figure 11). The altitude and surface area of the lake is 2115 m and 0.11 km^2, respectively. The lake has no permanent input and output flowing with a maximum water depth of 8.6 m, and surface water freezes over winter (from the middle of November to May). The pH of the lake water is approximately 5, making no fish habitable in the lake. Phytoplankton can bloom in spring and autumn, but the concentration of chlorophyll *a* is lower than 2 μg/L even for blooming

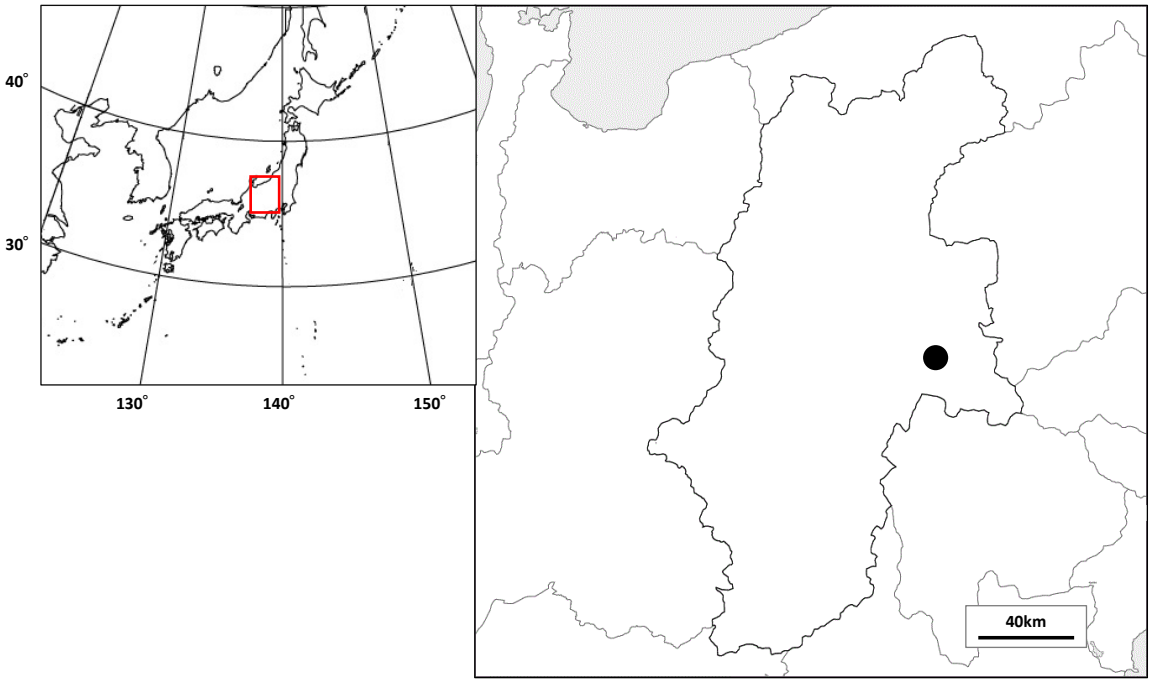

Figure 11. Geological location of sampling site, Shirakoma-ike, at Nagano pref., Japan.

periods and further decreased to 0.5 μg/L for winter (Table 1). The daphnia *Daphnia longispina* and the copepod *Acanthodiaptomus pacificus* are dominant zooplankton species, and the daphnia is found only in spring-autumn (20-120 × 10^3 individuals/m^2), whereas the copepod is found in the whole season (50-300 × 10^3 individuals/m^2) (Table 1). Water mites, phantom midge, and dragonfly larva may be high TP omnivores or carnivores in this lake (Lee et al., 2002).

The daphnia and the copepod were collected from around the center of the lake in spring (June), summer (August), autumn (November), and winter (December, but *A. pacificus* only because absence of *D. longispina*) in 2015. These two species were sorted under a dissecting microscope, freeze-dried, and kept at room temperature until the isotope analysis. According to no substantial contribution of gut contents to the isotope analysis (e.g., Hirahara et al., 2015), these species' gut content was not eliminated before analysis.

3.2.2 Stable nitrogen isotopic ratio analysis

The dried samples (approximately 1.0 mg) were prepared for stable nitrogen isotopic composition analysis of amino acids, after HCl hydrolysis and N-pivaloyl/isopropyl (Pv/OiPr) derivatization, according to the procedure in Chikaraishi et al. (2009). The isotopic composition was determined by gas chromatography/isotope ratio mass spectrometry (GC/IRMS) using a 6890N GC (Agilent Technologies, USA) instrument coupled with a DeltaplusXP IRMS instrument through combustion (950 ºC) and reduction (550 ºC) furnaces via a GC-C/TC III interface (Thermo Fisher Scientific, USA).

Table 1. Seasonal change in chlorophyll a and density of zooplankton in Shirakoma-ike.

	Unit	2011								2012						
		May	Jun	Jul	Aug	Sep	Oct	Nov	Dec	Jan	Mar	Apr	May	Jun	Jul	Aug
Chl.a	μg/L	0.79	1.83	1.38	1.83	1.47	1.81	1.29	0.86	0.47	0.23	0.26	1.23	0.88	1.34	1.49
Zooplakton Density																
D.longispina	$\times 10^3$ ind/m^2	0.3	28.0	93.7	45.8	40.3	30.7	11.7	1.5	0.0	0.0	0.0	15.0	39.4	114.9	32.3
A.pacificus	$\times 10^3$ ind/m^2	121.2	154.3	125.8	89.7	73.5	54.5	46.8	58.2	51.2	44.4	55.0	104.2	294.2	97.9	95.9
Rate of having egg																
D.longispina	%	0.0	16.0	1.1	1.6	39.2	12.3	3.2	0.0	0.0	0.0	0.0	0.0	13.8	22.7	52.1
A.pacificus	%	0.0	1.8	3.0	0.0	13.0	10.7	63.4	60.5	65.2	56.9	20.5	11.1	8.7	8.3	0.0

The isotopic composition was expressed relative to atmospheric nitrogen ($\delta^{15}N$, ‰ vs. AIR) on a scale normalized to the known $\delta^{15}N$ values of isotope reference amino acids (from −26.1 to +45.7 ‰, Indiana University and SI science Corp., Sato et al., 2014). The accuracy and precision for the isotope measurements of the reference amino acids were 0.0 ‰ (mean of Δ) and 0.5 ‰ (mean of 1σ), respectively. The TP was calculated using the equation (1), with $\delta^{15}N_{Glu}$ and $\delta^{15}N_{Phe}$ for each sample, which determined in the present study, and with −3.4 ‰ for the β value (Chikaraishi et al., 2009).

3.3 Results

3.3.1 The $\delta^{15}N$ values and the estimated TP

A little change in the $\delta^{15}N_{Glu}$ and $\delta^{15}N_{Phe}$ values was found in daphnia (i.e., from +6.2 to +8.0 ‰ and from −5.4 to −4.1 ‰, respectively) in spring-autumn, resulting in no substantial change in the estimated TP (2.1 ± 0.0) through season (Table 2, Figure 12a). On the other hand, a gradual increase in the $\delta^{15}N_{Glu}$ and $\delta^{15}N_{Phe}$ values was apparently found in copepods (from +6.0 to +10.8 ‰ and −6.2 to −3.6 ‰, respectively) from spring to winter (Table 2, Figure 12b). Moreover, a zigzag change in the TP was obtained in copepods, as the TP for spring and autumn (TP=2.1, n=2) is lower than that for summer and winter (TP=2.6, n=2). Thus, the TP of zooplankton indicates the foraging strategy specific to species, which may be related to the absence of daphnia vs. the presence of copepods in winter (i.e., limited primary production in the freezing period) of the lake (see below).

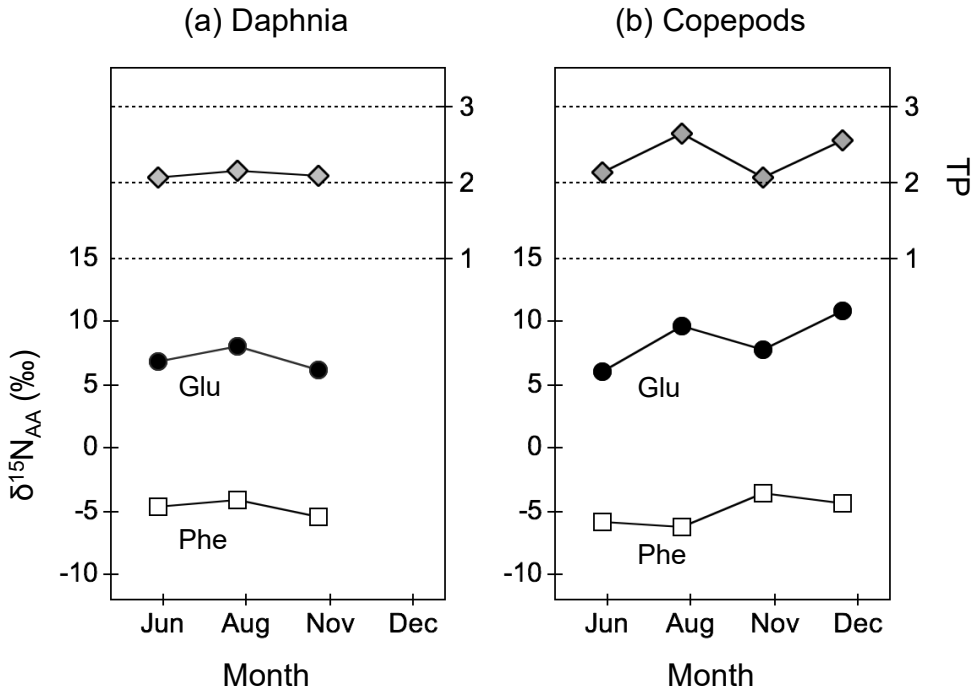

Figure 12. The $\delta^{15}N_{Glu}$ (filled circle) and $\delta^{15}N_{Phe}$ values (open square), and TP (gray diamond) of daphnia and copepods in Sirakoma-ike.

Table 2. Nitrogen isotopic composition of amino acids in *A.pacificus* and *D. longispina*.

	Collection date	$\delta^{15}N$(‰, vs Air)							$TP_{Glu/Phe}$※
		Alanine	Glycine	Valine	Leucine	Isoluecine	Glutamic acid	Phenyl alanine	
A.pacificus	Jun.	3.2	-13.5	4.5	-2.7	0.0	6.0	-5.9	2.1
	Aug.	9.6	-5.1	6.9	3.1	3.3	9.6	-6.2	2.6
	Nov.	5.5	-10.6	6.6	-1.2	0.7	7.8	-3.6	2.1
	Dec.	12.5	-3.2	8.3	3.1	5.6	10.8	-4.4	2.6
D.longispina	Jun.	3.2	-10.4	5.8	0.9	3.2	6.8	-4.7	2.1
	Aug.	n.d.	-4.0	11.8	5.6	7.9	8.0	-4.1	2.1
	Nov.	3.2	-12.3	3.5	1.1	1.2	6.2	-5.4	2.1

※$TP_{Glu/Phe}=[(\delta^{15}N_{Glu}-\delta^{15}N_{Phe}-3.4)/7.6]+1$

3.4 Discussion

3.4.1 Foraging strategy

It is known that the $\delta^{15}N_{Phe}$ values in consumers principally reflects an integrated value for that of basal recourses of the consumers in food webs. Furthermore, the $\delta^{15}N_{Phe}$ values of autochthonous sources (e.g., phytoplankton) are much lower (by ~11.8‰) than those of allochthonous inputs (e.g., plant leaves) (e.g., Chikaraishi et al., 2014; Ohkouchi et al., 2017). According to this knowledge, overlapping in the $\delta^{15}N_{Phe}$ range between daphnia (from −5.4 to −4.1 ‰) and copepods (from −6.2 to −3.6 ‰) was observed in this study (Table 2) clearly indicates that these two zooplankton species belong to the same food web in this lake. Also, these low $\delta^{15}N_{Phe}$ values and their small variation suggest little or negligible input from allochthonous food sources to these zooplankton species in this lake.

On the other hand, a difference in TP trend through the season (Figure 12) reveals a distinct foraging strategy for these two zooplankton species in this lake. Based on the potential estimation error in the TP (i.e., 0.2 units, Chikaraishi et al., 2009), the TP for the daphnia (2.1±0.0) and the copepods (2.3±0.3) indicates that they contribute mainly as herbivorous and omnivorous zooplankton, respectively, in the food webs of this lake. Moreover, such herbivory for the daphnia did not change through the season. Besides the daphnia, the degree of omnivory for the copepods is variable, and shows a difference between seasons as more herbivory (TP=2.1, n=2) that feeds on phytoplankton for spring and autumn than omnivory (TP=2.6, n=2) that feeds on both phytoplankton and heterotrophic

microbes (e.g., protists and bacteria) for summer and winter. Thus, these results reveal strong herbivory for the daphnia compared to dietary plasticity and facultative omnivory for the copepod in this lake.

In the observation, the population size of daphnia (20−120 × 10^3 individuals/m^2) was much smaller than that of copepods (50−300 × 10^3 individuals/m^2) in this lake. Moreover, the life cycle of daphnia is somewhat different from that of copepods: daphnia produce resting eggs (or sometimes called winter eggs) for over-wintering, whereas copepods can survive winter even in adult stages (e.g., Carvalho and Wolf, 1989, Wolf and Carvalho, 1989). Although based on the TP and the $\delta^{15}N_{Phe}$ values, we cannot fully explain these differences in the population and life cycle between the two zooplankton species, we predict the following foraging strategy and life cycle:

Daphnia: They feed predominantly on phytoplankton in spring-autumn, even under the strong limitation of the phytoplankton biomass, particularly for summer. However, they produce resting eggs for adapting to the extreme limitation of phytoplankton biomass in the freezing period.

Copepods: Like daphnia, they feed preferentially on phytoplankton in spring and autumn. However, their diet is shifted from phytoplankton to other food sources – probably heterotrophic microbes such as protists and bacteria – in summer and winter because copepods production cannot be supported only from the phytoplankton biomass.

There is a major paradox that these zooplankton species have more biomass than phytoplankton in this lake, and therefore a number of previous studies have investigated potential diet sources (instead of phytoplankton) for this zooplankton (e.g., Kadota, 1960; Lee et al., 2002). However, based on the

results of this study, (1) the TP for the daphnia (2.1±0.0) and the copepods (2.3±0.3) and (2) the low $\delta^{15}N_{Phe}$ values and their small variation (from −6.2 to −3.6 ‰) suggests that the phytoplankton production mainly supports these two zooplankton species, although the concentration of chlorophyll *a* determined is only 1.5 μg/L during the open ice season. In the field observation, short (within a few days) bloom of phytoplankton frequently appears after temporal inputs of snow melting-water and/or rainwater. The short bloom of phytoplankton may partially support the biomass of these zooplankton species.

Heterotrophic microbes (e.g., protists and bacteria) potentially have the TP close to 1.0 (as phytoplankton), because they de novo synthesize amino acids from carbon sources and ammonia (Yamaguchi et al., 2017), and may supply autochthonous food sources to these zooplankton species in freshwater lake (e.g., Janson et al., 2000; Karlsson et al., 2003; Cole et al., 2011). However, we assume that bioavailable carbon sources (e.g., glucose, boiled starch, but not starch, cellulose, lignin, etc.) are very limited or absent in the lake if allochthonous (e.g., plant leaves) inputs are significantly large. In this study, although we cannot accurately estimate the contribution of such microbes to the TP=1 organisms, we predict that phytoplankton is a major source to support these two zooplankton biomass species.

3.4.2 Potential uncertainty in the TP estimate

Applying this new methodology, we should consider the universality of the TP estimation for the

zooplankton species. Chikaraishi et al. (2009) first established the equation (1) for marine zooplankton and fish, based on large and small trophic enrichment $^{15}N_{Glu}$ and $^{15}N_{Phe}$, respectively. Moreover, the applicability of this equation (1) has been confirmed in diverse organisms including fungi, bacteria, insects, fish, and mammals (e.g., Steffan et al., 2015; Yamaguchi et al., 2017). However, trophic elevation in the $\delta^{15}N_{Glu}$ value may vary unique to species and/or among growth conditions such as the quality of diets (Chikaraishi et al., 2015; McMahon et al., 2015; McMahon and McCarthy, 2016). Little trophic elevation in the $\delta^{15}N_{Glu}$ value was reported in protozoan (Gutoérrez-Rodríguz et al., 2014) and protistan (microzooplankton) (Décima et al., 2017). More recently, Choi et al. (2018) reported that the TP of herbivorous gastropod estimated is lower than 2.0, because of the metabolic flux of amino acids unique to these species. Thus, trophic elevation in the $\delta^{15}N_{Glu}$ and $\delta^{15}N_{Phe}$ values is universal in many species, but is not always in all species, including several zooplanktons. Based on these findings, we suggest that further studies are required for the estimation of accurate TP of zooplankton with respect to the metabolic flux of amino acids in each species.

Chapter 4: Methanogenesis and methane cycle: Deep methanogenesis with unique microorganisms in an organic- and iodine-rich aquifer

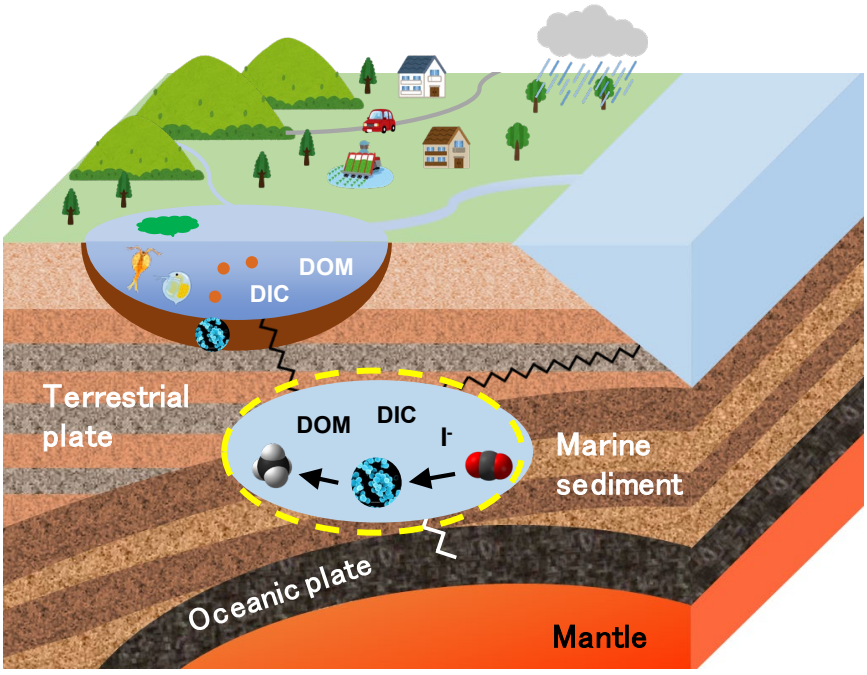

4.1 Aim of this study

Methane, the most reduced carbon compound, is widely distributed in surface environments and in deep subsurface environments on Earth. The global budget of atmospheric methane is 500–600 Tg year^{-1}, of which biogenic methane accounts for approximately 69% (Conrad, 2009). Biogenic methane is produced by methanogenic archaea living in terrestrial and oceanic anaerobic environments (e.g., Thauer et al., 2008; Valentine, 2011), including deeply buried marine sediments down to 2.5 km below the seafloor (e.g., Inagaki et al., 2015; Sass et al., 2019). However, the ecology of deep subsurface environments is still unclear because of the limited number of surveys utilizing culture-based approaches (Teske and Sorensen, 2008; Imachi et al., 2011; Mayumi et al.,2016); hence, it is difficult to assess the deep methane cycle in anaerobic subsurface environments directly. Methanogenic archaea has been found to use three general methanogenic pathways (Thauer, 1998, Figure 13). Coenzyme factor 430 (hereafter, F430) is a hydrocorphinoid nickel complex and is the prosthetic group of methyl-coenzyme M reductase (MCR), which catalyzes the final step in all methanogenesis pathways (Thauer, 1998; Ermler et al., 1997; Duin, 2009, Figure 13). Because F430 is a common coenzyme of methanogenic archaea and is directly involved in methanogenesis, quantitative analysis of F430 enables the determination of potential in situ methanogenic activity (Thauer and Bonacker, 1994; Passaris et al., 2018; Thauer, 2019).

A unique feature of our sampling site in the Southern Kanto gas field is that the brine-rich water originating from ancient seawater contains high concentrations of dissolved organic matter (DOM),

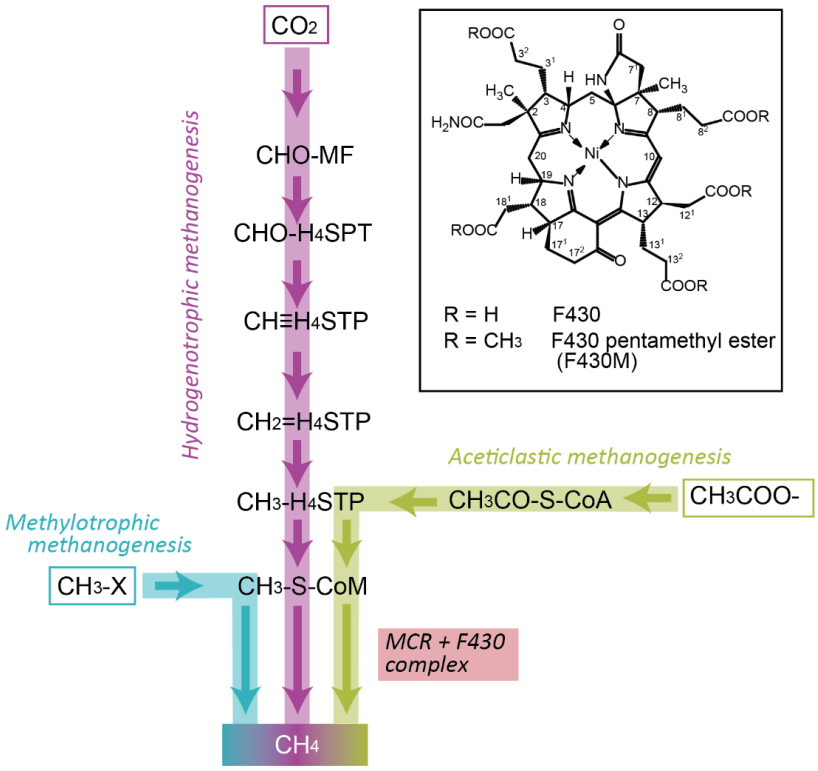

Figure 13. Biological methanogenesis pathways and the molecular structure of coenzyme factor 430 (Kaneko et al., 2014).

including humic substances, with the total organic carbon (TOC) concentration reaching approximately 82 mg L^{-1}(Katayama et al., 2015). DOM and methane originate from primary producers buried in the accretionary prism, but the relative contributions of modern carbon and organic compounds in Cenozoic sediments to the huge methane production are poorly understood so far. Furthermore, the brine-rich water also contains a high concentration of iodine (<1.2 mM, Amachi et al., 2005), which is approximately two thousand times that of modern seawater (0.5 μM). Iodine production from the gas field comprises 30% of the commercially available world production (Muramatsu et al., 2001).

To identify the characteristics of microorganisms, including methanogenic archaea, in the deep aquifer, we determined the ratio between Bacteria and Archaea as well as the relative biomass of methanogens (%) by using three parallel approaches. The first was lipid-based organic analysis based on archaeal ether lipids and bacterial fatty acids. Bacterial membrane lipids generally involve ester bonds between fatty acids and glycerol, whereas archaeal membrane lipids involve ether bonds between an isoprenoid hydrocarbon chain and glycerol (e.g, Killops and Killops, 2005). The second approach was community structure analysis based on small-subunit (SSU) rRNA gene tag sequencing. The third approach was identifying the potential for ongoing methanogenesis based on the concentration of F430, a key molecule of methanogenic archaea.

To assess the origin of methane molecules, we conducted methane-specific stable and radiocarbon measurements (i.e., $\delta^{13}C_{methane}$ and $\Delta^{14}C_{methane}$) to further elucidate the deep methanogenesis in the

brine-rich aquifer. Radiocarbon (^{14}C) has been utilized as a tracer to understand the biogeochemical carbon cycle (e.g., Larsen et al., 2018; Blattman et al., 2019; Ishikawa et al., 2019; Wyatt et al., 2019; Nishida et al., 2020; Kelsey et al., 2020), and ^{14}C measurements have been performed on methane and carbon dioxide from deep subsurface sources (e.g., Proskurowski et al., 2008; Kawagucci et al., 2013; McDermott et al., 2015; Takano et al., 2018; Nomaki et al., 2019).

4.2 Materials and Methods

4.2.1 Geological setting

The Southern Kanto gas field, located on the Boso Peninsula (Figure 14a), is the largest natural gas-dissolved-in-water field in Japan (e.g., Ueno et al., 1964). This gas field's reservoir rocks consist of turbidites (alternating beds of sandstone and mudstone) in the Umegase to Katsuura formations of the Kazusa Group. The formations' depths and ages are about 100–3000 m and about 0.8–2.4 Ma, respectively (Suganuma et al., 2018; Unosawa et al., 1983). The gas field does not contain oil because of the low geothermal heat flow and the short duration (and rapidity) of sedimentation (Sano et al., 2017; Kunisue et al., 2002). Previous studies reported that methane in the Southern Kanto gas field has a typical biogenic origin and was formed by a type of hydrogenotrophic methanogenesis, as indicated by its gas composition and methane isotopic ratios ($C_1/C_2 = 6.1 \times 10^3$, $\delta^{13}C_{methane}$, −67 ‰ vs. Vienna Pee Dee Belemnite [VPDB] and $\delta D_{methane}$, −185 ‰ vs. Standard Mean Ocean Water, Igari and Sakata, 1989; Kaneko et al., 2002). Based on archaeal 16S rRNA gene analysis and culturing of

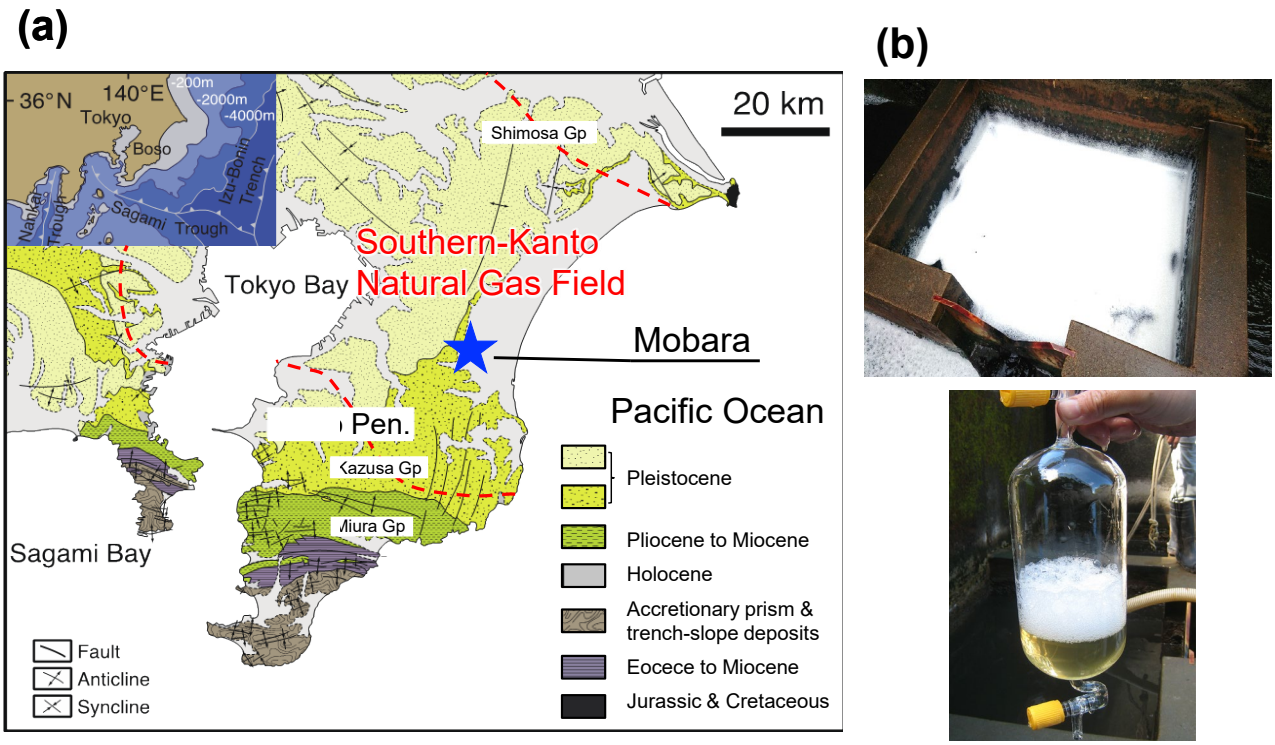

Figure 14. (a) Geological setting of the sampling site on the Boso Peninsula, Mobara, Japan. The broken red line shows the Southern Kanto gas field (Sawaki ei al., 2015). The geological profiles showing Holocene sediment and forearc basin deposits associated with the Shimousa, Kazusa, and Miura groups are modified after a previous study (Ito et al., 2016b). (b) Photographs of the well at the study site (KTG3). Upper: Vent of the deep aquifer after separation of methane gas. The photograph was taken just after the oversaturated gas from the well had blown out like a geyser. Lower: Gas phase, bubbles scum and brine samples collected by the water displacement method; the gas phase is >99 % methane. The bubbled scum and yellow brine-rich water are also visible.

brine-rich water from the deep subsurface environment at Mobara, it has been suggested that there are methanogenic communities presently living in the deep aquifer (Katayama et al., 2015; Mochimaru et al., 2007; Ishii et al., 2019). However, some organic geochemical aspects of the microbial ecology in the organic and iodine-enriched deep biosphere are still unknown.

4.2.2 Sampling procedure

We collected gas phase, brine-rich water, and bubbled scum from gas production wells KTG3 and KTG4 in the Southern Kanto gas field (Chiba, Japan; Figure 14a). The brine-rich water ranges from brownish to yellowish (Figure 14b) because of high concentrations of DOM. In KTG3, brownish brine-rich water flows into the well through openings in the well casing and rises to ground level by natural water pressure; in contrast, at KTG4 yellowish brine-rich water is brought to ground level by a gas lift system. The brine-rich water is sent to a separation tank where methane is separated under atmospheric pressure. The gas phase and brine-rich water were collected from the pipes before entering the separation tank. The bubbled scum was collected from the vent of the deep aquifer after the separation of methane gas. The bubbled scum appeared immediately after the oversaturated gas from the well had blown out like a geyser, and then covered the water surface (Figure 14b, on the left). The basic characteristics of the brine-rich water are summarized in Table 3.

Table 3. Geochemical characteristics of brine-rich water. ORP is an abbreviation for Oxidation Reduction Potential. "–" means unmeasured. The data of MOB4 and MOB7 was quoted from Mochimaru et al. (2007).

Property	Unit	KTG3	KTG4	MOB4*	MOB7*
Na^+	mg/L	7563	11287	11000	12000
NH_4^+	mg/L	167	243	280	290
K^+	mg/L	223	324	360	400
Mg^{2+}	mg/L	196	305	430	400
Ca^{2+}	mg/L	104	210	180	210
Cl^-	mg/L	12669	19171	18000	19000
Br^-	mg/L	83	124	145	160
SO_4^{2-}	mg/L	<10	<10	24	23
NO_2^-	mg/L	–	–	0.023	0.025
NO_3^-	mg/L	–	–	<0.005	<0.005
I^-	mg/L	70.6	106.5	120.0	150.0
TOC	mg/L	69	–	−57	−65
ORP	mV	−261	−234	−438	−411
Depth	m	274−715	714−1398	347−759	619−1132
Temp.	°C	21.9	33.0	19.1	26.7
Number of cells	cells/L	7.04×10^7	1.97×10^8	$<1.0 \times 10^4$	$<1.0 \times 10^4$

* Mochimaru et al. (2007)

4.2.3 Prokaryotic lipid analysis

Bacterial and archaeal lipids were analyzed as outlined in Figure 15. Samples (100 mL) were lyophilized and then saponified with 0.5 M KOH in methanol/water (95/5, w/w) in a sealed vial at 80 °C for 2 h. The neutral lipid fraction was extracted from the alkaline medium with *n*-hexane. After adding HCl to the residue, the fatty-acids fraction was extracted from the acid medium with dichloromethane. The fatty-acid fraction was methyl esterified with MeOH and HCl at 80 °C overnight and then purified by silica gel column chromatography by elution with dichloromethane. The neutral lipid fraction was subjected to ether cleavage treatment with 57 wt% HI (in H_2O) at 110 °C for 4 h (Takano et al., 2018). After the addition of 5 wt% NaCl (aqueous) and *n*-hexane, the *n*-hexane fraction was recovered by liquid-liquid extraction; n-hexane and PtO_2 were then added, and hydrogenation was performed by gentle bubbling with H_2 gas at room temperature for 45 min. Bacterial and archaeal lipids were identified by gas chromatography/mass spectrometry (GC/MS; 7890B GC and 5975C MSD, Agilent Technologies, USA) with a VF-5MS column (30 m × 0.25 mm i.d., 0.10 μm film thickness, Agilent Technologies, USA). Quantification was achieved by gas chromatography/flame ionization detector (GC/FID; 6890N, Agilent Technologies, USA) with a DB-5MS column (30 m × 0.25 mm i.d., 0.10 μm film thickness, Agilent Technologies, USA).

4.2.4 Coenzyme factor 430 analysis

Coenzyme F430 analysis followed the method described in previous studies (Takano et al., 2013;

Kaneko et al., 2014, 2016). After filtering the water (5 L) through a PTFE filter (0.2 μm, Advantec Corp., Tokyo, Japan), the filter was extracted with 1% formic acid by ultrasonication for 30 min on ice, followed by centrifugation (10,000 × g; 30 min at 4 °C) to recover the supernatant. The supernatant was introduced to an anion exchange column (Q Sepharose column; GE Healthcare, USA) that had been equilibrated with 50 mM Tris-HCl (pH 7.5) and washed with deionized water prior to use. The recovered eluent was introduced to a C18 SPE column (Sep-Pack; Waters Corp., USA) conditioned with 5 mL of 1% formic acid. A yellowish band on the column (F430 fraction) was eluted with methanol. The dried F430 fraction was reacted with BF_3 in methanol in a closed vial at 40 °C for 3.5 h to convert F430 to its pentamethyl ester (F430M). Distilled water was added, and the aqueous phase was extracted with dichloromethane and dried under a gentle N_2 stream. The F430M fraction was dissolved in a water/acetonitrile solution (85/15, v/v). F430M was quantified with high-performance liquid chromatography (HPLC; 1200 series, Agilent Technologies, USA) with a ZORBAX Eclipse XDB-C18 column (4.6 × 250 mm; 5 μm p.s., Agilent Technologies, USA) and a guard column. The column temperature was set at 30 °C throughout the analysis. Absorbance was measured at 430 and 560 nm using an online diode array detector (DAD). The mobile phases were 100 mM $NaClO_4$ (A) and acetonitrile (B) at a flow rate of 0.5 mL min^{-1}. The elution gradient started at 0 % B, shifting to 30 % B after 3 min and then 90 % B after 90 min.

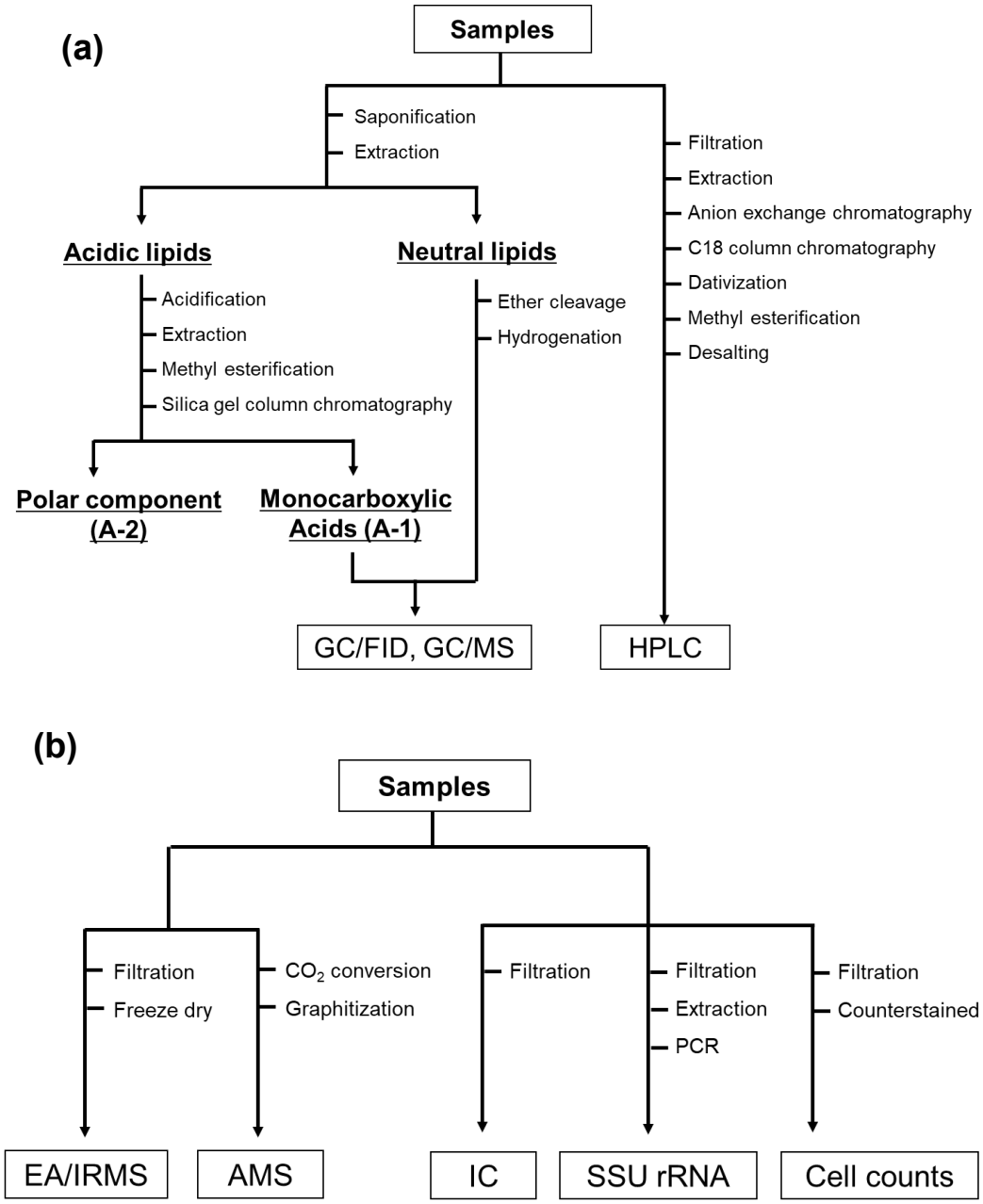

Figure 15. Flowcharts of analysis. (a) Prokaryotic lipid and F430 analysis. (b) rRNA gene, total cell counts, ionic composition, and isotope analysis ($\delta^{13}C$ and $\Delta^{14}C$). AMS, accelerator mass spectrometry; EA/IRMS, elemental analysis/isotope ratio mass spectrometry; GC/FID, gas chromatography/flame ionization detection; GC/MS, gas chromatography/mass spectrometry; HPLC, high-performance liquid chromatography; IC, ion chromatography; PCR, polymerase chain reaction; SSU rRNA, small-subunit rRNA.

4.2.5 SSU rRNA gene tag sequencing

DNA extraction and polymerase chain reaction (PCR) mixture preparation were performed on a clean bench to reduce contamination. DNA was extracted from samples by using DNeasy PowerSoil Kit (Qiagen, USA) as described previously (Nakahara et al., 2019). PCR amplification of the SSU rRNA gene was performed using TaKaRa LA Taq (TaKaRa Bio Inc., Japan) with a universal primer pair (530F/907R, Nunoura et al., 2012), which contained overhang adapters at the 5′ ends. The detailed procedures for library construction, sequencing by MiSeq (Illumina, USA), and data analysis were described previously (Ishii et al., 2019). The SSU rRNA gene tag sequencing data from this study have been deposited in a short read archive with the accession numbers SRS5817427–5817429 and SRX7574760.

4.2.6 Bulk stable carbon and nitrogen isotopic ratio analysis

The lyophilized bubbled-scum samples (1 mg) were dissolved in trichloromethane and transferred to tin capsules. The samples were then carefully dried before analysis. The samples were analyzed for stable carbon and nitrogen isotopes with an ultrasensitive elemental analyzer connected to an isotope ratio mass spectrometer (nano-EA/IRMS; Flash EA1112 connected to a Thermo Finnigan Delta plus XP via ConFlo III, Thermo Finnigan, USA) as described previously (Ogawa et al., 2010). The isotopic compositions of carbon and nitrogen are presented in conventional delta notation (‰) expressed as $\delta^{13}C$ (‰ vs. VPDB) and $\delta^{15}N$ (‰ vs. AIR), respectively:

$$\delta^{13}C\ (‰) = [(^{13}C/^{12}C)_{sample}/(^{13}C/^{12}C)_{standard} - 1] \times 1000$$

$$\delta^{15}N\ (‰) = [(^{15}N/^{14}N)_{sample}/(^{15}N/^{14}N)_{standard} - 1] \times 1000$$

The carbon and nitrogen contents and their isotopic compositions were calibrated by L-tyrosine (BG-T: C, 59.7 %; N, 7.74 %; $\delta^{13}C$, –20.83 ± 0.10 ‰; $\delta^{15}N$, +8.74 ± 0.09 ‰). The analytical errors for the isotopic compositions estimated by repeated analyses of BG-T (2.80–74.59 μgC, 0.66–9.67 μgN) are ± 0.25 ‰ (s.d. 1σ, n = 9) for $\delta^{13}C$ and ± 0.23 ‰ (s.d. 1σ, n = 10) for $\delta^{15}N$.

4.2.7 Radiocarbon measurements

We performed ^{14}C analysis using an accelerator mass spectrometer (AMS) for dissolved inorganic carbon (DIC) in the brine-rich water using a method that was previously reported (Yokoyama et al., 2010; Satoh et al., 2019). The brine-rich water was collected in a glass bottle (250 mL, Shibata Scientific Technology LTD., Japan). The bottle's lid was replaced with one having a vacuum line attachment in an ultra-pure-grade-argon tent and then connected to a DIC extraction line. CO_2 gas was extracted by acidification with 85 % phosphoric acid and bubbling with ultra-high-purity helium gas. The extracted CO_2 gas was cryogenically purified, quantified by a manometer at the cold finger portion of the vacuum line, and a suitable amount of purified CO_2 gas was transferred to the graphitization part of the vacuum line. The rest of the graphitization process was the same as for regular CO_2 glass-

ampoule samples.

Gas samples were collected in an aluminum multilayer gas sampling bag (10 L, GL Sciences, Japan). CH_4 was converted to CO_2 as described previously (Kawagucci et al., 2020). The gas sampling bag was connected to the vacuum line of the preparation system, and the gas sample containing an amount of CH_4 gas equivalent to 1 mg carbon was introduced into the vacuum line and captured with a cryogenic trap filled with silica gel beads. The trapped gas sample was forced to the flow-through portion of the preparation system by ultra-high-purity helium gas. The flow-through line has a number of CO_2, H_2O, CO, and condensable-gas traps to eliminate undesirable gases. CH_4 gas was captured in a trap containing HayeSep D (GL Sciences, Japan) at −130 °C, and non-condensable gases such as helium, hydrogen, nitrogen, oxygen, and argon were vented. Purified CH_4 gas was carried by the helium flow to an oxidation reactor (a quartz-tube reactor filled with platinum, palladium, nickel oxide, and copper oxide wires) and converted to CO_2 at 1000 °C. A magnesium perchlorate trap removed the water generated by the CH_4 conversion, and the CO_2 gas was further purified by cryogenic coolant and liquid nitrogen followed by flame sealing in a 9-mm-diameter borosilicate glass ampoule. The ampoules containing converted CO_2 were graphitized at the Atmosphere and Ocean Research Institute (AORI) at the University of Tokyo.

Radiocarbon was quantified by AMS using methods described previously (Yokoyama et al., 2010, 2019; Yamane et al., 2019). Here, we cross-checked the ^{14}C-depleted reference gas (GL Sciences, Japan) originating from petroleum by the parallel handling procedure. The isotopic composition of

radiocarbon is presented in delta notation ($\Delta^{14}C$, ‰) using the following equation:

$$\Delta\,^{14}C\ (‰) = \delta^{14}C - 2(\delta^{13}C + 25)(1 + \delta^{14}C/1000)$$

4.2.8 Cation and anion analysis

Cation and anion concentrations were measured by an ion chromatography (IC; Metrohm 930 Compact IC Flex, Metrohm AG, Swiss) coupled to an HPLC (1260 Infinity II, Agilent Technologies, USA). The samples were eluted for cations through a Metrohm Metrosep C6-250/4.0 column with 8 mM ultrapure HNO_3 at a flow rate of 0.9 mL min^{-1}. Anions were measured with a Metrohm Metrosep A Supp4-250/4.0 column with a chemical suppressor module with the mobile phase consisting of a mixture of 1.8 mM Na_2CO_3 and 1.7 mM $NaHCO_3$ at a flow rate of 0.9 mL min^{-1}. The chemical suppressor module (Metrohm MSM) was used to decrease the background conductivity of the eluent and to transform analytes into free anions. The column temperature was set at 35 °C throughout the analysis. Cations and anions, except for iodide, were detected with an electrical conductivity detector and an authentic standard. The waste line of the IC was connected to the HPLC with a DAD for the determination of iodide in the presence of high concentrations of chloride (Ito, 1997). Absorbance was measured at 226 nm. The delay time between the IC and the HPLC was initially calibrated using the flow delay sensor.

4.3 Results and Discussion

4.3.1 Bacteria/Archaea ratio and microbial community analysis by parallel molecular methods

In the brine-rich water and bubbled-scum samples, we detected the fatty acids, which originate from bacteria, and the ether lipids, which originate from archaea (Figure 16). Bacterial fatty acids are mainly C_{16} and C_{18}, within the typical range of C_{13}–C_{18} (e.g., Killops and Killops, 2005). Because most fatty acids in the deep sub-surface are considered to originate from bacteria, fatty-acid analysis can provide an overview of bacterial biomass (e.g., Baird et al., 1985). Archaeal membrane lipids are mainly diether and tetraether lipids: archaeol is a diether lipid with two C_{20}-isoprenoids (phytanes), whereas glycerol dialkyl glycerol tetraether (GDGT) is a lipid with two C_{40}-isoprenoids (biphytanes). Although potential contributions from photosynthetic microorganisms (including the remains of ancient cells) should be considered, the SSU rRNA gene data for the living prokaryotic biomass in the deep sub-surface are not consistent with a significant amount of phytol derived from chlorophyll side chains; hence, the ether lipids are likely to have been mostly derived from archaeal membrane lipids. Based on these observations, we concluded that the detected phytane and biphytane were derived from archaeal cells, and C_{16} and C_{18} fatty acids were derived from bacterial cells in a deep habitat below 274 m below the surface.

We estimated the proportions of Bacteria and Archaea in the brine-rich water and bubbled scum (Figure 17). From the results of lipid-based biomarkers, less than 10 % of lipids in the brine-rich water and bubbled scum were archaeal lipids (3.6–8.6 %) (Figure 17i), implying the dominance of bacteria

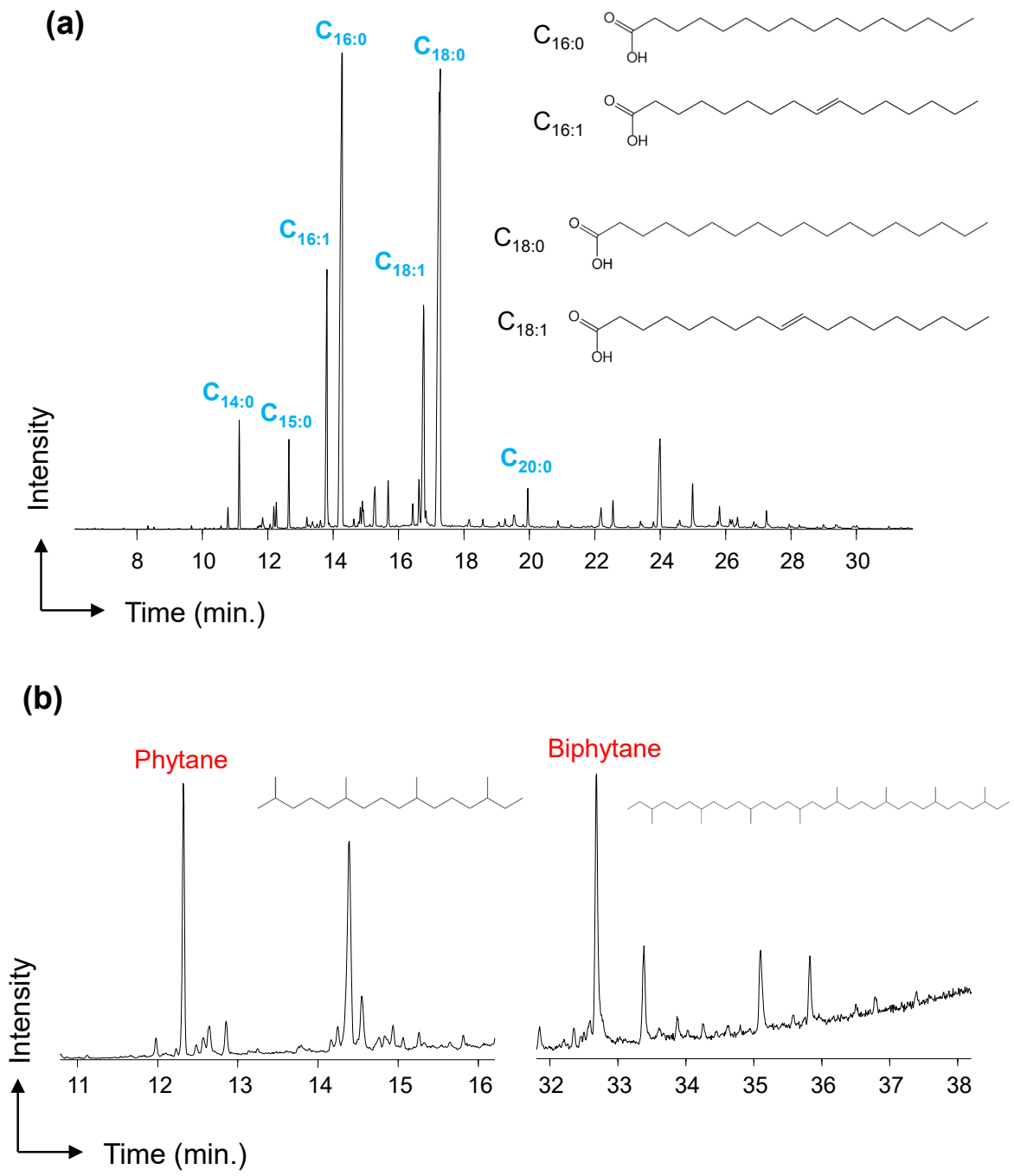

Figure 16. Chromatograms of brine-rich water samples analyzed by GC/MS. (a) Fatty-acid fraction showing bacterial lipid composition; (b) neutral ether lipid fraction showing archaeal lipid composition. Bacterial fatty acids were identified using the fatty acid methyl ester standard; archaeal phytane and biphytane were identified using the standard from *Methanobacterium* sp. Culture (Takano et al., 2009).

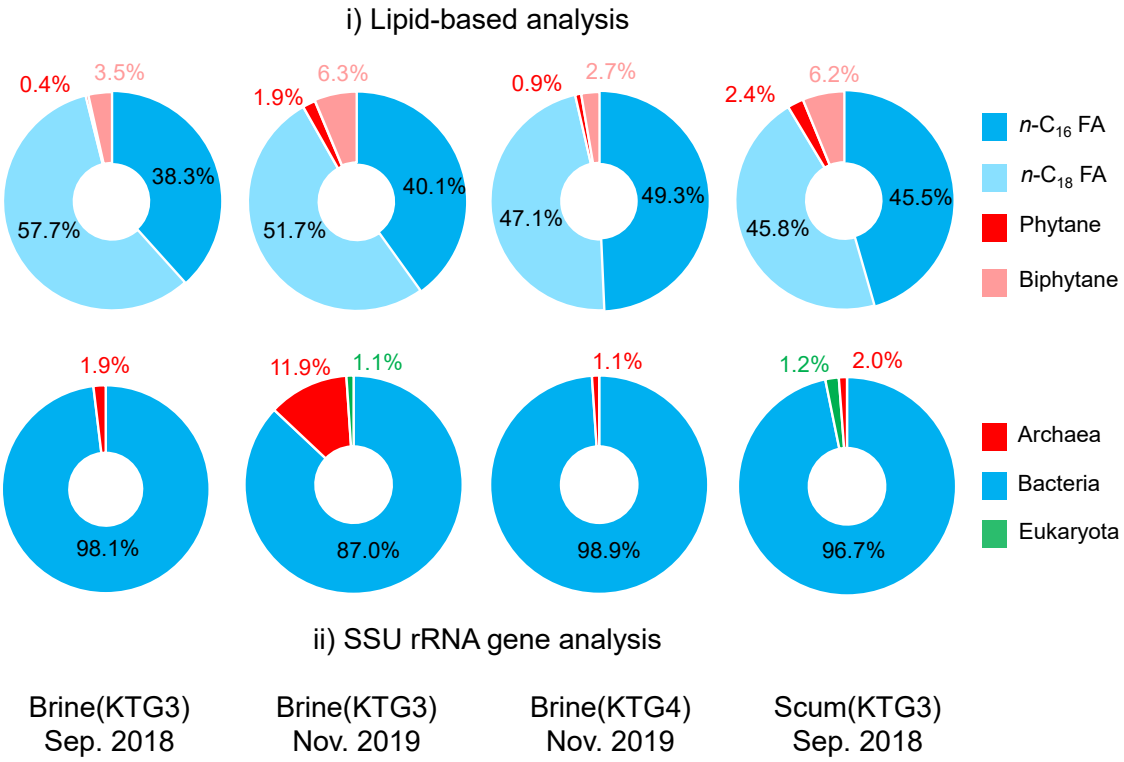

Figure 17. Proportions of prokaryotic archaea (red) and bacteria (blue) in brine-rich water and bubbled scum, cross-validated by (i) lipid-based analysis and (ii) SSU rRNA gene analysis. Membrane lipids of microorganisms are known to be the most representative biomarkers for characterizing prokaryotes. We calculated the proportions assuming that C_{16} and C_{18} fatty acids originated from bacterial cells and phytane and biphytane originated from archaeal cells.

in the deep aquifer. The SSU rRNA gene sequence analysis of the same samples supported the estimation of the proportions of Bacteria and Archaea from the lipid-based analysis (Figure 17ii). In addition, methanogenic archaea-related sequences (e.g., *Methanosarcinales, Methanobacteriales*, and *Methanomicrobiales* of the phylum *Euryarchaeota*) were detected, with relative abundances of 0.04 to 0.25 % of the total population (Figure 18). Several genera of methanogenic archaea (e.g., *Methanocalculus, Methanobacterium, Methanosarcina*, and *Methanothrix*) had been ubiquitously detected in 24 commercial production wells at the Southern Kanto gas field, with different diversities in each well (Katayama et al., 2015). Within them, the dominant methanogenic archaea were *Methanocalculus* and *Methanobacterium* in almost all wells, and the relative abundances of them were 2.4 to 99.6 % in the archaeal population (Katayama et al., 2015). In our study, the relative abundances of methanogenic archaea in KTG3 and KTG4 were 0.34 to 24.35% of the archaeal population, slightly lower than the values reported previously (Katayama et al., 2015). Variations in the chemical composition and temperature of brine-rich water between wells might have influenced these differences, and differences in the chosen PCR primers likely resulted in the detection of different microbial community compositions. We found that the community profiles in brine-rich water from KTG3 differed between September 2018 and November 2019 (Figure 18), suggesting a continuously changing community in the brine-rich water even within a single well. This result also indicates that brine-rich water is welling up from different regions.

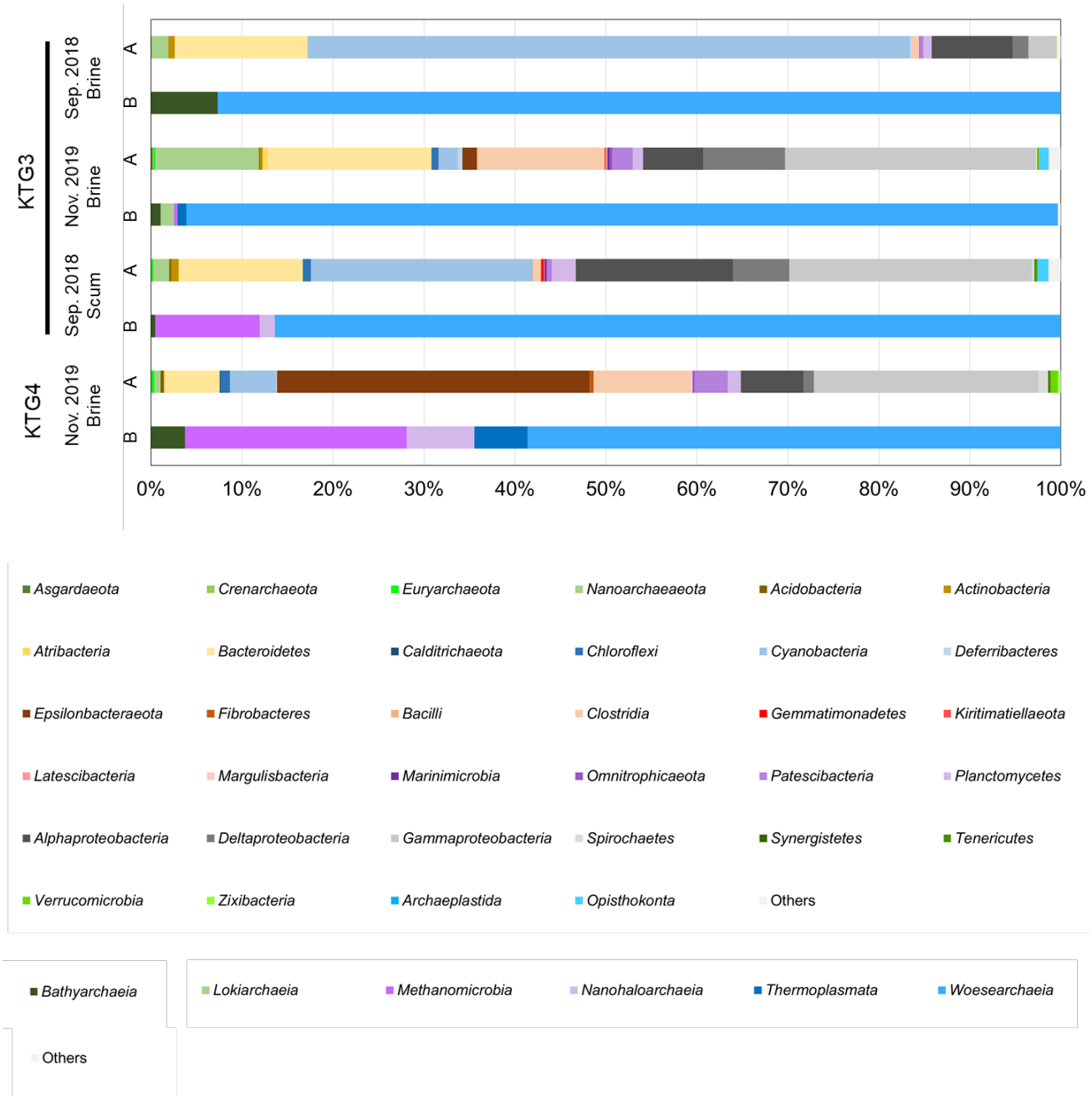

Figure 18. Taxonomic distributions of the rRNA community profiles in brine and scum samples. A: Total population. B: Archaeal population.

In addition to methanogenic archaea, many *Woesearchaeota*-related sequences were detected and accounted for 0.62 to 11.40 % of the total population (Figure 18). *Woesearchaeota*-related sequences have been detected in other environments worldwide, such as groundwater, freshwater lakes, and marine sediments (Ortiz-Alvarez and Casamayor, 2016; Liu et al., 2018; Román et al., 2019). A potential syntrophic relationship between *Woesearchaeota* and methanogenic archaea has been proposed, supported by metabolic modeling (Liu et al., 2018). The detection of abundant *Woesearchaeota* in the methane-rich deep aquifer may be due to its coexistence with methanogenic archaea; however, its lipid composition, physiology, and metabolic and ecological functions remain unclear due to the lack of an isolation culture.

There have been pioneering investigations into iodine–microbe interactions in natural environments (Sheppard and Hawkins, 1995; Yoshida et al., 1999; Amachi et al., 2008) and into iodine-accumulating and iodide-oxidizing bacteria (Amachi et al., 2005; Ito et al., 2016a; Khaing et al., 2019). It is interesting to note that iodine often acts as a sterilizing agent for microbial deactivation and also shows a high affinity for buried organic carbon in marine sediment (Malcolm and Price, 1984). Our understanding of microbial interactions in this context is currently limited (e.g., Ortiz-Alvarez and Casamayor, 2016; Román et al., 2019); however, the methanogenic microbial community is one that is tolerant of and active in the iodine-rich deep aquifer in the forearc basin, Boso Peninsula.

4.3.2 F430 profiles and ongoing methanogenesis by deep methanogenic archaea

The quantitative analysis of F430 is the most powerful method to determine whether the methanogenic archaea detected in this study are actively producing methane in the deep aquifer (e.g., Diekert et al., 1981; Mayr et al.,2008). Our HPLC–DAD analysis detected high concentrations of native F430 in the brine-rich water from well KTG3 (Figure 19), whereas F430 epimer, a diagenetic form of native F430, was detected in only trace amounts (Kaneko et al., 2016). The F430 concentration of 1.67×10^4 femto mol L^{-1} was substantially higher than the concentrations observed in previous studies (Ita-wari, a hot-spring water in Shizuoka Pref., Table 4). F430 degrades quickly when released into extracellular space because it is unstable and rapidly epimerizes to the thermodynamically more stable forms 13-epi-F430M and 12,13-diepi-F430M. This process occurs at a daily scale even at room temperature (e.g., Diekert et al., 1981; Mayr et al.,2008); therefore, the native F430 concentrations reflect the abundance of living methanogenic archaea and ongoing methanogenic reactions. The F430 determination clearly indicates that methanogenic archaea are highly active in the iodine-rich deep subsurface aquifer, consistent with the methanogenic archaea detected by SSU rRNA gene sequences having originated from living, rather than dead, cells. For comparison, the methane-rich (93.9 %) Ita-wari hot-spring water in an accretionary prism setting (~200 km west of the Southern Kanto gas field) had an F430 concentration of 8.11×10^2 femto mol L^{-1} (Kaneko et al., 2014; Matsushita et al., 2016), suggesting that subsurface methanogenesis in the Southern Kanto gas field is potentially two orders of magnitude greater than at the Ita-wari site. As these are the first data on F430 concentrations in a

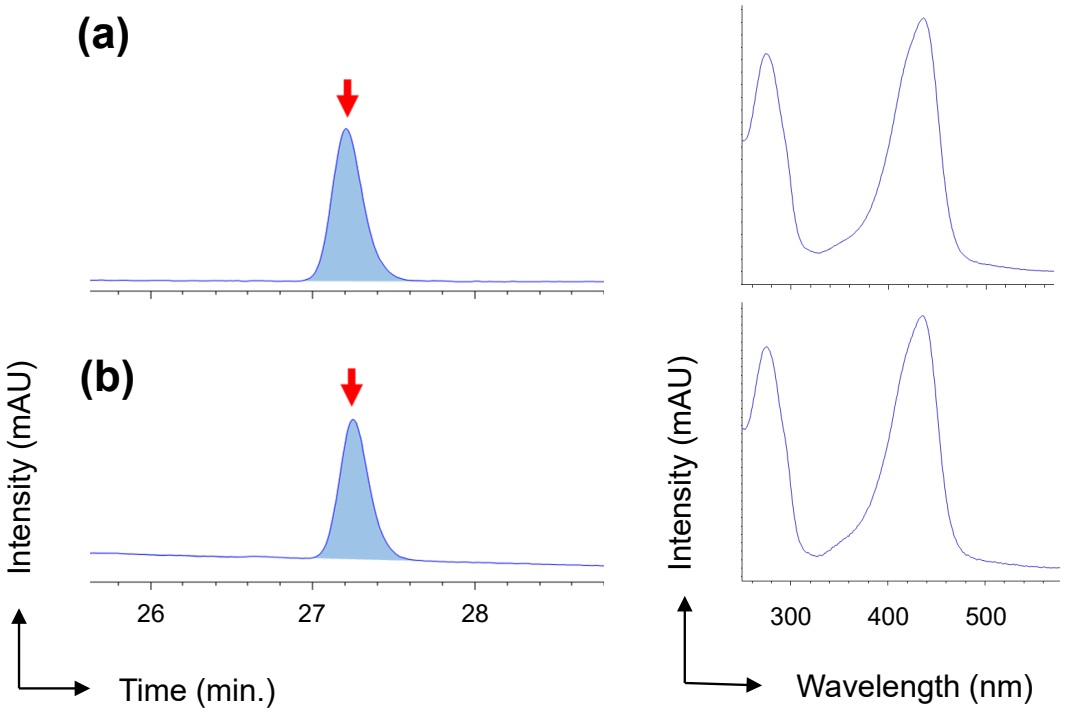

Figure 19. Chromatograms (430 nm) and photoabsorption spectra of the F430M fraction. (a) F430M working standard derived as described previously (Takano et al., 2013; Kaneko et al., 2014). (b) Brine-rich water from KTG3 (September 2018).

Table 4. Concentrations of F430 in environmental samples.

Sample name	Depth	Type	Concentration		Reference
KTG3	274-715 m	Deep aquifer	1.67×10^{4}	femto mol/L	This study
Ita-wari	1,489 m	Deep aquifer	8.11×10^{2}	femto mol/L	Kaneko et al.(2014)
Kawatabi	0 m	Paddy soil	8.70×10^{2}	femto mol/g-wet	Kaneko et al.(2014)
Chikugo RSC	0 m	Paddy soil	1.06×10^{3}	femto mol/g-wet	Kaneko et al.(2014)
Shimokita 8-4	1,249 m (69 mbsf*)	Marine sediments	5.29×10^{2}	femto mol/g-wet	Kaneko et al.(2016)
Nankai 7H7	2,687 m (60 mbsf*)	Marine sediments	3.14×10^{1}	femto mol/g-wet	Kaneko et al.(2016)

*mbsf: meter below the seafloor

natural gas field, reporting of F430 concentrations in other natural gas fields will make it possible to compare ongoing biological methanogenesis potentials using F430 concentrations.

Previous studies made the plausible assumption that F430 concentrations can be converted to methanogen cell numbers (Takano et al., 2013; Kaneko et al., 2014, 2016). The mean weight of F430 per prokaryotic cell was determined by the cultivation of a model methanogenic archaeon, which yielded the following equation:

$$n\ (\text{cells g}^{-1}) = C_{\text{F430 in sample}} / (C_{\text{F430 in culture}} \times m\text{cell})$$

where $C_{\text{F430 in sample}}$ and $C_{\text{F430 in culture}}$ denote the concentrations of F430 in the sample and the culture, respectively, and *m*cell denotes the mean weight of a cell (Takano et al., 2013; Kaneko et al.,2014). Using this equation, the density of methanogenic archaea in the brine-rich water was estimated to be 4.7×10^8 cells L^{-1}; however, this value is greater than the total cell density in the brine-rich water (7.0×10^7 cells L^{-1}). This contradiction has also been observed in other studies (e.g., Kaneko et al., 2016). The main reason is considered to be that the parameters of the equation have large errors (e.g., $C_{\text{F430 in culture}}$ is 580 ± 240 nmol g dry cell^{-1}, which is an average value for six methanogenic archaea, Diekert et al., 1981) and/or there are undiscovered methanogenic archaea that are too small to see under a microscope.

4.3.3 Origin of methane in the deep aquifer inferred from ^{13}C- and ^{14}C-depleted profiles

The carbon stable isotope ratios and radiocarbon content of methane and DIC from the Southern Kanto gas field are provided in Table 5. Figure 20 shows the isotopic data as a cross plot between $\delta^{13}C$ and $\Delta^{14}C$ for methane, DIC, and atmospheric CO_2, as well as data from previous studies for reference (Quay et al., 1999; Kessler et al., 2005; Slater et al., 2006; Proskurowski et al., 2008; Machida et al., 2013; Simkus et al., 2016; Schwab et al., 2019, Figure 16). Methane in natural gas (i.e., a closed system) was depleted in both ^{13}C and ^{14}C (Figure 20, bottom left), and its values were different from those of wetlands and rice paddies that fix modern CO_2 from the current atmosphere (i.e., open systems, upper left). It is apparent that the cross plot can potentially provide clear criteria for assessing the origin of methane, DIC, and other organic matter. For instance, methane collected from the Lost City hydrothermal field on the Mid-Atlantic Ridge, a geological source of ultramafic materials, plotted in a different area than methane obtained from natural gas (Quay et al., 1999; Proskurowski et al., 2008), suggesting that different methanogenesis processes produced those methane samples.

As for stable isotopic signature, the $\delta^{13}C_{methane}$ values at KTG3 and KTG4 were −67.9 ± 0.8 ‰ and −71.4 ± 0.7 ‰, respectively. These values are in a range typical of biogenic methane (<−60 ‰, Bernard et al., 1977; Whiticar, 1999) and consistent with those determined in previous studies (Igari and Sakata, 1989; Kaneko et al., 2002; Sano et al., 2017). In contrast, the $\delta^{13}C_{DIC}$ values at KTG3 and KTG4 were +8.2 ± 0.8 ‰ and +3.6 ± 1.1 ‰, respectively. Since isotope fractionation associated with methane production using CO_2 is reportedly up to 80 ‰ (e.g., Whiticar et al., 1986; Londry et al.,

2008),

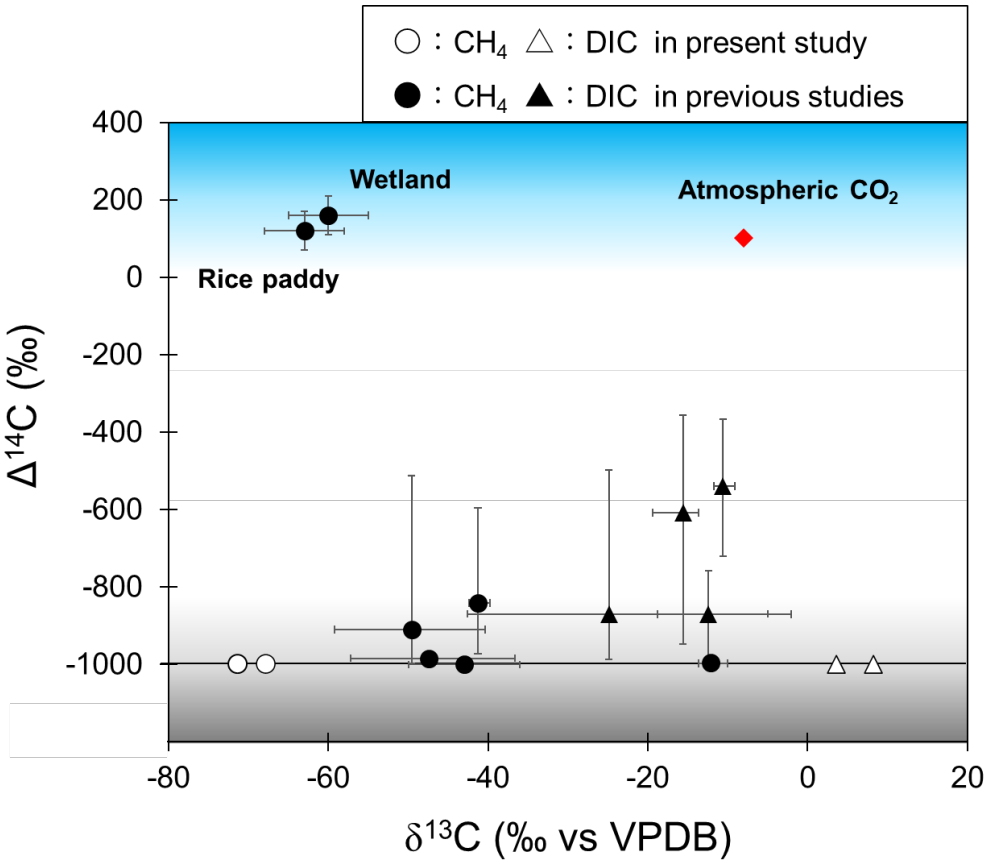

Figure 20. Cross plots of $\delta^{13}C$ and $\Delta^{14}C$ of methane (circles), DIC (triangles), and atmospheric CO_2 (diamond). Open symbols are results from the present study; solid symbols are from previous studies (Quay et al., 1999; Kessler et al., 2005; Slater et al., 2006; Proskurowski et al., 2008; Machida et al., 2013; Simkus et al., 2016; Schwab et al., 2019). The blue shaded area indicates an origin from modern carbon, and the gray area indicates an origin from deep subsurface carbon, which has been isolated from the atmosphere.

Table 5. Carbon isotopic compositions of methane and DIC. The standard methane gas originated from petroleum (GL Sciences, Japan) and can be used to test for contamination during the pretreatment process. These results are expressed as $\delta^{13}C$, $\Delta^{14}C$, and percent modern carbon (pMC, reflecting the concentration of ^{14}C in the sample).

Sample name	Type	$\delta^{13}C$ (‰ vs. VPDB)	$\Delta^{14}C$ (‰)	pMC (%)
KTG3	Methane	−67.9 ± 0.8	< −997.51	< 0.27
	DIC	+8.2 ± 0.8	−999.0 ± 0.3	0.10 ± 0.01
KTG4	Methane	−71.4 ± 0.7	< −997.42	< 0.29
	DIC	+3.6 ± 1.1	-999.2 ± 0.4	0.32 ± 0.01
Ref. Gas	Methane	−41.8 ± 1.0	< −996.06	< 0.24

the differences between $\delta^{13}C_{methane}$ and $\delta^{13}C_{DIC}$ at KTG3 and KTG4 are within the expected range. In addition, our SSU rRNA gene analysis also supported that methanogenic archaea in the deep aquifer is mainly a type of CO_2 reduction (Figure 18). The values of $\delta^{13}C_{DIC}$ are heavier than those in water collected from wells on the western Boso Peninsula (Machida et al., 2013): the $\delta^{13}C_{DIC}$ values in a deep aquifer (270–500 m) ranged from −21.5 to −12.5 ‰. This contrast suggests that methanogenic archaea make heavier DIC because they produce lighter methane. The $\delta^{13}C_{scum}$ and $\delta^{15}N_{scum}$ values at KTG3 were −18.7 ‰ and +2.5 ‰, respectively, and the C/N ratio was 18.5 (w/w) (Table 6). Ammonia could serve as a nitrogen source for the microbial communities in scum because brine-rich water contains high concentrations of ammonia (Table 3). The $\delta^{13}C_{scum}$ was slightly heavier than that of ordinary marine sediments (−30 to −20‰, Maslin et al., 2006), also suggesting that methanogenic archaea make heavier membrane components because they produce lighter methane.

As for radioisotopic signature, both methane and DIC from KTG3 (274–715 m) and KTG4 (714–1398 m) were significantly depleted in ^{14}C ($\Delta^{14}C < -997.5$‰) (Tables 3 and 5). The F430 concentrations indicate a high abundance of living methanogenic archaea and ongoing methanogenic reactions, mainly hydrogenotrophic methanogenesis. As the substrate DIC is ^{14}C-depleted, the methane produced by ongoing methanogenesis is also ^{14}C-depleted, meaning that ^{14}C measurements cannot distinguish between the methane produced by ongoing methanogenesis and that preserved in the deep aquifer. Thus, it is currently difficult to perform a quantitative assessment of the extent to which ongoing methane production by methanogenic archaea contributes to the methane reservoir.

Table 6. Carbon and nitrogen stable isotopic compositions and C/N ratio of bubbled scum from KTG3. Values were determined from duplicate analyses for each sample.

Sample name	Type	$\delta^{13}C$ (‰ vs. VPDB)	$\delta^{15}N$ (‰ vs. AIR)	C (wt%)	N (wt%)	C/N (w/w)
KTG3	Scum	-18.7	2.5	1.3	0.07	18.5
	Scum (with HCl)	-23.2	13.9	0.67	0.34	2.0

The reservoir rocks of the gas field are alternating beds of sandstone and mudstone, with potential water-permeable layers. In fact, there are several places around the study sites where natural gas spontaneously springs up with brine-rich water. It is therefore possible that modern carbon is supplied to the deep aquifer along tectonic faults and the forearc basin (Figure 14a). In addition, chloride and sodium ions in brine-rich water at KTG3 (Na^+ = 7563 mg L^{-1}, Cl^- = 19,171 mg L^{-1}) are present in lower concentrations than in modern seawater, suggesting a contribution of rainwater to the deep aquifer (Table 3). This is in line with the finding from a previous study, which demonstrated that the $\Delta^{14}C_{DIC}$ in the deep aquifer on the western Boso Peninsula ranged widely from −948 to −355‰ (Machida et al., 2013). These results suggest that modern carbon is supplied up to about 500 meters below the surface on the western Boso Peninsula. However, $\Delta^{14}C_{methane}$ and $\Delta^{14}C_{DIC}$ values at Mobara (Eastern Boso Peninsula) clearly indicate that there has been little contribution of modern carbon to the deep subsurface (Figure 20, Table 5). These results suggest that the deep aquifer has been contaminated with a small amount of rainwater that has not affected the carbon pool. Alternatively, the deep aquifer was contaminated by stormwater prior to 50,000 years ago, but may now be a closed environment. In future work, further confirmation of the deep carbon cycle and a comprehensive description of the subterranean microbial ecosystem in the complex geological setting at Mobara (Snelgrove et al., 2018) will require verification of the $\Delta^{14}C$ values of methane, DIC, and DOM in the deep aquifer at other wells, where modern carbon may flow into the deep aquifer from shallower and/or nearer-shore settings.

Chapter 5: Methanogenesis and methane cycle: Simultaneous occurrence of cyanobacterial bloom and methanogenic archaea in a freshwater lake

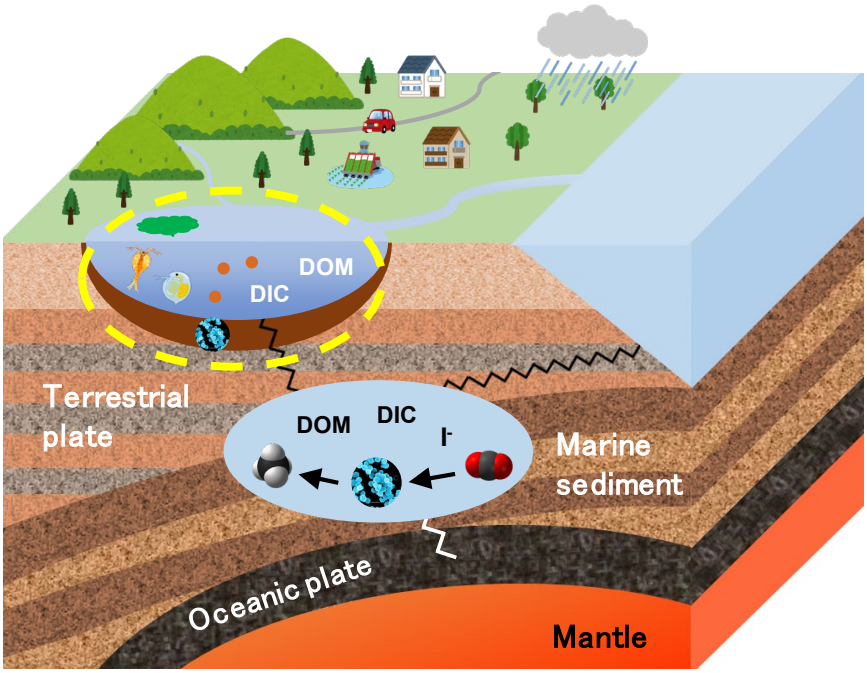

5.1 Aim of this study

Freshwater lakes in terrestrial environments are thought to be one of the main natural sources of methane (CH_4) and are estimated to account for 6 to 16% of all-natural sources (e.g., Bastviken et al., 2004; Sherwood et al., 2006; Cole et al., 2007; Holgerson and Raymond, 2016; Günthel et al., 2019). It is generally believed that the major CH_4 fraction released from freshwater lakes is produced in anoxic sediments by methanogenic archaea in the terminal step of organic matter decomposition (e.g., Borrel et al., 2011; Bukin et al., 2018). Through this process, heterotrophic microbes degrade organic matter to H_2, CO_2, acetate, and methylated compounds, which are then used as the principal substrates for hydrogenotrophic, aceticlastic, or methylotrophic methanogenic pathways by methanogenic archaea. The CH_4 produced in anoxic sediments then diffuses into the atmosphere or is oxidized by anaerobic or aerobic microbial processes in the lacustrine water column (e.g., Bastviken et al., 2002; Thauer et al., 2008; Conrad, 2009; Kojima et al., 2014; Deutzmann et al., 2014; Donis et al., 2017; Iwata et al., 2018).

In recent decades, biogeochemical evidence for CH_4 accumulation in oxygen-saturated freshwater and marine environments, commonly known as the 'methane paradox,' has emerged (e.g., Repeta et al., 2016; Encinas Fernández et al., 2016; Tang et al., 2016; Günthel et al., 2019). The following three main hypotheses have been proposed to explain this enigmatic phenomenon: (i) methanogenesis by methanogenic archaea in anoxic microenvironments, such as detritus or animal guts (Oremland, 1979; Burke et al., 1983; De Angelis and Lee, 1994; Schmale et al., 2018); (ii) CH_4 release as a by-product

of the bacterial decomposition of potential precursors (e.g., methylphosphonate and dimethylsulfoniopropionate) under aerobic conditions (Damm et al., 2010; Wang et al., 2017; Khatun et al., 2019); and (iii) methanogenesis by methanogenic archaea associated with photoautotrophic consortia in lacustrine environments (Grossart et al., 2011; McGinnis et al., 2015).

Cyanobacteria grow rapidly and form blooms under certain environmental conditions, including high nutrient levels, warm temperatures, and sun exposure (e.g., Park et al., 1998; Yan et al., 2017), and it is suggested that these cyanobacterial blooms stimulate CH_4 production in sediments by increasing the supply of organic matter (e.g., Wang et al., 2006; Yan et al., 2017). If microbial CH_4 production associated with methanogenic archaea and cyanobacteria occurs in natural environments, it is hypothesized that cyanobacterial blooms may promote microbial CH_4 production as a nutrient. Recently, Bižić et al. (2020) demonstrated CH_4 production in pure cyanobacteria cultures in marine, freshwater, and terrestrial environments. Although it has been suggested that some versatile methanogenic archaea thrive in anoxic microenvironments within cyanobacterial consortia (Batista et al., 2019), the entire CH_4 production process in natural environments remains unclear.

Previously, Grossart et al. (2011) reported the coexistence of methanogenic archaea and cyanobacteria in the surface water of an oligotrophic lake based on molecular analyses targeting small subunit (SSU) rRNA gene and the methyl coenzyme M reductase A gene (*mcrA*), which encodes the alpha subunit of methyl coenzyme M reductase (MCR) (e.g., McGinnis et al., 2015). As SSU rRNA and *mcrA* gene analysis can effectively identify species, these methods are commonly used to screen

for methanogenic archaea in the environment. However, they cannot accurately evaluate microbial biomass and activity because they detect genes that are present in biological remains, and are less accurate in environments with extremely low microbial biomass (e.g., deep marine sediments, Inagaki et al., 2015).

Quantification of coenzyme factor 430 (F430; Figure 13), a key molecule with a specific and common function in methanogenic archaea, clearly indicates in situ abundance and ongoing microbial activity of methanogenic archaea (e.g., Takano et al., 2013; Kaneko et al., 2014; Inagaki et al., 2015) as it rapidly decomposes to its relic forms. Using the highly sensitive analytical method developed by Kaneko et al. (2014, 2016), we quantified F430 in cyanobacterial bloom and surface sediment samples, thereby providing direct evidence of planktonic methanogenic activity in the surface water of Lake Suwa, a shallow eutrophic lake in Japan, during a cyanobacterial bloom. To our knowledge, this is the first study to report F430 concentrations in a freshwater lake environment. We confirmed active CH_4 emission from the surface sediments of Lake Suwa. This CH_4 is thought to be produced by methanogenic archaea in the benthic sediment; however, the biomass and activity of these species in benthic sediments have not been quantified. Molecular SSU rRNA and *mcrA* gene analyses were also performed to elucidate the microbial community structure in the planktonic cyanobacterial bloom with a reference benthic habitat sample. Thus, we present evidence that planktonic methanogenic archaea exist in a seasonal cyanobacterial bloom in the freshwater environment at Lake Suwa.

5.2 Materials and Methods

5.2.1 Geological setting and sampling procedure

Lake Suwa is located in Nagano Prefecture in the central part of Honshu Island, Japan, on the Itoigawa-Shizuoka tectonic line (Figure 21). The lake has a surface area of 13.3 km^2 and mean and maximum depths of 4.3 m and 6.4 m, respectively, with a particularly high estimated sedimentation rate near the estuary (~1 cm $year^{-1}$) and a bottom with organic-rich sediment (Nakazato et al., 1998; Suwa Construction Office, 2019). Lake Suwa is a typical Japanese eutrophic lake that is considerably affected by anthropogenic impacts from nearby cities, despite being surrounded by mountains (Park et al., 1993; 1998). Cyanobacterial blooms, particularly those caused by *Microcystis* spp., have occurred regularly during the summer since the 1970s (Park et al., 1993, 1998; Watanabe et al., 2012).

Samples were collected from the southeast shore of the lake (36°2'46.92"N, 138°6'30.94"E; Figure 22a) at a water depth of 1.8 m on September 28, 2018, and June 29, 2019. Water samples were collected in serum vials to measure the dissolved CH_4 concentration, whereas the cyanobacterial bloom floating on the surface (Figure 22b) was collected using a plankton net (10 μm mesh) and placed in polypropylene bottles (Figure 22c). Sediment surface samples were collected from a 0–10 cm depth in September 2018 and a 0–3 cm depth in June 2019 using a gravity core sampler (50 cm in length, 4 cm in diameter, Figure 22d). Cyanobacterial bloom and sediment samples were preserved in an icebox and transported to the laboratory, where they were frozen and stored at −30 °C. Cyanobacterial bloom samples were observed microscopically (PX-51; Olympus, Japan). Water temperature

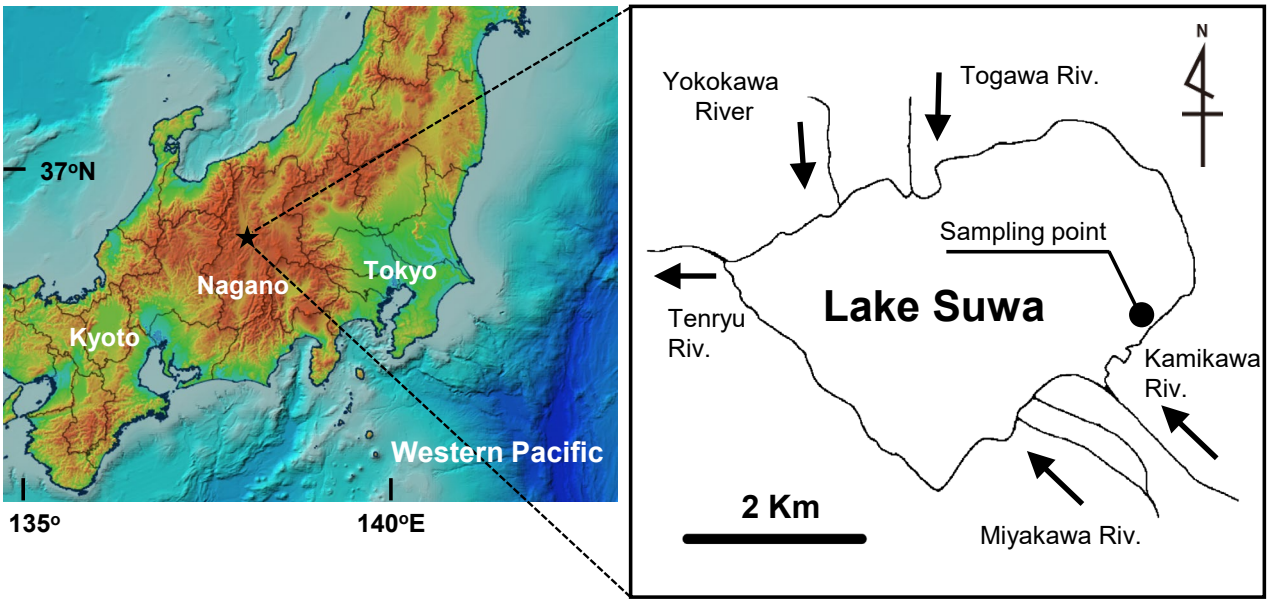

Figure 21. Map of the study site location. Lake Suwa lies in the central part of Honshu Island, Japan (36°2'46.92"N, 138°6'30.94"E); the surrounding cities contribute large anthropogenic inputs. Water flows into the lake from 31 rivers, with a single outlet (Tenryu River). Samples were collected from the southeastern shore of Lake Suwa.

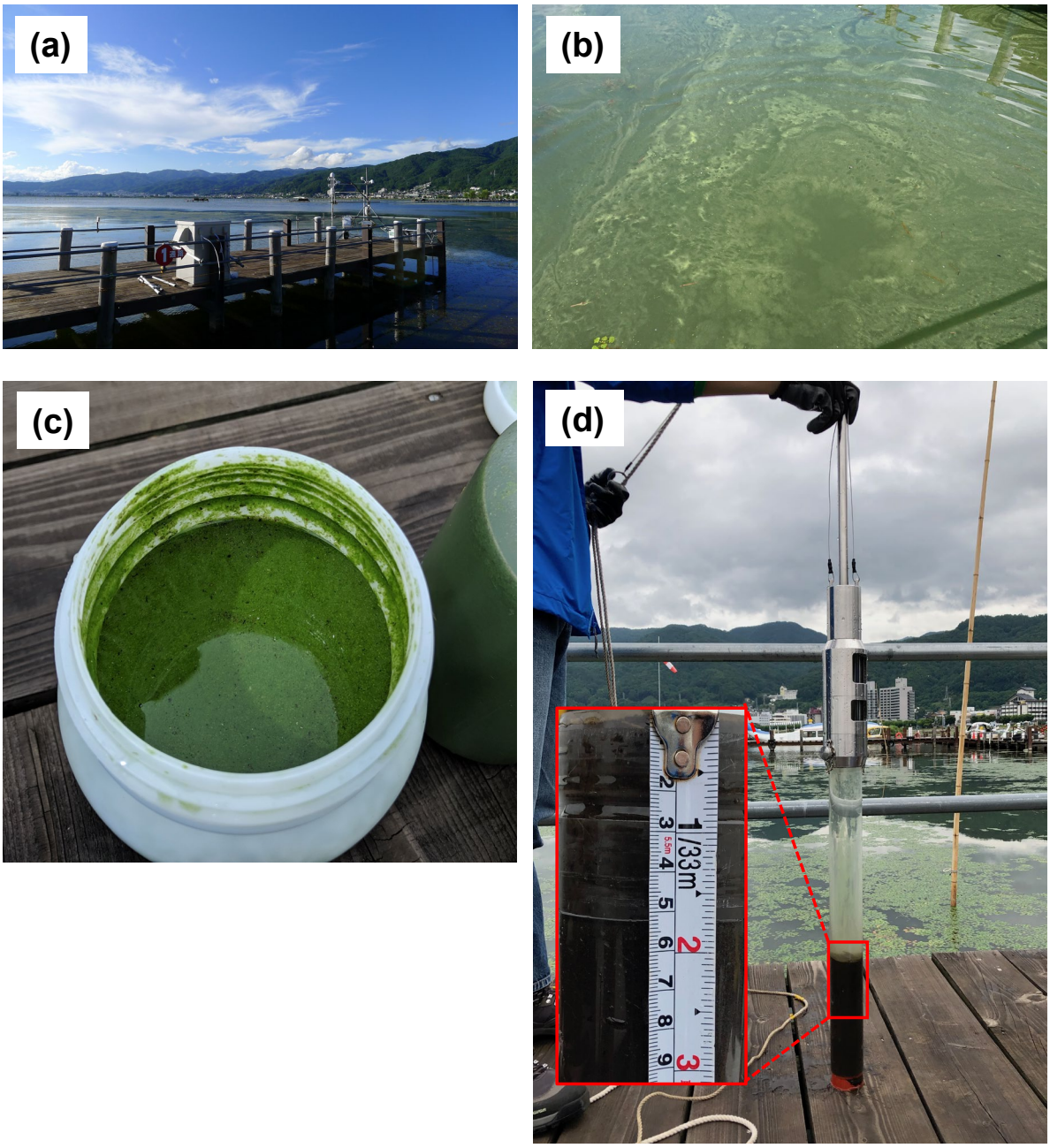

Figure 22. (a) Photographs of the sampling site. The pier extends ~40 m from the lakeshore and has a depth of ~1.8 m. (b) Floating cyanobacterial bloom around the pier in June 2019. (c) Cyanobacterial bloom sample collection. (d) Sediment core collection using a gravity core sampler in June 2019.

and dissolved oxygen (DO) concentration were measured on-site at each depth using a DO meter (HQ-30D; Hach, Loveland, USA).

5.2.2 Measurement of dissolved CH_4

The concentration of CH_4 dissolved in the lake water samples was analyzed on June 27 and September 28, 2018, and on June 28, August 29, and October 10, 2019, as per methods described previously (Itoh et al., 2015). Lake water was collected in 30 mL vials from several locations of different depths (0, 10, 50, 100, 130, 150, and 160 cm) using syringes and tubes attached to a pier. CH_4 was quantified using a gas chromatograph with a flame-ionization detector (GC-14B; Shimadzu, Japan) and a packed column (Porapack-Q, 80/100 mesh, 1.5 m × 3.0 mm i.d.; GL Sciences, Japan). The concentration of dissolved CH_4 was calculated using the ideal gas law and the Bunsen solubility coefficient (Magen et al., 2014).

5.2.3 F430 extraction

F430 analysis was performed according to a previously described method (Takano et al., 2013; Kaneko et al., 2014). Briefly, F430 was extracted from freeze-dried cyanobacterial bloom and wet sediment samples collected in September 2018 and June 2019 using 1% formic acid followed by ultrasonication for 30 min on ice and centrifugation (10,000 × g; 30 min; 4°C). The supernatant was then recovered, and this step was repeated three times. The combined supernatants were introduced

into an anion-exchange column (Q Sepharose; GE Healthcare, USA) that had been equilibrated with 50 mM Tris-HCl (pH 7.5) and washed with deionized water before use. The recovered eluent was introduced into a C18 SPE column (Sep-Pack; Waters, USA) that had been equilibrated with methanol and conditioned with 1% formic acid. F430 was eluted with methanol and converted into F430 methyl ester (F430M) by derivatization with BF_3–methanol (40°C, 3.5 h) before being extracted with dichloromethane. To remove the organic matrix, the F430M fraction extracted from the samples collected in September 2018 was purified by silica gel chromatography (Kaneko et al., 2016). This pretreatment eliminates any potential analytical artifacts that may affect ultra-small-scale analyses (~femto mol; Kaneko et al., 2014; Isaji et al., 2020) of tetrapyrrole compounds with chromatographic separation that induce ion suppression and enhancement effects (Mallet et al., 2004; Taylor, 2005) in liquid chromatography/electrospray ionization–mass spectrometry (LC/ESI–MS).

5.2.4 F430 qualification and quantification using LC/ESI–MS

The concentration of extracted F430M was determined using high-performance liquid chromatography/electrospray ionization mass spectrometry (HPLC/ESI–MS/MS; 1260 Infinity II LC System coupled to a 6490 Triple Quadrupole LC-MS system with an Agilent jet stream; Agilent Technologies, USA) in the positive ion mode. Chromatographic separation was performed using the ZORBAX Eclipse XDB-C18 column (4.6 × 150 mm; 5 μm, Agilent Technologies). Multiple reaction monitoring analysis was performed with a fragment voltage of 380 V and a collision energy of 70 V.

The F430M product ion was set to m/z 844.3. The mobile phases comprised 10 mM ammonium acetate with 1% acetonitrile (A) and acetonitrile (B), with a flow rate of 16 μL min^{-1} and the following gradient: 0 % B, 30 % B after 3 min, and 90 % B after 90 min (Mayr et al., 2008). The F430M concentration was determined using an external F430M standard (Kaneko et al., 2014, 2016).

5.2.5 SSU rRNA gene tag sequencing

Total DNA was extracted from the cyanobacterial bloom and sediment samples collected in September 2018 using the Plant Genomic DNA Extraction Miniprep System (Viogene, Taiwan) and the DNeasy Power Soil Kit (Qiagen, USA), respectively. The concentration of the extracted DNA was measured using the Quant-iT™ dsDNA HS Assay Kit and the Qubit Fluorometer (Thermo Fisher Scientific, USA). The SSU rRNA genes in the extracted DNA were amplified by polymerase chain reaction (PCR) using TaKaRa LA Taq (TaKaRa Bio, Japan) according to the manufacturer's instructions. The 530F/907R primer set (V4–V5 regions) that covers most bacterial, archaeal, and eukaryotic SSU rRNA genes (Nunoura et al., 2012) was used. The PCR amplification conditions were as per those described previously (Hirai et al., 2017). The amplified SSU rRNA gene sequences were analyzed using MiSeq (Illumina, USA) as per methods described previously (Imachi et al., 2019). PCR primers were removed from the merged sequences using Cutadapt v1.10 (Martin, 2011). Low-quality (Q score < 30 in over 3% of the sequences) and short reads (< 150 bp) were filtered out using a customized Perl script. After chimeric sequences had been removed with Usearch61 (Edgar, 2010) in

QIIME (Caporaso et al., 2010), the operational taxonomic units (OTUs) with a 97% similarity level were selected using UCLUST (Edgar, 2010) and were assigned to a taxon (at the phylum, class, order, family, and genus levels) using the SILVA 132 database (Quast et al., 2013). The SSU rRNA gene tag sequence data reported in this manuscript have been deposited in BioProject PRJNA 9444 under the accession number DRA009781.

5.2.6 PCR amplification of archaeal 16S rRNA and *mcrA* genes

To confirm the presence of methanogenic archaea in the samples, the archaeal 16S rRNA and *mcrA* genes were amplified from the extracted DNA by PCR with TaKaRa LA Taq (TaKaRa Bio), according to the manufacturer's instructions. The archaeal 16S rRNA gene was amplified using the 340F/1000R primer set (Gantner et al., 2011, Table 7), while the *mcrA* genes were amplified using the Luton-*mcrA* F/R, MCR F/MCR R, ME 3F/ME 2R, and mlas/*mcrA*-rev primer sets (Springer et al., 1995; Luton et al., 2002; Steinberg and Regan, 2008; Sørensen et al., 2009, Table 7). The PCR conditions involved denaturation at 95°C for 9 min, followed by 45 cycles of denaturation at 94°C for 40 s, annealing at 50°C, 52°C, or 55°C for 30 s, and extension at 72°C for 40 s, followed by a final extension step at 72 °C for 7 min. The annealing temperature for each primer set is listed in Table 7. The size of the PCR products was analyzed by 1.5 % agarose gel electrophoresis stained with the RedSafe™ Nucleic Acid Stain Solution (FroggaBio, Canada).

Table 7. PCR primers for archaeal 16S rRNA and *mcrA* genes.

Target	Primer name	Direction	Sequences (5' → 3')	Hybridization Temperature (°C)	References
Archaeal 16S rRNA gene	340F	Forward	CCCTAYGGGGYGCASCAG	52	Gantner et al. (2011)
	1000R	Reverse	GGCCATGCACYWCYTCTC		
mcrA gene	Luton-mcrA F	Forward	GGTGGTGTMGGATTCACACARTAYGCWACAGC	50	Luton et al. (2002)
	Luton-mcrA R	Reverse	TTCATTGCRTAGTTWGGRTAGTT		
mcrA gene	MCR F	Forward	TAYGAYCARATHTGGYT	50	Springer et al. (1995)
	MCR R	Reverse	ACRITCATNGCRTARTT		
mcrA gene	ME 3F	Forward	ATGTCNGGTGGHGTMGGSTTYAC	55	Sørensen et al. (2009)
	ME 2R	Reverse	TCATBGCRTAGTTDGGRTAGT		
mcrA gene	mlas	Forward	GGTGGTGTMGGDTTCACMCARTA	55	Steinberg et al. (2008)
	mcrA-rev	Reverse	CGTTCATBGCGTAGTTVGGRTAGT		

5.2.7 Bulk stable carbon and nitrogen isotopic ratio analysis

Total organic carbon (TOC) and total nitrogen (TN) contents and their stable isotopic ratios ($^{13}C/^{12}C$ and $^{15}N/^{14}N$, respectively) were measured in the cyanobacterial bloom and sediment samples collected in September 2018. All samples were freeze-dried, crushed, and homogenized prior to analysis. Sediment samples were treated with 1 M HCl to remove carbonates, centrifuged (~ 2,000 × g) for 5 min, and the precipitate was washed well with deionized water. This procedure was repeated 3–5 times before the sample was dried and pulverized. Measurements were performed using an ultrasensitive elemental analyzer connected to an isotope ratio mass spectrometer (Flash EA1112 connected to the Thermo Finnigan Delta plus XP via ConFlo III; Thermo Finnigan, USA), as per methods described previously (Ogawa et al., 2010). Isotopic compositions were expressed using the conventional δ notation:

$$\delta = (R_{sample}/R_{standard} - 1) \times 1000 \ (‰)$$

where R represents the $^{13}C/^{12}C$ or $^{15}N/^{14}N$ ratio. The carbon and nitrogen isotope standards included Vienna Pee Dee Belemnite (VPDB) and atmospheric N_2 (AIR). Carbon and nitrogen contents and their isotopic compositions were calibrated against three reference materials, namely L-tyrosine (BG-T: C, 59.7 %; N, 7.74 %; $\delta^{13}C$, −20.83 ± 0.10 ‰; $\delta^{15}N$, +8.74 ± 0.09 ‰), DL-alanine (CERKU-01: C, 40.4 %; N, 15.7 %; $\delta^{13}C$, −25.36 ± 0.08 ‰; $\delta^{15}N$, −2.89 ± 0.04 ‰), and glycine (CERKU-03: C, 32.0 %; N: 18.7% ; $\delta^{13}C$, −34.92 ± 0.07 ‰; $\delta^{15}N$, +2.18 ± 0.04 ‰) (Tayasu et al., 2011). The analytical

errors for the isotopic compositions estimated by repeated analyses of BG-T (5.8−22.7 µg C; 0.75−2.9 µg N) were ± 0.07‰ (1σ; n = 9) for $\delta^{13}C$ and ± 0.18‰ (1σ; n = 9) for $\delta^{15}N$.

5.3 Results

5.3.1 Water column chemical profiles with carbon and nitrogen contents

First, we generated water column profiles from the measurements obtained in September 2018 (Figure 23). Both water temperature and DO decreased with depth and ranged from 20.8 to 17.2 °C and 10.97 to 6.76 mg L^{-1}, respectively. DO saturation ranged from 134 to 77%, suggesting that the water column was well oxygenated from the surface to the bottom. The maximum CH_4 concentration was observed between depths of 100 and 160 cm (3.5−3.6 µM) and decreased from 3.5 to 1.5 µM in water shallower than 100 cm. Similar trends were observed on the other days examined (Table 8).

We also analyzed the carbon and nitrogen contents and stable isotopic ratios of the samples collected in September 2018 (Table 9). In the cyanobacterial bloom samples, the TOC and TN contents were 41.1 ± 1.8 wt% and 7.7 ± 1.08 wt%, with $\delta^{13}C$ and $\delta^{15}N$ values of −26.5 ± 0.3 ‰ and +8.8 ± 0.5 ‰, respectively. Conversely, the sediment samples displayed lower TOC and TN contents of 5.5 ± 0.9 wt% and 0.3 ± 0.04 wt%, with $\delta^{13}C$ and $\delta^{15}N$ values of −27.6 ± 0.4 ‰ and +3.0 ± 0.9 ‰, respectively. The observed carbon and nitrogen isotopic compositions were typical of the lacustrine range in Lake Suwa (Yoshioka et al., 1988, 1994), and the cyanobacterial bloom and sediment samples demonstrated TOC/TN ratios of 5.4 ± 0.6 and 17.2 ± 0.6, respectively.

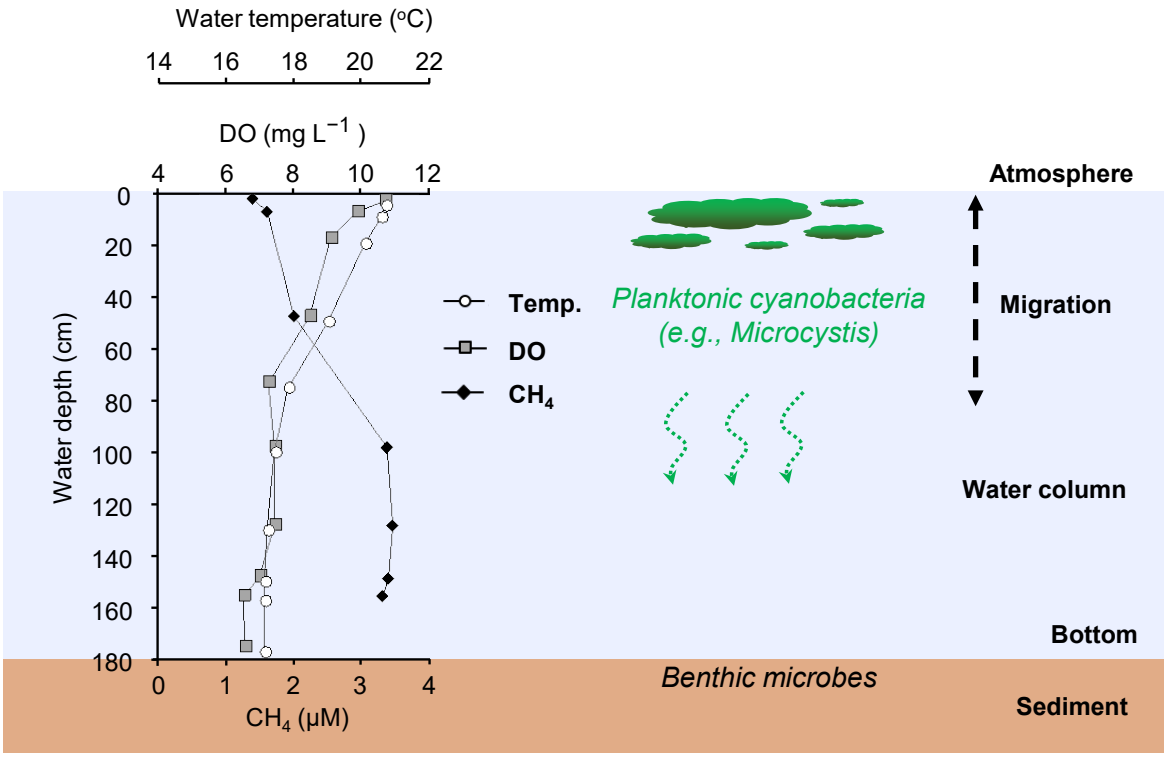

Figure 23. Cross-section of Lake Suwa and water column profiles measured in September, 2018. Cyanobacterial blooms migrate to a lower water layer at night and rise to the surface layer before dawn (Reynolds, 1987). Blooms are thought to migrate vertically to avoid predation by zooplankton and to supplement their nutrients in the lower layer.

Table 8. Water column profiles at the sampling site between June 2018 and October 2019.

Date	Depth cm	Temp. ℃	DO mg/L	CH_4 mmol/L
2018.6.27	0	—	—	1.80
	5	24.5	8.61	—
	10	24.5	8.61	2.09
	20	24.5	8.61	—
	50	24.5	8.66	2.05
	75	24.5	8.58	—
	100	24.5	8.64	2.26
	130	24.5	8.43	1.83
	150	24.5	7.83	2.05
	160	24.5	7.16	2.36
	180	24.5	6.48	—

Date	Depth cm	Temp. ℃	DO mg/L	CH_4 mmol/L
2018.9.28	0	—	—	—
	5	20.8	10.97	1.52
	10	20.7	10.11	1.73
	20	20.2	9.34	—
	50	19.1	8.74	2.13
	75	17.9	7.5	—
	100	17.5	7.68	3.5
	130	17.3	7.67	3.6
	150	17.2	7.24	3.53
	160	17.2	6.76	3.45
	180	17.2	6.8	—

Date	Depth cm	Temp. ℃	DO mg/L	CH_4 mmol/L
2019.6.28	0	—	—	0.92
	5	22.9	7.16	—
	10	22.9	7.13	1.07
	20	23	7.12	—
	50	23	7.11	1.17
	75	23	6.94	—
	100	23	6.85	1.43
	130	22.9	6.31	2.25
	150	22.8	5.75	2.76
	160	22.7	4.92	3.03
	180	22.7	4.84	—

Date	Depth cm	Temp. ℃	DO mg/L	CH_4 mmol/L
2019.8.29	0	—	—	2.78
	5	25.7	7.49	—
	10	25.6	7.51	0.61
	20	25.5	7.54	—
	50	25.4	7.4	0.37
	75	24.4	3.22	—
	100	23.9	1.32	0.23
	130	23.4	2.77	0.94
	150	22.6	1.86	3.38
	160	22.4	1.22	13.59
	180	22.3	0.83	—

Date	Depth cm	Temp. ℃	DO mg/L	CH_4 mmol/L
2019.10.10	0	—	—	0.32
	5	20.9	10.06	—
	10	20.9	10.06	0.29
	20	20.9	10.08	—
	50	20.8	10.06	0.99
	75	18.9	8.98	—
	100	17.8	7.01	0.90
	130	16.9	5.5	1.83
	150	16.9	5.45	2.36
	160	16.8	5.23	2.37
	180	16.8	5.07	—

Table 9. Carbon and nitrogen contents and stable isotope ratios in the samples.

Sample	TOC (wt%)	TN (wt%)	$\delta^{13}C$ (‰, vs VPDB)	$\delta^{15}N$ (‰, vs AIR)	TOC/TN (wt%)
Cyanobacterial bloom (September 2018)	41.1 ± 1.8	7.7 ± 1.1	−26.5 ± 0.3	+8.8 ± 0.5	5.4 ± 0.6
Sediment 0–10 cm depth (September 2018)	5.5 ± 0.9	0.3 ± 0.0	−27.6 ± 0.4	+3.0 ± 0.9	17.2 ± 0.6

5.3.2 F430 concentration

We detected F430 in the cyanobacterial bloom and benthic surface sediment samples using LC/ESI–MS/MS (Figure 24). The cyanobacterial bloom samples collected in September 2018 and June 2019 displayed F430 concentrations of 6.8×10^2 and 3.5×10^3 femto mol g-wet^{-1}, respectively (Table 10), or 9.2×10^3 and 5.6×10^4 femto mol g-dry^{-1} when considering the water content of the cyanobacterial bloom samples (both water content of the cyanobacterial bloom samples were 92.5 % and 93.8 %, respectively). Conversely, the F430 concentrations in the sediment samples from September 2018 and June 2019 were 8.5×10^2 and 8.6×10^3 femto mol g-wet^{-1}, respectively. The peak ratios of native F430 to epimers were 3.3 and 3.8 in the cyanobacterial bloom samples and 9.0, and 11.1 in the sediment samples (Table 10), respectively. The small amounts of F430 epimers detected in the samples of this study (Figure 24) indicated that most methanogenic archaea were in an active state.

5.3.3 Microbial community structure in cyanobacterial bloom and benthic sediment

Next, we investigated the microbial communities' structure in the cyanobacterial bloom and surface sediment samples. Figure 25 shows a photomicrograph of a cyanobacterial bloom sample collected in June 2019, in which a large number of cells (a few micrometers in diameter) were confluent and formed colonies with a morphology that was similar to that of cyanobacteria of the genus *Microcystis* (Xu et al., 2016).

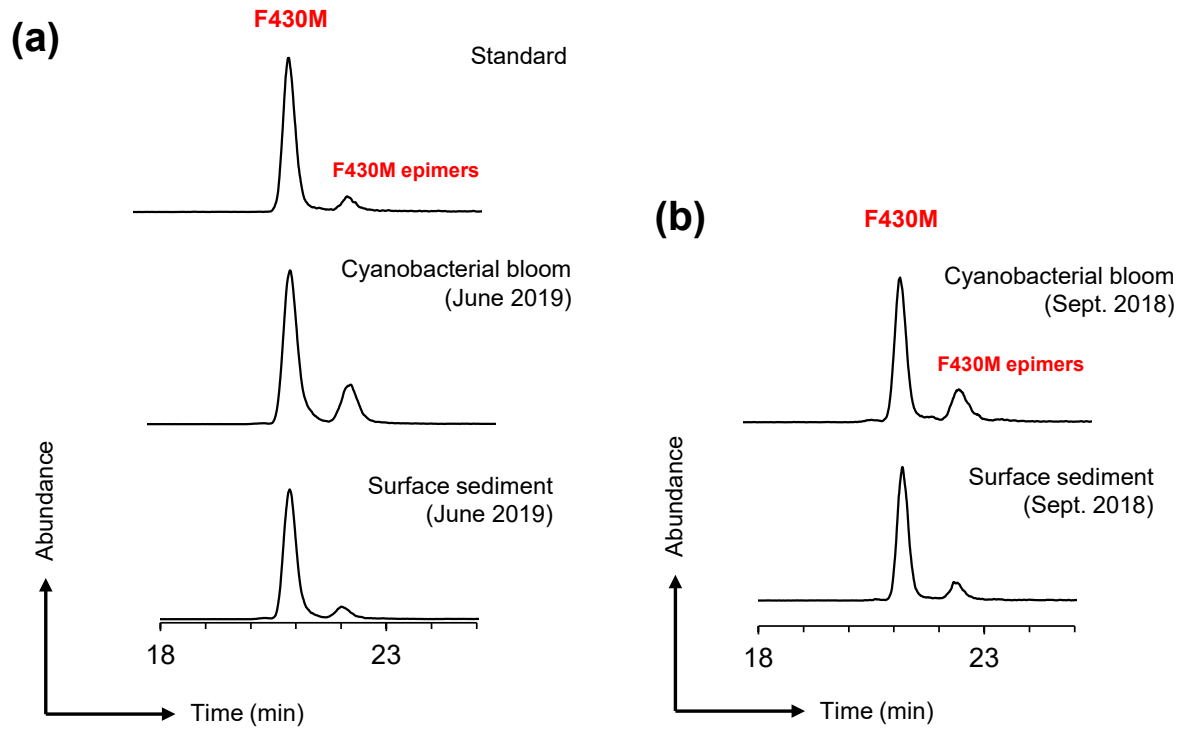

Figure 24. Chromatograms of the cyanobacterial bloom and surface sediment samples analyzed using LC/ESI–MS/MS in the MRM mode. The F430M product ion was set to m/z 844.3. (a) June 2019. (b) September 2018.

Table 10. Concentrations of F430 and its epimers in environmental samples obtained from Lake Suwa.

Sample type	Sample name	Concentration	F430 / F430epimer	Reference
Planktonic bloom	Cyanobacterial bloom (September 2018)	6.8×10^2 femto mol g-wet^{-1}	3.3	This study
	Cyanobacterial bloom (June 2019)	3.5×10^3 femto mol g-wet^{-1}	3.8	This study
Sediment	Sediment 0-10 cm depth (September 2018)	8.5×10^2 femto mol g-wet^{-1}	9.0	This study
	Sediment 0-3 cm depth (June 2019)	8.6×10^3 femto mol g-wet^{-1}	11.1	This study
	Kawatabi (Paddy soil)	8.7×10^2 femto mol g-wet^{-1}	-	Kaneko et al. (2014)
	Shimokita 11-4 (Marine sediment)	6.3×10^1 femto mol g-wet^{-1}	-	Kaneko et al. (2014)

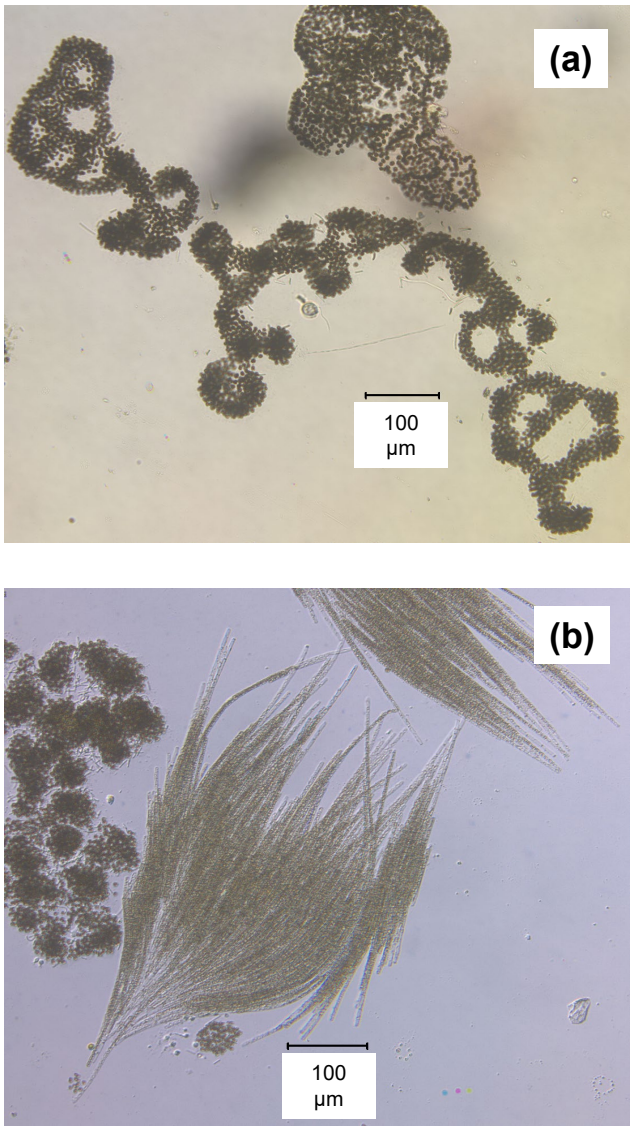

Figure 25. Photomicrograph of a cyanobacterial bloom sample collected in June 2019. The cyanobacterial bloom in Lake Suwa mainly comprised *Microcystis* (a) but also contained other cyanobacteria, such as *Aphanizomenon* (b).

The detailed structures of the microbial communities in the cyanobacterial bloom and sediment samples collected in September 2018 were investigated using SSU rRNA gene tag sequencing analysis. A total of 66,092 reads were obtained from the cyanobacterial bloom sample, of which 99.2 % were assigned to bacteria (Figure 26a). Archaeal sequences accounted for only eight (0.012 %) of the total sequence reads, six of which were singleton sequences closely related to the phyla *Euryarchaeota*, *Altiarchaeota*, *Bathyarchaeota*, and *Nanoarchaeota*. Consequently, only two reads were assigned to known methanogenic archaea of the orders *Methanomicrobiales* and *Methanomassiliicoccales*, and no 16S rRNA genes from anaerobic methane-oxidizing archaea (ANME) were detected. Owing to their extremely low sequence abundance, these archaeal reads were considered as 'not significant' (Figure 26b). More than 50 % of the bacterial reads were assigned to a single OTU and were closely related to the cyanobacterium genus *Microcystis* in the order *Nostocales* (Figure 26c). We also detected another cyanobacterium genus *Pseudanabaena* in the order *Pseudanabaenales*. In addition to the cyanobacteria, bacteria closely related to the orders *Acetobacterales* (mainly *Acetobacteraceae*), *Betaproteobacteriales* (mainly uncultured *Nitrosomonadaceae*, *Azohydromonas*, *Ramlibacter*, and *Noviherbaspirillum*), *Caulobacterales* (mainly uncultured *Caulobacteraceae*), and *Cytophagales* (mainly uncultured *Microscillaceae*) were detected, which are generally known to be aerobic heterotrophic, or aerobic ammonia-oxidizing bacteria. A small proportion (0.3 %) of the total sequence reads were assigned to eukaryotic 18S rRNA genes, mainly from *Cnidaria, Conthreep, Bilateria*, and *Heterotrichea*.

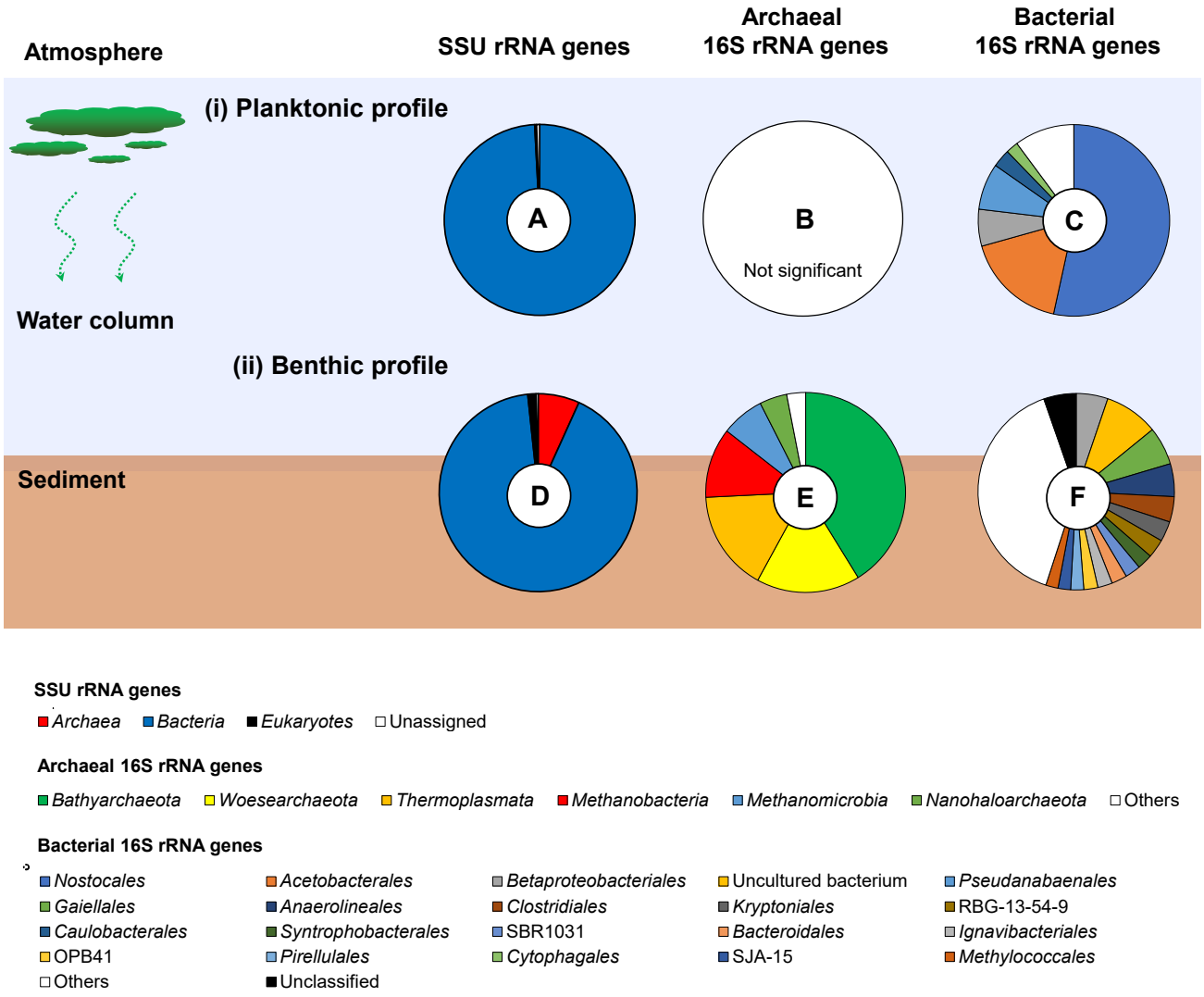

Figure 26. Cross-section of Lake Suwa and SSU rRNA gene tag sequencing analysis of the cyanobacterial bloom sample (a, b, c) and sediment sample (d, e, f) collected in September 2019. Relative abundance of each domain (a, d), archaeal community (b, e), and bacterial community (c, f) based on the number of sequence reads obtained. Singleton sequences based on taxonomic classification were excluded when estimating the microbial community structure in the samples.

A total of 46,801 reads were obtained from the sediment samples, of which 91.5 % and 6.8 % were assigned to bacteria and archaea, respectively (Figure 26d). Methanogenic archaea belonging to the classes *Methanobacteria* (*Methanobacterium*) and *Methanomicrobia* (mainly *Methanoregula*, *Methanothrix*, *Methanosarcina*, and *Methanocella*) were confirmed in the archaeal community (Figure 26e). The majority of archaeal reads were assigned to the phylum *Bathyarchaeota*, the phylum *Woesearchaeota*, and the class *Thermoplasmata* (mainly Marine Benthic Group-D). Although these predominant archaeal groups are also frequently found in marine and freshwater ecosystems, groundwater, and thermal springs, little is known about their physiology or metabolism due to the lack of cultured representatives (Evans et al., 2015; Tarnovetskii et al., 2018; Zhou et al., 2018, 2019). The bacterial community in the sediment samples was extremely diverse compared to that in the cyanobacterial bloom sample (Figure 26f), with relatively abundant bacterial reads that were closely related to the orders *Betaproteobacteriales* (mainly *Sulfuritalea*, *Quatrionicoccus*, uncultured *Nitrosomonadaceae*, and uncultured *Burkholderiaceae*), *Gaiellales* (mostly uncultured), *Anaerolineales* (mostly uncultured *Anaerolineaceae*), and *Clostridiales* (mainly *Romboutsia*, *Clostridium*, and *Sarcina*). These bacteria include aerobic heterotrophic (*Burkholderiaceae*), anaerobic autotrophic (*Sulfuritalea*), anaerobic heterotrophic (*Anaerolineales*, *Clostridiales*), and ammonia-oxidizing (*Nitrosomonadaceae*) species that have often been reported in the sediments of freshwater lakes (Buckles et al., 2013; Watanabe et al., 2017; Chen et al., 2017). Additionally, only a small proportion (0.3 %) of the total sequence reads were assigned to eukaryotes, mainly *Cnidaria*,

Peridiniphycidae, *Conthreep*, and *Streptophyta*.

5.3.4 Genomic indicators of methanogenic archaea

To detect methanogenic archaea in the cyanobacterial bloom and sediment samples, we amplified the archaeal 16S rRNA and *mcrA* genes in the total extracted DNA using PCR with one and four previously reported primer sets, respectively (Table 7). The archaeal 16S rRNA and *mcrA* genes were successfully amplified from the sediment samples (Table 11), but no PCR amplicons were obtained from the cyanobacterial bloom sample, despite repeated attempts.

5.4 Discussion

5.4.1 CH_4 production in the cyanobacterial phycosphere

F430 is unstable and quickly epimerizes to its relic forms (13-epi-F430M and 12,13-diepi-F430M), via a process that occurs on a daily basis, even at room temperature (e.g., Diekert et al., 1981; Mayr et al., 2008); therefore, the native form of F430 is unlikely to accumulate in the environment after the death of methanogenic archaeal cells. In this study, we detected native F430 in cyanobacterial bloom samples (6.8×10^2 to 3.5×10^3 femto mol g-wet^{-1}), clearly indicating the presence of methanogenic archaea in this oxidative environment. (Figure 24). Additionally, the F430 concentration in the cyanobacterial bloom was equal to or higher than that of the benthic sediment of Lake Suwa (8.5×10^2 to 8.6×10^3 femto mol g-wet^{-1}) and paddy soil (8.7×10^2 femto mol g-wet^{-1}, Kaneko et al.,

Table 11. PCR amplification of the archaeal 16S rRNA gene and the *mcrA* gene. PCR products were loaded onto a 1.2 % agarose gel with negative and positive controls and a DNA ladder. Presence (+) and absence (−) of PCR products are shown.

Target	Archaeal 16S rRNA gene	*mcrA* gene			
PCR primer set	340F/1000R	Luton-mcrA F/R	MCR F/MCR R	ME 3F/ME 2R	mlas/mcrA-rev
Cyanobacterial bloom (September 2018)	—	—	—	—	—
Sediment 0–10 cm depth (September 2018)	+	+	—	+	+

2014), suggesting that cyanobacterial blooms possessed the same CH_4 emission potential as benthic sediment and paddy soil.

We also found that the F430 concentration in the cyanobacterial bloom sample collected in June 2019 was approximately five times higher than that in the sample collected in September 2018, suggesting that the activity of methanogenic archaea was higher in June 2019 (Table 10). It is possible that active cyanobacteria photosynthesis increases the supply of organic substrates to heterotrophic bacteria and that these metabolites are provided to methanogenic archaea. The water temperature in September 2018 and June 2019 supported this hypothesis as it was higher in June 2019 than that in September 2018. Although active photosynthesis simultaneously generates oxygen, some methanogenic archaea have been hypothesized to tolerate oxygen exposure for long periods (Angel et al., 2011), and/or they are attributed to anoxic microniches such as extracellular polysaccharides. Therefore, the methanogenic archaea in a cyanobacterial bloom may produce CH_4 when oxygen production via photosynthesis stops and an anoxic microenvironment is established, such as that at night. The hypothesis is supported by the results of a previous study by Bižic et al. (2020); the authors reported that peak CH_4 production was confirmed under dark conditions and that it shifted with the peak of O_2 production (under light conditions) in cultured experiments.

F430 epimers were also detected in the cyanobacterial bloom samples; however, the ratio of native F430/F430 epimer in these samples ranged from 3.3 to 3.8 (Table 10), suggesting that methanogenic archaea were active in cyanobacterial blooms and contributed to CH_4 production in surface water. The

ratio of F430/F430 epimer in cyanobacterial bloom was lower than that in benthic sediments (9.0 to 11.0), suggesting that the activity of methanogenic archaea in benthic sediment was higher than that in cyanobacterial bloom or that the degradation of F430 was higher in the water column. Our data support previous studies that have reported the occurrence of cyanobacteria-associated methanogenic archaea that thrive in anoxic microenvironments in the cyanobacterial phycosphere (Grossart et al., 2011; Berg et al., 2014). Assemblages of heterotrophic bacteria are present within the cyanobacterial phycosphere, and their respiration activity leads to an oxygen gradient in the bloom (Ploug, 2008; Dziallas and Grossart, 2012; Batista et al., 2019).

Previous studies have estimated the in situ cellular abundance of methanogenic archaea based on F430 concentrations (Takano et al., 2013; Kaneko et al., 2014, 2016) using the following equation:

$$n\ (\text{cells g}^{-1}) = C_{\text{F430 in sample}} / (C_{\text{F430 in culture}} \times m\text{cell})$$

where $C_{\text{F430 in sample}}$ and $C_{\text{F430 in cell}}$ denote the F430 concentrations in the sample and a single cell, respectively, and *m*cell denotes the mean weight of the cell. Using the F430 concentration reported in seven species of cultured methanogens (580 ± 240 nmol g-dry cells^{-1}, Diekert et al., 1981) and the average prokaryotic cell weight (8.6×10^{-14} g, Whitman et al., 1998; Lipp et al., 2008; Braun et al., 2016), we estimated the abundance of methanogenic archaea in the cyanobacterial bloom samples to be 3.0×10^{7} cells g-wet^{-1} in September 2018 and 1.5×10^{8} cells g-wet^{-1} in June 2019 (Table 10).

According to the average cellular dry weight of *Microcystis* (2.0×10^{-11} g, *M. aeruginosa*; Li et al., 2014), the abundance of *Microcystis* cells in the cyanobacterial bloom sample was 5.0×10^{10} cells g-dry^{-1}. The cellular abundance of methanogenic archaea relative to *Microcystis* was thus determined to be 0.79% in September 2018 and 4.9% in June 2019, which was calculated considering the water content of cyanobacterial bloom; however, uncertainty in the actual relative abundance of methanogenic archaea that arises from the sample matrix of extracellular polysaccharides in the cyanobacterial consortium must be taken into consideration. Additionally, we noted that the values obtained by these formulas contained large errors; the cellular dry weight of *Microcystis* is calculated using cultured experiments. Grossart et al. (2011) reported the direct attachment of methanogenic archaea to cyanobacteria as observed by fluorescence in situ hybridization (FISH). As we did not directly observe microbial cells in the cyanobacterial bloom using FISH technique, the coexistence of methanogenic archaea and the bloom requires clarification. To elucidate the physical symbiosis between cyanobacterial blooms and methanogenic archaea, we will microscopically observe cells in cyanobacterial blooms using FISH in future studies.

SSU rRNA gene tag sequencing analysis detected a large number of 16S rRNA genes from aerobic heterotrophic bacteria, including *Acetobacterales* and *Betaproteobacteriales*, in the cyanobacterial bloom samples (Figure 26), suggesting that the respiration of these aerobic bacteria created a niche for methanogenic archaea within the cyanobacterial bloom. Moreover, some *Acetobacterales* species are known to produce acetate as a metabolite (Vu et al., 2019); therefore, these

heterotrophic bacteria may supply methanogenic archaea with methanogenic substrates via decomposition of the organic matter produced during cyanobacterial photosynthesis. Berg et al. (2014) have proposed that hydrogenotrophic methanogenic archaea utilize hydrogen generated by cyanobacteria during nitrogen fixation; however, as *Microcystis*, which were predominant in our samples (Figure 26c), lacks nitrogenase for nitrogen fixation (Kim et al., 2019), its contribution toward CH_4 production appears to be less remarkable in surface water. Although F430 levels were detected in the oxygenated cyanobacterial bloom sample, which were similar to those in anoxic sediments such as paddy fields (Figure 24, Table 10), the samples contained extremely low numbers of SSU rRNA gene sequences from known methanogenic archaea and no PCR amplicons from archaeal 16S rRNA and *mcrA* genes (Figure 24, Table 11). This discrepancy between F430 and molecular analyses was consistent with the findings of a previous study that targeted the microbial community in deep subseafloor coal beds (e.g., Inagaki et al., 2015), and might be attributable to the extremely low abundance of methanogenic archaea. Furthermore, the bulk DNA extracted from the cyanobacterial bloom sample might contain high concentrations of *Microcystis*-derived polysaccharides, which might have interfered with or inhibited the amplification of archaeal 16S rRNA and *mcrA* genes during PCR (Yoshida et al., 2003). Additionally, as cyanobacterial blooms are heterogeneous, unlike cultured cyanobacteria, it is possible that archaeal DNA were not extracted efficiently.

The F430 concentrations measured in the cyanobacterial bloom strongly suggest that CH_4 production occurs in the lake water column; however, the depth profile of dissolved CH_4 in the water

column reveals particularly high concentrations in water from the bottom of the lake but absence of CH_4 accumulation in surface water (Figure 23, Table 8). Consistently, similar trends were observed in the water temperature and DO profiles throughout all seasons. CH_4 accumulation in the surface water of other freshwater lakes has often been reported in thermoclines (Tang et al., 2016).

As CH_4 emissions from benthic sediments are larger than those from cyanobacterial blooms, CH_4 accumulation in the surface water was not observed in Lake Suwa. For instance, Grossart et al. (2011) estimated the rate of microbial CH_4 production in the oxygenated surface water of Lake Stechlin (Germany) as 1.8–2.4 nmol L^{-1} h^{-1}, and Bižic et al. (2020) reported the rate of CH_4 production from cultured experiments with *Microcystis aeruginosa* to be up to 1.0 µmol L^{-1} h^{-1}. The CH_4 production rate in benthic sediment (5–30 cm depth) in Lake Suwa was reported to be 7.8–19.8 nmol g-dry^{-1} h^{-1} at the typical summer maximum surface sediment temperature (Iwata et al., 2020). To evaluate the actual CH_4 production rate in the surface water of Lake Suwa, incubation experiments will be required using surface water and cyanobacterial bloom samples collected from the lake.

5.4.2 CH_4 production in benthic sediment

We quantified F430 in sediment samples collected in September 2018 (8.5×10^2 femto mol g-wet^{-1}) and June 2019 (8.6×10^3 femto mol g-wet^{-1}), revealing levels similar to or higher than those previously reported in marine sediment ($0.026–1.9 \times 10^3$ femto mol g-wet^{-1}, Kaneko et al., 2014, 2016) and paddy soil ($0.3–2.0 \times 10^3$ femto mol g-wet^{-1}, Kaneko et al., 2014, 2016), which suggest ongoing

archaeal methanogenesis in the surface sediment. Although ANME also utilize F430 for reverse methanogenesis (e.g., Krüger et al., 2003; Maryr et al., 2008; Shima et al., 2011), 16S rRNA gene sequences of the ANME were not detected from cyanobacterial bloom and benthic sediment, suggesting that F430 detected from these samples originated from methanogenic archaea. The abundance of methanogenic archaea in benthic sediments calculated from the F430 concentrations was 3.7×10^7 cells g-wet^{-1} in September 2018 and 3.8×10^8 cells g-wet^{-1} in June 2019 (Table 10). These values are approximately in the same range as those reported for other lake sediments, as determined using microscopic and molecular techniques (e.g., Zepp Falz et al., 1999; Chan et al., 2005). As Lake Suwa is a eutrophic lake, its surface sediment contains high concentrations of organic carbon (Table 9); therefore, this nutrient-rich substrate can support high levels of benthic microbial CH_4 production.

5.4.3 Planktonic cyanobacterial bloom and benthic archaeal community shift

Our analysis of archaeal 16S rRNA and *mcrA* genes revealed the presence of methanogenic archaea closely related to *Methanobacteriales* and *Methanomicrobiales* in surface sediment (Figure 26, Table 11), including hydrogenotrophic, aceticlastic, and methylotrophic methanogenic archaea (e.g., Sakai et al., 2012; Schirmack et al., 2014). Additionally, the 16S rRNA genes of anaerobic heterotrophic bacteria were also detected in the sediment sample (Figure 26). Members of *Anaerolineales* and *Clostridiales* are known to anaerobically decompose organic matter by fermentation and supply methanogenic archaea with their metabolites, such as H_2, acetate, formate,

and methanol (Yamada et al., 2006; Nishiyama et al., 2009). Although water from the bottom of the lake contains dissolved oxygen (Figure 24), this is thought to be rapidly utilized by aerobic heterotrophic bacteria in surface sediment, suggesting that CH_4 is produced in surface sediment via the anaerobic decomposition of organic matter by fermentative bacteria and methanogenic archaea. Surface sediment samples were abundant with the 16S rRNA genes of archaea closely related to *Bathyarchaeota*, whose genomes reportedly contain divergent homologs of the genes required for methane metabolism (Evans et al., 2015). Thus, uncultured archaea belonging to *Bathyarchaeota* may also be involved in CH_4 production in surface sediment.

The microbial community structure differed dramatically between surface sediment and surface water. A wide variety of archaeal and bacterial taxa were present in the surface sediment. For instance, members of the phylum *Cyanobacteria* were predominant in the water column. These findings were consistent with those of a previous study in which a cyanobacterial bloom in Lake Suwa was mainly caused by *Microcystis* spp. (Park et al., 1993) and involved the aggregation of thick mucilage composed of complex polysaccharides. Although dead cyanobacterial cells from surface blooms sink rapidly through the water column, SSU rRNA genes from cyanobacteria constituted an extremely minor fraction (~2 % of all sequences) in the sediment. Previously, Yan et al. (2017) have reported that the decomposition of cyanobacterial cells produces nutrients (nitrate, phosphate, and organic substances) that stimulate benthic microbial CH_4 production. Further, a positive relationship was clearly observed between CH_4 flux rate and productivity normalized to the chlorophyll a concentration

in freshwater environments (Beaulieu et al., 2019). Therefore, this process may explain the seasonal fluctuations in F430 concentrations observed throughout our study. As the depth of the study site was shallow (1.8 m), it is possible that methanogenic archaea derived from benthic sediments attached to cyanobacterial bloom owing to the mixing of lake water. However, the results of SSU rRNA gene analysis clearly indicated that the microbial community structure differed dramatically between benthic sediment and cyanobacterial bloom. Additionally, Iwata et al. (2020) reported the observations of seasonal variations in the meteorological and limnological environment of Lake Suwa during 2016-2017, which indicated a stable stratification from May to September and a difference in temperature between the surface and bottom layer. These results suggested that the contamination of microorganisms derived from benthic sediment to cyanobacterial bloom was negligible.

Chapter 6: Interaction between surface hydrosphere and deep sub-surface aquifer in an active fault lake: Scope of surface and deep subsurface methanogenesis.

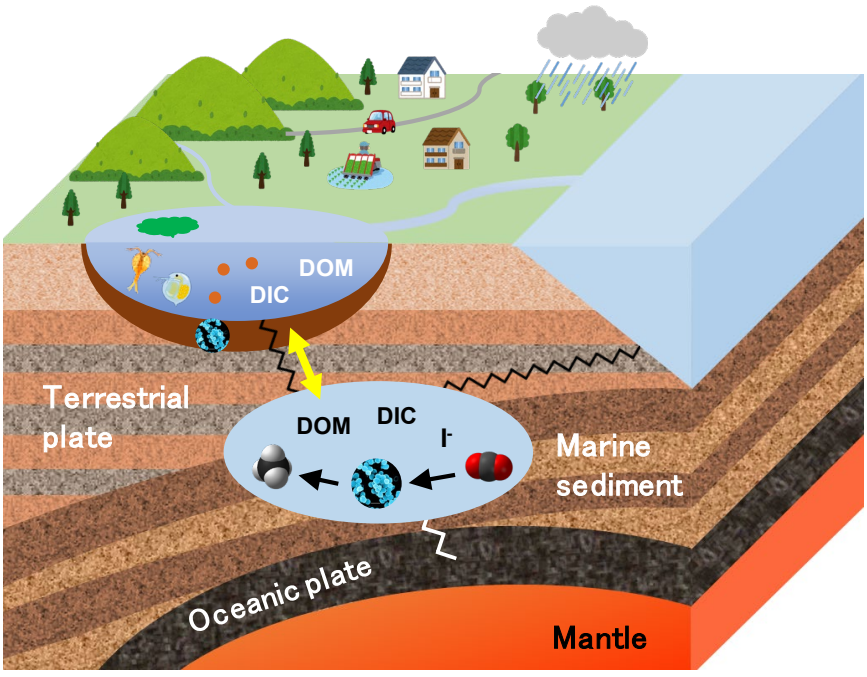

6.1 Aim of this study

Methane (CH_4) is the final decomposition product of organic matter and is produced by biogenic and thermogenic processes, which have occurred in an anaerobic environment when inorganic oxidants are depleted (e.g., nitrate, ferric iron, or sulfate). Because direct observation of biogeochemical processes in the deep subsurface environment is demanding, upwelling gas, including CH_4, is important as information of a deep subsurface environment. Since these processes are recorded as an isotopic ratio of carbon and hydrogen ($^{13}C/^{12}C$ and $^{2}H/^{1}H$), CH_4 has been used as an indicator to understand the biogeochemistry process in anaerobic environments.

Itoigawa-Shizuoka Tectonic Line (ISTL) is located on central Honshu Island, Japan (Figure 27), and is considered to be a plate boundary between the North American and the Eurasian plates. ISTL is the most active fault zone in Japan: previous studies reported that left-lateral slip is up to 10.0 ± 2.6 mm/yr just south of the intersection with the Median Tectonic Line (MTL) (Loveless et al., 2010). Since there are also many hot springs around ISTL, geological and geochemical studies have been reported using a gas associated with hot spring water. For instance, Umeda et al. (2013) investigated changes in the subsurface environment before and after the 2011 Nagano central earthquake by gas composition and helium isotope ratio analysis for gas collected from wells and hot spring water around ISTL. Suda et al. (2014) investigated the deep methanogenesis by serpentinite-hosted hydrothermal conditions in Hakuba Happo hot spring located on the west of ISTL, Nagano, Japan. Matsushita e al. (2016, 2018) reported the microbial and thermogenic origins of CH_4, the gas is associated with hot

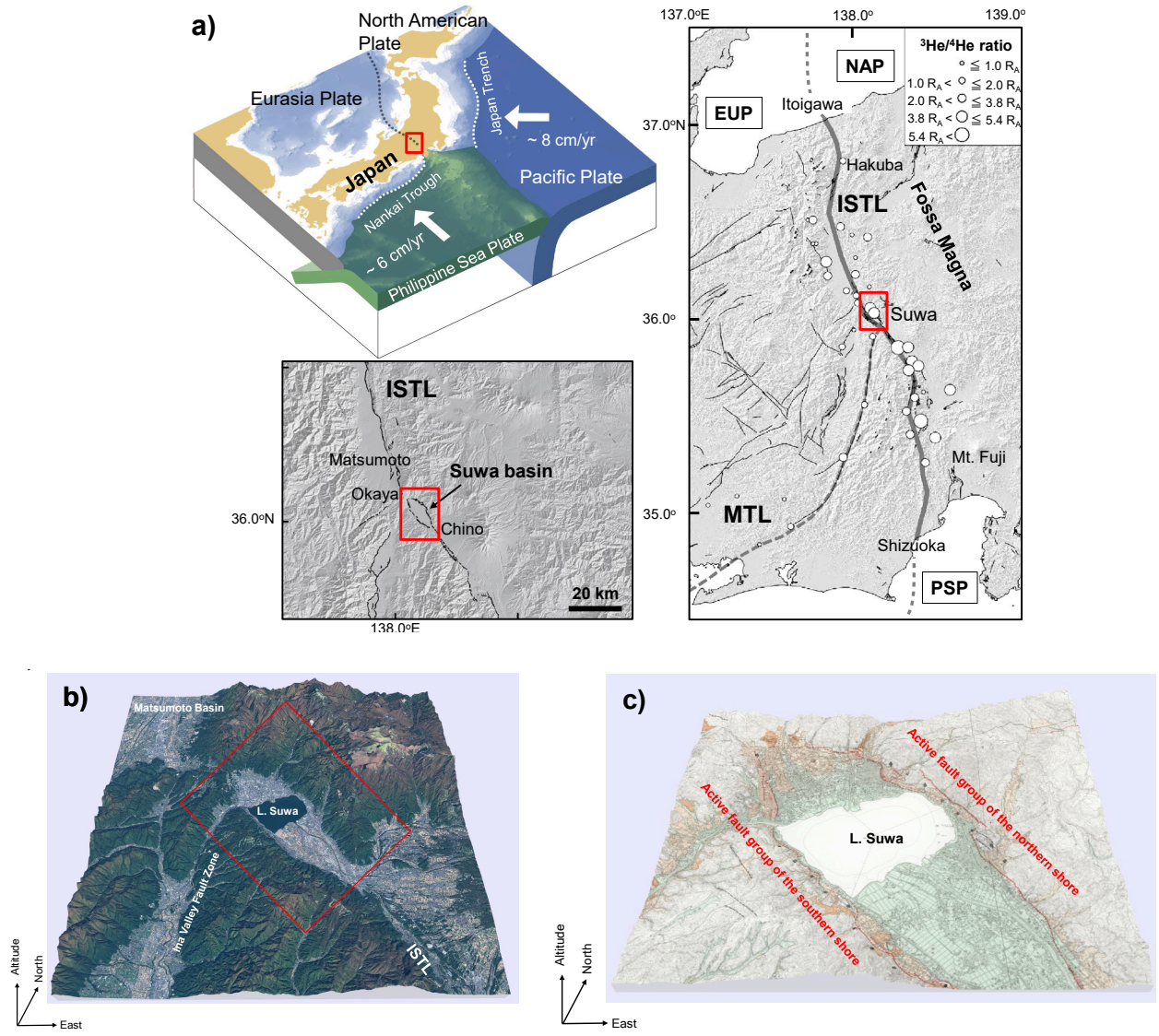

Figure 27. (a) Geological setting of the study site Lake Suwa locating at Suwa basin on the Itoigawa-Shizuoka Tectonic Line (ISTL) and the crossing point of Median Tectonic Line (MTL). The surrounding plates of North American Plate (NPA), Eurasia Plate (EUP), Philippine Sea Plate (PSP), Pacific Plate (Lin et al., 2016; Ikeda et al., 2004) are compiled with the profile of Helium isotope ratio ($^3He/^4He$) along with ISTL and MTL before the 2011 central Nagano earthquake (Umeda et al., 2013). (b), (c) Three-dimensional geological map from the bird eyes view and active fault transforms (The raw data profiles were courtesy from Geospatial Information Authority of Japan).

spring water located on the south end of ISTL, Shizuoka, Japan, using stable carbon and hydrogen isotopic ratio and small sub-unit rRNA gene analyses.

Radiocarbon measurements ($^{14}C/^{12}C$) is a powerful tracer for determining the origins of carbon. Radiocarbon is produced by nitrogen (^{14}N) and cosmic rays in the atmosphere, which half-life is 5730 years. While the biosphere, which interacts with the atmosphere, is ^{14}C-rich, the lithosphere isolated from the atmosphere is ^{14}C-depleted. Radiocarbon measurement using accelerator mass spectrometry (AMS) enables the measurement of ^{14}C in carbon on the order of 100 micrograms or less (e.g., Pearson et al., 1998; Yokoyama et al.,2010).

In this study, we performed radiocarbon measurements of CH_4 and CO_2 to elucidate the origin of CH_4 in Lake Suwa, which has two sources of CH_4 emission; it is considered that one is seeping from the deep sub-surface and the other is produced in the benthic sediment. Furthermore, to assess the contribution of CH_4 to the lake ecosystem, we determined the ^{14}C content of phytoplankton collected from Lake Suwa.

6.2 Materials and Methods

6.2.1 Geological setting

Lake Suwa is located in Nagano Prefecture, in the central part of Honshu Island, Japan (Figure 27). The surface area and altitude are 13.3 km^2 and 759 m, respectively, and it has mean and maximum depths of 4.3 m and 6.4 m, respectively. Lake Suwa is recognized to be formed on ISTL and the

crossing point of MTL. ISTL around Lake Suwa, which is about 50 km, consists of left-lateral slip faults (Sagiya et al., 2002; Loveless et al., 2010) (Figure 28). Since Lake Suwa has a large catchment area (512 km^2) and 31 inflowing rivers, it has more than 370 m of sedimentary layer with a high annual sedimentation rate (~1 cm yr^{-1}, Nakazato et al., 1998; Suwa Construction Office, 2019). Lake Suwa is a typical eutrophic lake due to the influence of residential and agricultural areas. Cyanobacterial blooms, particularly those caused by *Microcystis* spp., have occurred regularly during the summer (Park et al., 1993, 1998).

6.2.2 Sampling procedure

6.2.2.1 Methane seep samples

We collected the gas phase and water samples from methane gas seep sites (Site #1, #2) at the south side of Lake Suwa on June 29, 2019 (Figure 29). The distance from the shore of both sites and the water depth is about 100 m and 3 m, respectively. Site #1 is the most active methane seep site in Lake Suwa, with a large number of fine bubbles. Site #2 is different from site #1; large bubbles have been regularly released. Seep gas was collected by a water displacement method using a bucket, which connects an aluminum multilayer gas sampling bag (10 L, GL Sciences, Japan) by a tube and a gas syringe (100mL, GL Sciences, Tokyo, Japan). Surface water was collected in a glass bottle (250 mL, Shibata Scientific Technology LTD., Japan). To eliminate the effects of microorganisms, we added 50 μL of an aqueous solution of mercury chloride to the glass bottle.

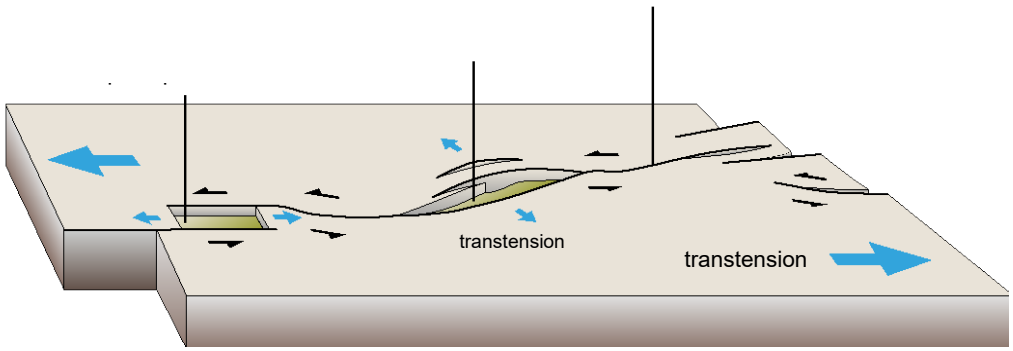

Figure 28. Conceptual diagram showing the geometry of typical pull-apart basin and oblique pull-apart basin in a transform fault system. The black and blue arrows stand for the direction of transform and transmission, respectively (Frisch et al., 2011).

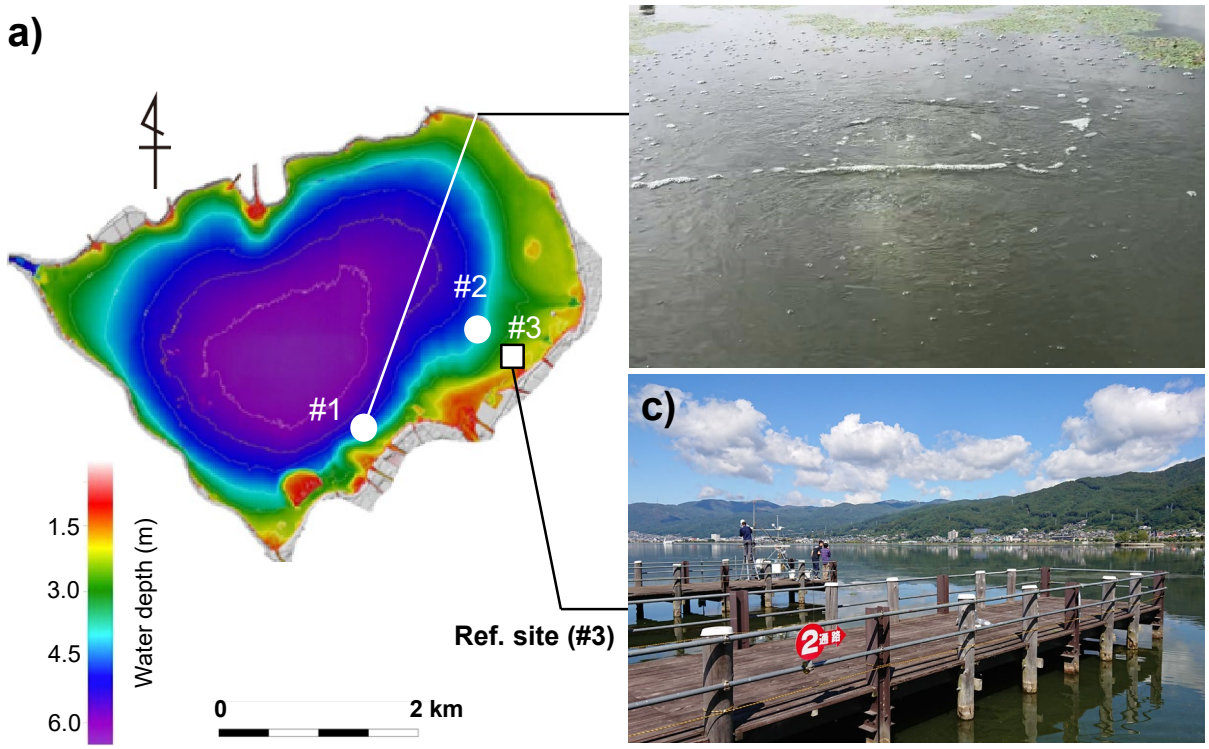

Figure 29. (a) Sampling location of the study site, (b) the seep methane gas (#1, #2), and (c) the surface methane gas (#3, reference site) at lake Suwa.

6.2.2.2 Reference samples

We also collected these samples from the pier site (Site #3) as a reference site (Figure 29). The distance from the shore and the water depth is 50 m and 1.8 m, respectively. Although there is not springing up of gas as the site #1, stimulation of the surface deposits with a rod releases a large amount of CH_4-rich bubbles. The sampling method was the same used for the seep sites.

6.2.3 Gas composition analysis

As to Ar, O_2, N_2, CH_4, and CO, Micropacked GC column (Molseive 5A column, Restek, USA) and Agilent 7890A Gas chromatograph equipped with a thermal conductivity detector (TCD) (Agilent Technologies, USA). Oven temperature of –78 ℃ isothermal (dry ice – ethanol slush) was used to separate Ar and O_2, and oven temperature of +40 ℃ isothermal was used to analyze N_2, CH_4, and CO. As to CO_2, Micropacked GC column (Shincarbon ST column, Restek, USA) and Agilent 7890A Gas chromatograph equipped with a thermal conductivity detector (TCD) (Agilent Technologies, USA). Furthermore, as to C_2H_6, Micropacked GC column (Shincarbon ST column, Restek, USA) and GL4000 Gas chromatograph equipped with a flame ionization detector (FID) (GL Sciences, JAPAN).

6.2.4 Stable carbon isotopic ratio analysis and radiocarbon measurements

Stable carbon isotope and radiocarbon measurements for CH_4, CO_2, DIC, and cyanobacterial bloom were performed by accelerator mass spectrometer (AMS) using the method described as

previous studies (Yokoyama et al., 2010; Satoh et al., 2019). CO_2 gas was extracted from the water sample by acidification with 85% phosphoric acid and bubbling with ultra-high-purity helium gas. The extracted CO_2 gas was cryogenically purified, quantified by a manometer at the cold finger portion of the vacuum line, and a suitable amount of purified CO_2 gas was transferred to the graphitization part of the vacuum line.

The gas sampling bag was connected to the vacuum line of the preparation system, and CH_4 and CO_2 gases were separated and purified with a cryogenic trap filled with silica gel beads. The CO_2 was sealed in a 9-mm-diameter borosilicate glass ampoule. CH_4 was converted to CO_2 as described previously (Kawagucci et al., 2020). CH_4 gas was captured in a trap containing HayeSep D (GL Sciences, Japan) at −130 °C, and non-condensable gases such as helium, hydrogen, nitrogen, oxygen, and argon were vented. Then, purified CH_4 gas was carried to an oxidation reactor and converted to CO_2 at 1000 °C. The convert CO_2 gas was further purified by cryogenic coolant and liquid nitrogen followed by flame sealing in a 9-mm-diameter borosilicate glass ampoule.

We also used the cyanobacterial bloom sample collected by site#3 in a previous study (Urai et al., submitted). Lyophilized and pulverized cyanobacterial bloom samples were weighed and packed in tin capsules and converted to CO_2 gas by a conventional elemental analyzer (FlashEA 1112 Series, Thermo Fisher Scientific, USA). The exhaust line of the elemental analyzer is connected to the above mentioned CH_4 vacuum line (Kawagucci et al., 2020) with 1/16” o.d. stainless-steel tubing, and the CO_2 gas was carried to the vacuum line by the carrier helium gas of the elemental analyzer and trapped

by liquid nitrogen, purified by dry ice- ethanol slush, and flame sealed into a borosilicate glass tubings (Figure 30).

All CO_2 gases were graphitized at the Atmosphere and Ocean Research Institute (AORI) at the University of Tokyo. Here, for checking the contamination of modern carbon, we also analyzed the ^{14}C-depleted reference gas (GL Sciences, Japan) by the parallel handling procedure. The isotopic compositions of stable carbon and radiocarbon are presented in delta notation ($\delta^{13}C$, ‰ vs. VPDB and $\Delta^{14}C$, ‰) using the following equation:

$$\delta^{13}C\ (‰) = [(^{13}C/^{12}C)_{sample} / (^{13}C/^{12}C)_{standard} - 1] \times 1000$$

$$\Delta\ ^{14}C\ (‰) = \delta^{14}C - 2(\delta^{13}C + 25)(1 + \delta^{14}C/1000)$$

6.3 Results and Discussion

6.3.1 Deep origin of methane

The results of gas composition analyses in site #1 and #2 showed that CH_4 (90.1 and 93.2 vol.%) was the predominant gas in both seep sites, and other major gases were CO_2 (7.0 and 1.9 vol.%), N_2 (0.5 and 3.9 vol.%) and O_2 (0.5 and 0.7 vol.%) (Table 12). The gases in site #1 and #2 contained very little C_2H_6 (0.0041 and 0.0044 vol.%), and CH_4/C_2H_6 ratios were 2.2×10^4 and 2.1×10^4, respectively. In addition, values of $\delta^{13}C_{CH4}$ in site #1 and #2 were −66.5 ± 1.3 ‰ and −65.6 ± 1.5 ‰,

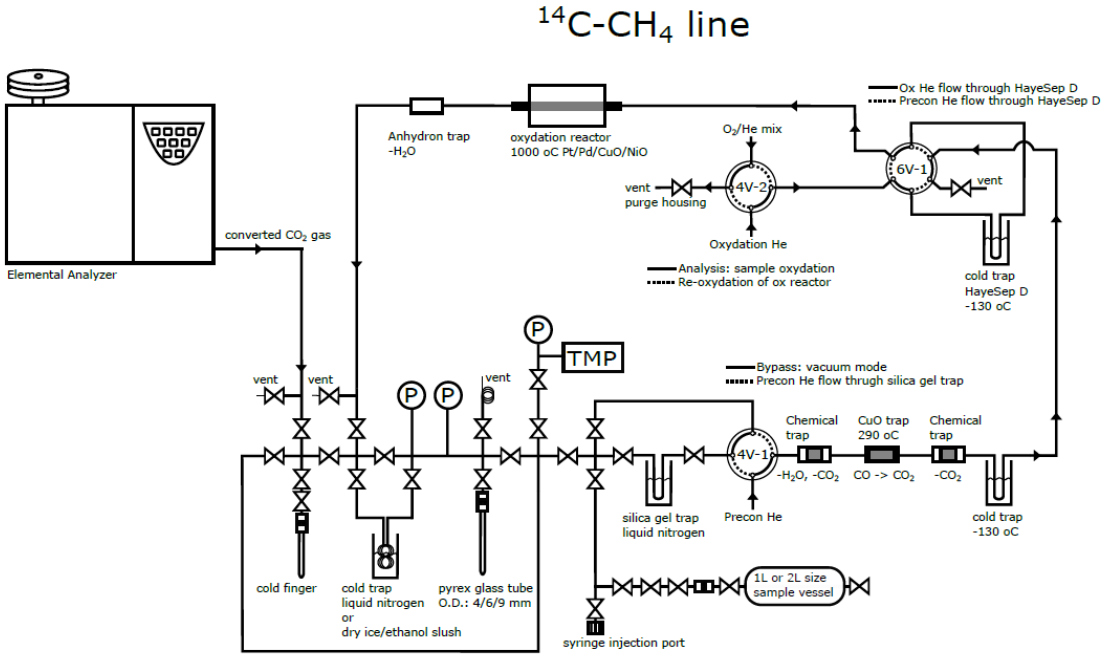

Figure 30. Purification and oxidation line.

Table 12. Chemical and isotopic compositions of lake water and gases collected from Lake Suwa.

Site name	N_2 (vol.%)	CO_2 (vol.%)	CO (vol.%)	O_2 (vol.%)	Ar (vol.%)	CH_4 (vol.%)	C_2H_6 (vol.%)	CH_4/C_2H_6
Site #1	0.5	7.0	<0.01	0.5	0.1	90.1	0.0041	2.2×10^4
Site #2	3.9	1.9	<0.01	0.7	0.1	93.2	0.0044	2.1×10^4
Site #3	5.4	5.5	<0.01	0.5	0.2	86.9	0.0049	1.8×10^4

Table 13. Carbon isotopic compositions of CH_4, CO_2, DIC, and Aoko (cyanobacterial bloom). The results are expressed as $\delta^{13}C$, $\Delta^{14}C$, and percent modern carbon (pMC, reflecting the concentration of ^{14}C in the sample).

Site name	Type	$\delta^{13}C$ (‰, vs VPDB)	$\Delta^{14}C$ (‰)	pMC (%)
Site #1	CH_4	−66.5 ± 1.3	−972.1 ± 0.5	2.79 ± 0.05
	CO_2	+3.5 ± 1.2	−917.5 ± 0.7	8.25 ± 0.07
	DIC	+4.1 ± 1.4	−630.6 ± 1.7	36.94 ± 0.17
Site #2	CH_4	−65.6 ± 1.5	−989.8 ± 0.3	1.02 ± 0.03
	CO_2	+7.8 ± 0.1	−951.2 ± 1.0	4.87 ± 0.10
	DIC	−6.8 ± 2.4	−103.1 ± 4.0	89.69 ± 0.40
Site #3	CH_4	−59.6 ± 1.5	+21.7 ± 3.8	102.17 ± 0.38
	CO_2	−3.0 ± 1.9	+6.2 ± 3.9	100.62 ± 0.39
	DIC	−7.8 ± 1.9	−100.9 ± 3.5	89.90 ± 0.35
	Aoko	−27.9 ± 0.7	−110.3 ± 2.7	88.96 ± 0.27

respectively (Table 13). These results indicated in a range typical of biogenic methane (e.g., Vogel et al., 1982; Belay and Daniels, 1988) and consistent with those reported in previous studies ($\delta^{13}C_{CH4}$ = − 66.1 to −75.0 ‰, Nakai et al., 1974). In contrast, values of $\delta^{13}C_{CO2}$ at site #1 and site #2 were +3.5 ± 1.2 ‰ and +7.8 ± 0.1 ‰, respectively, suggesting that CO_2 was produced by the decomposition of sediment and then used for methanogenesis by methanogenic archaea (Scott et al., 1994).

For comparison, Suda et al. (2017) reported that the values of $\delta^{13}C_{CH4}$ collected from Hakuba Happo hot spring were −34.5 to −33.7 ‰ (well depths are 515 to 700 m). Furthermore, Matsushita et al. (2016) performed stable isotopic ratio analysis and culture experiments for methanogenic archaea to identify the origin of CH_4 in deep aquifers located at Shizuoka, the southern end of ISTL (Figure 27). The values of $\delta^{13}C_{CH4}$ were −69.4 to −33.5 ‰ (well depths are 150 to 1500 m), suggesting that the origins of CH_4 associated with hot spring water in Shizuoka were mixing of the biogenic and thermogenic origin. Since previous studies have been collecting a sample at the hot spring well, we note that gases associated with hot spring water are susceptible to the effect of thermogenic origin.

There are also several hot spring wells (Kamisuwa and Shimosuwa Hot Spring) on the active fault group of the northern shore of Lake Suwa (Figure 27c). Umeda et al. (2013) measured helium and neon isotopic ratios of gas associated with hot spring water around the ISTL and MTL, including Kamisuwa and Shimosuwa Hot Springs. The results indicated that the gas associated with the hot spring water around Lake Suwa was contributed by the gas originated from the mantle. Since some hot spring wells have been observed in Lake Suwa, it is possible that the gas originated from hot spring

water contributes to the CH_4 reservoir in Lake Suwa.

As for radioisotope signature, both values of $\Delta^{14}C_{CH4}$ and $\Delta^{14}C_{CO2}$ in site #1 and #2 were depleted ($\Delta^{14}C = -989.8 \pm 0.3$ to -917.5 ± 0.7‰, Table 12). The ^{14}C ages of CH_4 and CO_2 calculated from $\Delta^{14}C$ were 28,757 ± 134 to 36,851 ± 249 yrBP and 20,044 ± 70 to 24,274 ± 166 yrBP, respectively. Although data on the well depths of site#1 and site #2 are unknown, the drilling survey of sediment core in Lake Suwa (near site #1) reported that the depth of CH_4 reservoir was about 130 to 210 m (Motojima et al. 1955). The age of this sedimentary layer for which the sedimentation rate is calculated is about 43,000 to 70,000 yrBP (Anma et al., 1990). The calculated ages of the sedimentary layer are older than the ^{14}C age of CH_4 and CO_2, suggesting that seep gases may contain the gas buried at shallow depths because of the upwelling process from CH_4 reservoirs into Lake Suwa.

6.3.2 Surface origin of methane

The gas composition of site #3 was similar to that of site #1 and #2 (Table 12). CH_4 concentration was lower than sites #1 and #2, and N_2 concentration was higher than the seep sites, indicating denitrification by microorganisms in the benthic sediments. For the results of $\delta^{13}C_{CH4}$ (-59.6 ± 1.5 ‰) and CH_4/C_2H_6 ratio (1.8×10^4) in site #3 also indicated in a range of biogenic methane (e.g., Vogel et al., 1982; Belay and Daniels, 1988). The previous study reported that total organic carbon in the benthic sediment (0−10cm) was 5.5 ± 0.9 wt% and that the benthic sediment contained a variety of archaea and bacteria, including methanogenic archaea (Urai et al., submitted). It is considered that a vast

amount of CH_4 is produced by these microorganisms as they decompose the organic matter. In contrast, the value of $\delta^{13}C_{CO2}$ in site #3 was −3.0 ± 1.9 ‰, which was different from site #1 and #2, suggesting that the effect of active exchange with atmospheric CO_2 is more significant than the isotope effect of methanogenesis.

As for radioisotopic signature, both values of $\Delta^{14}C_{CH4}$ and $\Delta_{14}C_{CO2}$ in site #3 were +21.7 ± 3.8 ‰ and +6.2 ± 3.9 ‰, respectively, indicating that these carbons have a typical range of modern carbon origin (Table 13). Although ^{14}C measurements for benthic sediments have not been performed in the present study, there is a river in the vicinity of site #3, which potentially provides a constant supply of fresh organic matter. In future work, ^{14}C measurements of benthic sediments should be performed to define the origin of CH_4 and CO_2 better.

6.3.3 Interaction between deep carbon and surface ecology

The values of $\Delta^{14}C_{DIC}$ in site #1, #2, and #3 were −630.6 ± 1.7 ‰, −103.1 ± 4.0 ‰, and −100.9 ± 3.5 ‰, respectively (Table 13). These samples were collected from surface water in Lake Suwa, an environment where the supply of atmospheric CO_2 is actively occurring. If the only source of DIC in the lake water is atmospheric CO_2, the DIC takes the same value as atmospheric CO_2 ($\Delta^{14}C = \pm 0$ ‰). The results clearly indicate that some CH_4 and CO_2, which do not contain ^{14}C, are dissolved in lake water when the deep gases are released into the lake water. Figure 31 summarized the isotopic data as a cross plot between the $\delta^{13}C$ and $\Delta^{14}C$ for CH_4, DIC, and CO_2, including the data of cyanobacterial

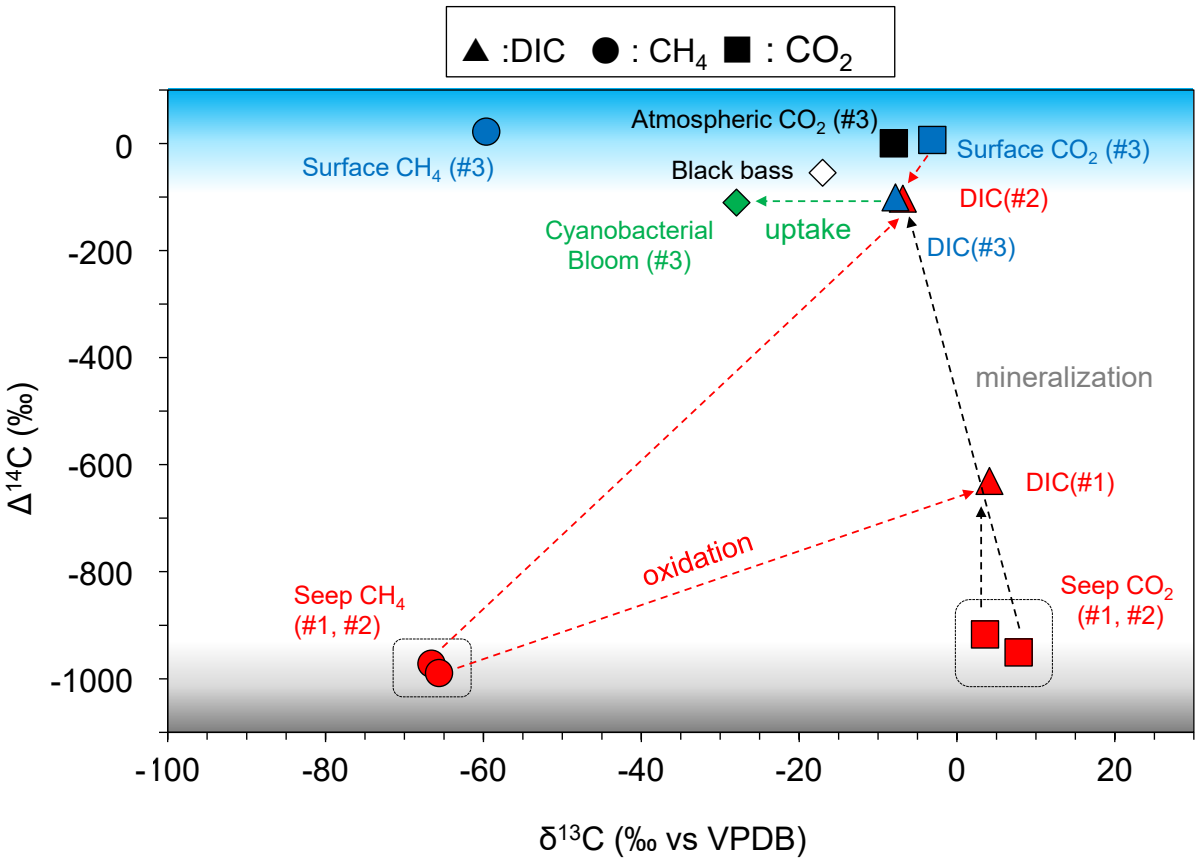

Figure 31. Diagram showing carbon isotopic composition ($\delta^{13}C$, ‰ vs. VPDB) and radiocarbon isotopic composition ($\Delta^{14}C$, ‰) of methane, CO_2, and dissolved inorganic carbon (DIC). Planktonic cyanobacterial bloom sample (Urai et al., submitted) and a bone collagen sample of black bass (Micropterus) (Miyata et al., 2011) collected from lake Suwa are also compiled for further understanding the carbon cycle and the interaction with ^{14}C-depleted deep methane sources.

bloom and black bass collected from Lake Suwa (Miyata et al., 2011; Urai et al., submitted). Deep carbon (site #1 and #2), which is a ^{14}C-depleted, are plotted in the gray area (seep CH_4 and CO_2 in site #1 and #2), while atmospheric carbon, which is ^{14}C-rich, is plotted in the blue area (surface CH_4 and CO_2 in site #3). For the results of DIC, they are plotted below the blue area; especially, DIC in site #1 ($\Delta^{14}C = -630.6 \pm 1.7$ ‰) is plotted much closer to the gray area than that in site #2 and #3 ($\Delta^{14}C = -103.1 \pm 4.0$ ‰, -100.9 ± 3.5 ‰, respectively). It is considered that site #1 not only has a higher volume of spring up, but the gas is released into the lake water in the form of fine bubbles, which promotes the dissolution of CH_4 and CO_2 more than the other sites. Considering the DIC carbon source as atmospheric- and deep-origin end-members, 63.0 % of DIC (#1), 10.3 % of DIC (#2) and 11.0 % of DIC (#3) are affected by deep-carbon. These results, especially considering the lack of a seep site in the vicinity of site #3, suggest that deep-carbon contributes to the DIC in Lake Suwa as a carbon source.

Furthermore, we performed ^{14}C measurements for cyanobacterial bloom collected from site #3 (Urai et al., submitted) to elucidate the contribution of deep-carbon to the lake ecosystem. The $\delta^{13}C$ and $\Delta^{14}C$ values of cyanobacterial bloom were -27.9 ± 0.7 ‰ and -110.3 ± 2.7 ‰, respectively (Table 13), which was the same ranges as the $\Delta^{14}C_{DIC}$ in site #2 and #3. Since algae use DIC as a carbon source, the $\Delta^{14}C$ values of algae are generally consistent with that of DIC (McCallister et al., 2018; Larsen et al., 2018). The results suggest that deep carbon originated from CH_4 is taken up by algae, including cyanobacteria, via DIC, and that potentially is spreading within the lake ecosystem. Miyata et al. (2011) performed ^{14}C measurements for black bass collected from freshwater lakes and reported

that the $\Delta^{14}C$ value of black bass collected from Lake Suwa was −55 ‰ (Figure 31), supporting the hypothesis of the present study. In contrast, benthic organisms (e.g., aquatic insects) have been reported to take up benthic CH_4 as a carbon source by preying on methane-oxidizing bacteria (MOB)(Kankaala et al., 2010; Yasuno et al., 2010; Jones and Grey, 2011; Brett et al., 2017). MOB (e.g., *Methylococcales* and *Methylococcales*) has been detected in the benthic sediments in Lake Suwa (Urai et al., submitted), suggesting that benthic organisms using MOB as a carbon source are taking up ^{14}C-rich CH_4; It means that the benthic organisms have low $\delta^{13}C$ values and high $\Delta^{14}C$ values. In addition, it has been reported that $\Delta^{14}C$ values of compound (e.g., chlorophylls and fatty acids) were different from those of bulk samples (e.g., Ishikawa et al., 2015,2020; Yamamoto et al., 2020). We note that these processes should be considered when we apply ^{14}C measurements to food web analysis in Lake Suwa.

Chapter 7. Executive Summary

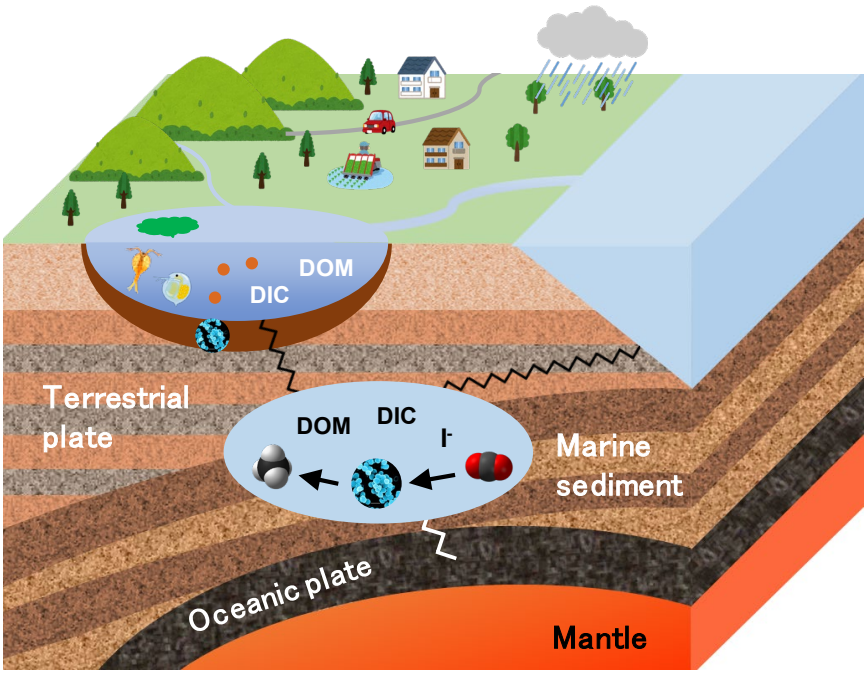

7.1 Biogeochemical carbon cycle: elucidating of interactions between the surface and deep subsurface

Microorganisms are closely related to the global carbon cycle to produce, decompose, and recycle organic matter. Since the focus on global warming issues for the past hundred years, the research to evaluate these microbial functions has been dramatically increased. While the carbon cycle in the surface and deep subsurface has been studied independently, there can be an interaction between the surface and deep subsurface (Figure 2). In this thesis, we assessed the microorganism's function on the carbon cycle focused in lake ecosystems and deep aquifer and elucidated the interaction of the carbon cycle between the surface and deep subsurface using the biomarkers and their isotopic ratios.

7.2 Freshwater environment with eukaryote community

The surface hydrosphere is an ecosystem composed mainly of eukaryotes. In terrestrial waters, including the surface ocean, the hydrosphere plays supply sediments with organic matter derived from terrestrial areas, and aquatic organisms in the hydrosphere plays decomposition, concentration, and reproduction of the organic matter (e.g., Bolin et al., 1979). Dissolved organic matter (DOM) accounts for 95% of the total organic carbon in the hydrosphere and is originated from multiple sources such as terrestrial plants and aquatic organisms (e.g., Repeta, 2015; Hansell and Carlson, 2015). Although DOM is affected by complicated transformation and degradation reactions in aquatic environments (e.g., Benner et al., 1992; McCarthy et al., 1998; McCallister et al. 2006a, 2006b), the formation process of DOM and its interaction between particulate organic matter (POM) and high molecular

weight-DOM (HMW-DOM) is still enigmatic. To further elucidate the origin of DOM and its interactions, we analyzed the sterol compositions and isotope ratio of sterol using the phytoplankton (100-40μm), POM (40-0.6μm), HMW-DOM (0.6μm-1000Da), and total-DOM (<0.6μm) isolated from three lakes. Although phytoplankton, POM, and total-DOM demonstrated similar sterol composition, HMW-DOM was different trends; the former was dominated by cholesterol throughout the year, while the latter was dominated by stigmasterol, which is regarded as a terrestrial plant origin, and decreased in winter. The results suggested that HMW-DOM has a unique cycle in which interactions was isolated from POM and total-DOM in the lakes. From the carbon and hydrogen isotope analysis of individual sterol, stigmasterol in HMW-DOM was strongly affected by a source of autochthonous algae in the lakes.

Phytoplankton and zooplankton, a primary source of POM and DOM, are the most important in lake ecosystems as primary producers and primary consumers. Although the primary consumers' biomass is controlled by that of primary producers, previous studies observed that many zooplankton are present in lakes where the biomass of phytoplankton is extremely low. In such an environment, the biological carbon cycle may behave differently than ordinary. The carbon and nitrogen isotopic ratio of bulk samples is widely applied for food web analysis (e.g., Lee et al., 2002; Wada, 2009). However, this method has a problem of large errors in food wed analysis because of the wide spatiotemporal variation of isotope ratios. In this study, understanding the foraging strategy of two dominant freshwater zooplankton species in an oligotrophic lake, we applied the method for estimating the

trophic position (TP) based on the nitrogen isotope ratio of amino acids in an oligotrophic lake, Shirakoma-ike. The surface water of this lake is frozen in winter, and the daphnia is found only in spring-autumn, whereas the copepod is found in a whole season. We found that the TP is 2.1±0.0 for the daphnia in spring-autumn and 2.3±0.3 for the copepod in a whole season, suggesting the strong herbivory for the daphnia compared to dietary plasticity and facultative omnivory for the copepod. The insight may explain why the daphnia is absent, whereas the copepod is present in the frozen lake in winter, where primary production is limited.

7.3 Deep aquifer environment with Prokaryote

The deep subsurface hydrosphere is an ecosystem dominated by eukaryotes (bacteria and archaea). Previous studies reported that archaeal biomass increased with depth (e.g, Lipp et al., 2008; Biddle et al., 2006, 2008), and that methanogenic archaea was detected in a marine sediment down to 2.5 km below the seafloor (e.g., Inagaki et al., 2015; Sass et al., 2019). Methanogenic archaea produce methane from carbon dioxide with hydrogen, acetic acid, and alcohol; this process is a final decomposer of organic matter. However, the ecology of methanogenic archaea still unclear because culture-based studies of methanogenic archaea are limited (Teske and Sorensen, 2008; Imachi et al., 2011; Mayumi et al.,2016). Coenzyme factor 430 (F430) is a compound-specific to all methanogenic archaea and can evaluate the ecology of in situ methanogenic archaea (e.g., Thauer et al., 2008). To elucidate the ecology of methanogenic archaea in deep methane-rich aquifer at the Southern Kanto gas

field, we performed parallel approaches; F430 analysis, small sub-unit rRNA gene sequencing, and membrane lipid analysis. Lipid analysis indicated that the biomass of archaea was less than 10% of the total population, and the SSU rRNA gene sequencing supported the estimation of the proportions. We successfully detected a high concentration of F430 in the absence of the F430 epimer in the deep aquifer, strongly indicating that high active methanogenesis potential mediated by the subsurface microbes. In addition, radiocarbon measurement ($^{14}C/^{12}C$) was also performed to assess the origin and fate of methane in the deep aquifer. Although Southern Kanto gas field is located at Boso Peninsula where are alternating beds of sandstone and mudstone, with potential water-permeable layers, radiocarbon measurements of methane and dissolved inorganic carbon (DIC) revealed ^{14}C-depleted (both $\Delta^{14}C_{methane}$ and $\Delta^{14}C_{DIC}$, <−997.4‰). The results suggest that modern carbon has contributed little to the deep subsurface, and that active living methanogenic archaea produce methane using a ^{14}C-depleted substrate.

7.4 Interaction between surface and subsurface hydrosphere with methane cycle

In this study, we separately elucidated the organism's function and the carbon cycle in lakes and deep aquifer. In contrast, deep carbon can affect the ecosystem and carbon cycle in the surface hydrosphere. Lake Suwa has a thick sedimentary layer (>370m), which contains a large amount of methane dissolved in deep aquifer. Therefore, the lake has two different sources of methane emissions; one is seeping from the deep sub-surface and the other is produced in the benthic sediment (e.g., Iwata

et al., 2020). Deep methane is released to the atmosphere via the lake water, and some methane may be dissolved in the lake water and converted to DIC, which affects the lake's carbon cycle and ecosystem. In this study, we performed radiocarbon measurements of deep methane and carbon dioxide to assess the contribution of methane to the lake ecosystem. Radiocarbon measurements of deep methane and carbon dioxide was depleted ($\Delta^{14}C_{methane}$ <−972.1‰), and DIC and cyanobacterial bloom (Aoko) collected from surface lake water contained ^{14}C-depleted carbon ($\Delta^{14}C_{DIC}$ = −630.6 to −103.1‰ and $\Delta^{14}C_{aoko}$ = −110.3‰), suggesting that 10-60% of DIC is affected by deep methane, which is also propagated through phytoplankton into lake ecosystems.

In addition, we successfully detected F430 in cyanobacterial bloom. Although methanogenic archaea is found only in anaerobic environments, previous studies reported that methane accumulation was observed under aerobic conditions such as oceans and lakes, which was call “methane Paradox” (e.g., Tang et al., 2016; Günthel et al., 2019). This result suggests the coexistence of methanogenic archaea with cyanobacterial bloom in the lake water under aerobic conditions and may provide insight into the methane paradox.

Appendix. The vent flora in KTG3

Acknowledgments

There are many people whom I would like to thank for their contribution, both directly and indirectly, to this thesis. I am deeply grateful to my supervisor, Prof. Ho Dong Park (Env. Sci, Shinshu Univ.) and Dr. Yoshinori Takano (BGC, JAMSTEC), for helpful support of my Ph.D. life. I would also like to thank Drs. Naohiko Ohkouchi, Nanako O Ogawa, Naoto F Ishikawa, Toshihiro Yoshimura, Yuta Isaji (BGC, JAMSTEC), and other BGC group members for your assistance and suggestions throughout my research.

It would not have been possible to write my Ph. D. thesis without the help and support of the kind people around me, to only some of whom it is possible to give particular mention here:

Drs. Hiroyuki Imachi, Shun'ichi Ishii, and Yohei Matsui (X-star, JAMSTEC) for cooperation and helpful discussions for my papers.

Dr. Masanori Kaneko, Satoshi Furota, and Makoto Matsushita (GSJ, AIST) for technical support with the coenzyme F430 analysis and helpful discussions.

Prof. Yusuke Yokoyama and Dr. Yosuke Miyairi (AORI, Univ. Tokyo) for performing the ^{14}C measurements and helpful discussions.

Profs. Hiroki Iwata and Yuichi Miyabara (Env. Sci, Shinshu Univ.) for providing assistance with our field survey and helpful discussions.

References

Amachi, S., Muramatsu, Y., Akiyama, Y., Miyazaki, K., Yoshiki, S., Hanada, S., Kamagata, Y., Bannai, T., Shinoyama, H., and Fujii, T. Isolation of iodide-oxidizing bacteria from iodide-rich natural gas brines and seawaters. *Microb. Ecol.* **49**, 547-557, 2005.

Amachi, S. Microbial Contribution to global iodine cycling: volatilization, accumulation, reduction, oxidation, and sorption of iodine. *Microbes Environ.* **23**, 269-276, 2008.

Angel, R., Matthies, D. and Conrad, R. Activation of methanogenesis in arid biological soil crusts despite the presence of oxygen. *PLoS One* **6**, 20453, 2011.

Anma, K., Nagaoka, M., Niwa, S., Sekimoto, K., Yoshioka, M., and Fujine, H. A geological survey for the study on neotectonic movement and geoenvironment of Lake Suwa, Nagano prefecture. *Mem. Geol. Soc. Jpn.* **36**, 179-194, 1990. (in Japanese with English abstract)

Baird, B. H., Nivens, D. E., Parker, J. H., and White, D. C. The biomass, community structure, and spatial distribution of the sedimentary microbiota from a high-energy area of the deep sea. *Deep Sea Research Part A. Oceanographic Research Papers* **32**, 1089-1099, 1985.

Bastviken, D., Ejlertsson, J., and Tranvik, L. Measurement of methane oxidation in lakes: a comparison of methods. *Environ. Sci. Technol.* **36**, 3354-3361, 2002.

Bastviken, D., Cole, J., Pace, M., and Tranvik, L. Methane emissions from lakes: dependence of lake characteristics, two regional assessments, and a global estimate. *Global Biogeochem. Cycles* **18**, GB4009, 2004.

Batista, A. M. M., Woodhouse, J. N., Grossart, H. P., and Giani, A. Methanogenic archaea associated to *Microcystis* sp. in field samples and in culture. *Hydrobiologia* **831**, 163-172, 2019.

Beaulieu, J. J., DelSontro, T.and Downing, J. A. Eutrophication will increase methane emissions from lakes and impoundments during the 21st century. *Nat. Commun.* **10**, 1375, 2019.

Belay, N. and Daniels, L. Ethane production by *Methanosarcina barkeri* during growth in ethanol supplemented medium. *Antonie Van Leeuwenhoek* **54**, 113-125, 1988.

Benner, R., Pakulski, J. D., McCarthy, M., Hedges, J. I., and Hatcher, P. G. Bulk chemical characteristics of dissolved organic matter in the ocean. *Science* **255**, 1561-1564, 1992.

Benner, R., Biddanda, B., Black, B., and McCarthy, M. Abundance, size distribution, and stable carbon and nitrogen isotopic compositions of marine organic matter isolated by tangential-flow ultrafiltration. *Mar. Chem.* **57**, 243-263, 1997.

Berg, A., Lindblad, P., and Svensson, B. H. Cyanobacteria as a source of hydrogen for methane formation. *J. Microbiol. Biotechnol.* **30**, 539-545, 2014.

Bernard, B., Brooks, J. M., and Sackett, W. M. A Geochemical model for characterization of hydrocarbon gas sources in marine sediments. *Offshore Technol. Conf.* 1977.

Biddle, J. F., Lipp, J. S., Lever, M. A., Lloyd, K. G., Sorensen, K. B., Anderson, R., Fredricks, H. F., Elvert, M., Kelly, T. J., Schrag, D. P., Sogin, M. L., Brenchley, J. E., Teske, A., House, C. H., and Hinrichs, K. U. Heterotrophic Archaea dominate sedimentary subsurface ecosystems off Peru. *Proc. Natl. Acad. Sci.* **103**, 3846-3851, 2006.

Biddle, J. F. and Teske, A. P. A genetic view of diversity beneath the seafloor. *Geochim. Cosmochim. Acta* **72**, A83-A83, 2008.

Bižić, M., Klintzsch, T., Ionescu, D., Hindiyeh, M. Y., Gunthel, M., Muro-Pastor, A. M., Eckert, W., Urich, T., Keppler, F., and Grossart, H. P. Aquatic and terrestrial cyanobacteria produce methane. *Sci. Adv.* **6**, eaax5343, 2020.

Blair, N., Leu, A., Munoz, E., Olsen, J., Kwong, E., and Des Marais, D. Carbon isotopic fractionation in heterotrophic microbial metabolism. *Appl. Environ. Microbiol.* **50**, 996-1001, 1985.

Blattmann, T. M., Wang, S. L., Lupker, M., Märki, L., Haghipour, N., Wacker, L., Chung, L. H., Bernasconi, S. M., Plötze, M., and Eglinton, T. I. Sulphuric acid-mediated weathering on Taiwan buffers geological atmospheric carbon sinks. *Sci. Rep.* **9**, 2945, 2019.

Bolin, B., Degens, E.T., Kempe, S., and Ketner, P. *Global carbon cycle*. John Wiley and Sons, New York, 1979.

Borrel, G., Jézéquel, D., Biderre-Petit, C., Morel-Desrosiers, N., Morel, J.P., Peyret, P., Fonty, G., and Lehours, A.C. Production and consumption of methane in freshwater lake ecosystems. *Res. Microbiol.* **162**, 832-847, 2011.

Braun, S., Morono, Y., Becker, K. W., Hinrichs, K.U., Kjeldsen, K. U., Jørgensen, B. B., and Lomstein, B. A. Cellular content of biomolecules in sub-seafloor microbial communities. *Geochim. Cosmochim. Acta* **188**, 330-351, 2016.

Brett, M. T., Bunn, S. E., Chandra, S., Galloway, A. W. E., Guo, F., Kainz, M. J., Kankaala, P., Lau, D.

C. P., Moulton, T. P., Power, M. E., Rasmussen, J. B., Taipale, S. J., Thorp, J. H., and Wehr, J. D. How important are terrestrial organic carbon inputs for secondary production in freshwater ecosystems? *Freshw. Biol.* **62**, 833-853, 2017.

Buckles, L. K., Villanueva, L., Weijers, J. W., Verschuren, D., and Damste, J. S. Linking isoprenoidal GDGT membrane lipid distributions with gene abundances of ammonia-oxidizing Thaumarchaeota and uncultured crenarchaeotal groups in the water column of a tropical lake (Lake Challa, East Africa). *Environ. Microbiol.* **15**, 2445-2462, 2013.

Bukin, S. V., Pavlova, O. N., Kalmychkov, G. V., Ivanov, V. G., Pogodaeva, T. V., Galach'Yants, Y. P., Bukin, Y. S., Khabuev, A. V., and Zemskaya, T. I. Substrate specificity of methanogenic communities from lake baikal bottom sediments associated with hydrocarbon gas discharge. *Microbiology* **87**, 549-558, 2018.

Burke, R. A., Reid, D. F., Brooks, J. M., and Lavoie, D. M. Upper water column methane geochemistry in the eastern tropical North Pacific1. *Limnol Oceanogr.* **28**, 19-32, 1983.

Caporaso, J. G., Kuczynski, J., Stombaugh, J., Bittinger, K., Bushman, F. D., Costello, E. K., Fierer, N., Peña, A. G., Goodrich, J. K., Gordon, J. I., Huttley, G. A., Kelley, S. T., Knights, D., Koenig, J. E., Ley, R. E., Lozupone, C. A., McDonald, D., Muegge, B. D., Pirrung, M., Reeder, J., Sevinsky, J. R., Turnbaugh, P. J., Walters, W. A., Widmann, J., Yatsunenko, T., Zaneveld, J., and Knight, R. QIIME allows analysis of high-throughput community sequencing data. *Nat. Methods* **7**, 335-336, 2010.

Carvalho, G. R., and Wolf, H. G. Resting eggs of lake- Daphnia I. Distribution, abundance and hatching of eggs collected from various depths in lake sediments. *Freshw. Biol.* **22**, 459-470, 1989.

Chan, O. C., Claus, P., Casper, P., Ulrich, A., Lueders, T., and Conrad, R. Vertical distribution of structure and function of the methanogenic archaeal community in Lake Dagow sediment. *Environ. Microbiol.* **7**, 1139-1149, 2005.

Chen, W. M., Xie, P. B., Young, C. C., and Sheu, S. Y. *Formosimonas limnophila* gen. nov., sp. nov., a new member of the family Burkholderiaceae isolated from a freshwater lake. *Int. J. Syst. Evol. Microbiol.* **67**, 17-24, 2017.

Chikaraishi, Y., Naraoka, H., and Poulson, S. R. Hydrogen and carbon isotopic fractionations of lipid biosynthesis among terrestrial (C3, C4 and CAM) and aquatic plants. *Phytochemistry* **65**, 1369-1381, 2004.

Chikaraishi, Y., Yamada, Y., and Naraoka, H. Carbon and hydrogen isotopic compositions of sterols from riverine and marine sediments. *Limnol. Oceanogr.* **50**, 1763-1770, 2005.

Chikaraishi, Y. Carbon and hydrogen isotopic composition of sterols in natural marine brown and red macroalgae and associated shellfish. *Org. Geochem.* **37**, 428-436, 2006.

Chikaraishi, Y., Kashiyama, Y., Ogawa, O. N., Kitazato, H., and Ohkouchi, N. Metabolic control of nitrogen isotope composition of amino acids in macroalgae and gastropods: implications for aquatic food web studies. *Mar. Ecol. Prog. Ser.* **342**, 85-90, 2007.

Chikaraishi, Y., Ogawa, N. O., Kashiyama, Y., Takano, Y., Suga, H., Tomitani, A., Miyashita, H.,

Kitazato, H., and Ohkouchi, N. Determination of aquatic food-web structure based on compound-specific nitrogen isotopic composition of amino acids. *Limnol. Oceanogr. Methods* **7**, 740-750, 2009.

Chikaraishi, Y., Steffan, S. A., Ogawa, N. O., Ishikawa, N. F., Sasaki, Y., Tsuchiya, M., and Ohkouchi, N. High-resolution food webs based on nitrogen isotopic composition of amino acids. *Ecol. Evol.* **4**, 2423-2449, 2014.

Chikaraishi, Y., Steffan, S. A., Takano, Y., and Ohkouchi, N. Diet quality influences isotopic discrimination among amino acids in an aquatic vertebrate. *Ecol. Evol.* **5**, 2048-2059, 2015.

Choi, B., Takizawa, Y., and Chikaraishi, Y. Compression of trophic discrimination in $^{15}N/^{14}N$ within amino acids for herbivorous gastropods. *Res. Org. Geochem.* **34**, 29-35, 2018.

Cole, J. J., Prairie, Y. T., Caraco, N. F., McDowell, W. H., Tranvik, L. J., Striegl, R. G., Duarte, C. M., Kortelainen, P., Downing, J. A., Middelburg, J. J., and Melack, J. Plumbing the global carbon cycle: integrating inland waters into the terrestrial carbon budget. *Ecosystems* **10**, 172-185, 2007.

Cole, J. J., Carpenter, S. R., Kitchell, J., Pace, M. L., Solomon, C. T., and Weidel, B. Strong evidence for terrestrial support of zooplankton in small lakes based on stable isotopes of carbon, nitrogen, and hydrogen. *Proc. Natl. Acad. Sci.* **108**, 1975-1980, 2011.

Conrad, R. The global methane cycle: recent advances in understanding the microbial processes involved. *Environ. Microbiol. Rep.* **1**, 285-292, 2009.

Damm, E., Helmke, E., Thoms, S., Schauer, U., Nöthig, E., Bakker, K., and Kiene, R. P. Methane production in aerobic oligotrophic surface water in the central Arctic Ocean. *Biogeosciences* **7**, 1099-1108, 2010.

de Angelis, M. A., and Lee, C. Methane production during zooplankton grazing on marine phytoplankton. *Limnol.Oceanogr.* **39**, 1298-1308, 1994.

Décima, M., Landry, M. R., Bradley, C. J., and Fogel, M. L. Alanine $\delta^{15}N$ trophic fractionation in heterotrophic protists. *Limnol. Oceanogr.* **62**, 2308-2322, 2017.

Deutzmann, J. S., Stief, P., Brandes, J., and Schink, B. Anaerobic methane oxidation coupled to denitrification is the dominant methane sink in a deep lake. *Proc. Natl. Acad. Sci.* **111**, 18273-18278, 2014.

Diekert, G., Konheiser, U., Piechulla, K., and Thauer, R. K. Nickel requirement and factor F430 content of methanogenic bacteria. *J. Bacteriol.* **148**, 459-464, 1981.

Donis, D., Flury, S., Stöckli, A., Spangenberg, J. E., Vachon, D., and McGinnis, D. F. Full-scale evaluation of methane production under oxic conditions in a mesotrophic lake. *Nat. Commu.* **8**, 1661, 2017.

Duin, E. C. Role of coenzyme F430 in methanogenesis in *Tetrapyrroles: Birth, Life and Death* (eds Martin J. W. and Alison G. S.). Springer New York, 352-374, 2009.

Dziallas, C. and Grossart, H. P. Microbial interactions with the cyanobacterium *Microcystis aeruginosa* and their dependence on temperature. *Mar. Biol.* **159**, 2389-2398, 2012.

Ebert., D. *Ecology, Epidemiology and Evolution of Parasitism in Daphnia*. Bethesda (MD): National Library of Medicine (US), National Center for Biotechnology Information, 2005.

Edgar, R. C. Search and clustering orders of magnitude faster than BLAST. *Bioinformatics* **26**, 2460-2461, 2010.

Encinas Fernández, J., Peeters, F., and Hofmann, H. On the methane paradox: Transport from shallow water zones rather than in situ methanogenesis is the major source of CH_4 in the open surface water of lakes. *J Geophys. Res. Biogeosci.* **121**, 2717-2726, 2016.

Ermler, U., Grabarse, W., Shima, S., Goubeaud, M., and Thauer, R. K. Crystal Structure of methyl-coenzyme M reductase: The key enzyme of biological methane formation. *Science* **278**, 1457-1462, 1997.

Evans, P. N., Parks, D. H., Chadwick, G. L., Robbins, S. J., Orphan, V. J., Golding, S. D., and Tyson, G. W. Methane metabolism in the archaeal phylum Bathyarchaeota revealed by genome-centric metagenomics. *Science* **350**, 434-438, 2015.

Frisch, W., Meschede, M., and Blakey, R. C. *Plate tectonics: continental drift and mountain building*. Springer, 2011.

Fukushima, K., Sasaki, T., and Park, H. D. Methylalkane composition of cultured strains of cyanophytae, *Microcystis* sp. *SIL Proceedings* **29**, 1280-1284, 2006.

Günthel, M., Donis, D., Kirillin, G., Ionescu, D., Bizic, M., McGinnis, D. F., Grossart, H.P., and Tang, K. W. Contribution of oxic methane production to surface methane emission in lakes and its

global importance. *Nat. Commun.* **10**, 5497, 2019.

Gantner, S., Andersson, A. F., Alonso-Sáez, L., and Bertilsson, S. Novel primers for 16S rRNA-based archaeal community analyses in environmental samples. *J. Microbiol. Methods* **84**, 12-18, 2011.

Goldfine, H. Lipids of Prokaryotes–structure and distribution in *Current Topics in Membranes and Transport Vol. 17* (eds Felix, B. and Arnost, K.) Academic Press, Oxford, 1-43, 1982.

Grossart, H. P., Frindte, K., Dziallas, C., Eckert, W., and Tang, K. W. Microbial methane production in oxygenated water column of an oligotrophic lake. *Proc. Natl. Acad. Sci.* **108**, 19657-19661, 2011. (ここまで)

Gutiérrez-Rodríguez, A., Décima, M., Popp, B. N., and Landry, M. R. Isotopic invisibility of protozoan trophic steps in marine food webs. *Limnol. Oceanogr.* **59**, 1590-1598, 2014.

Haghipour, N., Ausin, B., Usman, M. O., Ishikawa, N., Wacker, L., Welte, C., Ueda, K., and Eglinton, T. I. Compound-specific radiocarbon analysis by elemental analyzer–accelerator mass spectrometry: Precision and limitations. *Anal. Chem.* **91**, 2042-2049, 2019.

Hairston, N. G., Smith, F. E., and Slobodkin, L. B. Community structure, population control, and competition. *The American Naturalist* **94**, 421-425, 1960.

Hansell, D. A. and Carlson, C. A. *Biogeochemistry of Marine Dissolved Organic Matter. 2nd ed.*, Elsevier., 2015.

Hirabayashi, S., Yokoyama, Y., Suzuki, A., Miyairi, Y., and Aze, T. Multidecadal oceanographic changes in the western Pacific detected through high-resolution bomb-derived radiocarbon

measurements on corals. *Geochem Geophys. Geosys.* **18**, 1608-1617, 2017.

Hirahara, M., Chikaraishi, Y., and Toda, T. Isotopic discrimination of ^{15}N /^{14}N of amino acids among the calanoid copepod Acartia steueri and its food items, eggs, and fecal pellets. *Res.Org. Geochem.* **31**, 29-32, 2015.

Hirai, M., Nishi, S., Tsuda, M., Sunamura, M., Takaki, Y., and Nunoura, T. Library construction from subnanogram DNA for pelagic sea water and deep-sea sediments. *Microbes Environ.* **32**, 336-343, 2017.

Holgerson, M. A. and Raymond, P. A. Large contribution to inland water CO_2 and CH_4 emissions from very small ponds. *Nat. Geosci.* **9**, 222-226, 2016.

Igari, S. and Sakata, S. Origin of natural gas of dissolved-in-water type in Japan inferred from chemical and isotopic compositions: Occurrence of dissolved gas of thermogenic origin. *Geochem. J.* **23**, 139-142, 1989.

Ikeda, Y., Iwasaki, T., Sato, H., Matsuta, N., and Kozawa, T. Seismic reflection profiling across the Itoigawa-Shizuoka Tectonic Line at Matsumoto, Central Japan. *Earth, Planets and Space* **56**, 1315-1321, 2004.

Imachi, H., Aoi, K., Tasumi, E., Saito, Y., Yamanaka, Y., Saito, Y., Yamaguchi, T., Tomaru, H., Takeuchi, R., Morono, Y., Inagaki, F., and Takai, K. Cultivation of methanogenic community from subseafloor sediments using a continuous-flow bioreactor. *ISME J.* **5**, 1913-1925, 2011.

Imachi, H., Tasumi, E., Takaki, Y., Hoshino, T., Schubotz, F., Gan, S., Tu, T. H., Saito, Y., Yamanaka,

Y., Ijiri, A., Matsui, Y., Miyazaki, M., Morono, Y., Takai, K., Hinrichs, K. U., and Inagaki, F. Cultivable microbial community in 2-km-deep, 20-million-year-old subseafloor coalbeds through ~1000 days anaerobic bioreactor cultivation. *Sci. Rep.* **9**, 2305, 2019.

Inagaki, F., Hinrichs, K. U., Kubo, Y., Bowles, M. W., Heuer, V. B., Hong, W. L., Hoshino, T., Ijiri, A., Imachi, H., Ito, M., Kaneko, M., Lever, M. A., Lin, Y. S., Methé, B. A., Morita, S., Morono, Y., Tanikawa, W., Bihan, M., Bowden, S. A., Elvert, M., Glombitza, C., Gross, D., Harrington, G. J., Hori, T., Li, K., Limmer, D., Liu, C. H., Murayama, M., Ohkouchi, N., Ono, S., Park, Y. S., Phillips, S. C., Prieto-Mollar, X., Purkey, M., Riedinger, N., Sanada, Y., Sauvage, J., Snyder, G., Susilawati, R., Takano, Y., Tasumi, E., Terada, T., Tomaru, H., Trembath-Reichert, E., Wang, D. T., and Yamada, Y. Exploring deep microbial life in coal-bearing sediment down to ~2.5 km below the ocean floor. *Science* **349**, 420-424, 2015.

Isaji, Y., Ogawa, N. O., Takano, Y., and Ohkouchi, N. Quantification and carbon and nitrogen isotopic measurements of heme B in environmental samples. *Anal. Chem.* **92**, 11213-11222, 2020.

Ishii, S., Imachi, H., Kawano, K., Murai, D., Ogawara, M., Uemastu, K., Nealson, K. H., and Inagaki, F. Bioelectrochemical stimulation of electromethanogenesis at a seawater-based subsurface aquifer in a natural gas field. *Front. Energy Res.* **6**, 144, 2019.

Ishikawa, N. F., Hyodo, F., and Tayasu, I. Use of carbon-13 and carbon-14 natural abundances for stream food web studies. *Ecol. Res.* **28**, 759-769, 2013.

Ishikawa, N. F., Yamane, M., Suga, H., Ogawa, N. O., Yokoyama, Y., and Ohkouchi, N. Chlorophyll

a-specific $\Delta^{14}C$, $\delta^{13}C$ and $\delta^{15}N$ values in stream periphyton: implications for aquatic food web studies. *Biogeosciences* **12**, 6781-6789, 2015.

Ishikawa, N. F., Itahashi, Y., Blattmann, T. M., Takano, Y., Ogawa, N. O., Yamane, M., Yokoyama, Y., Nagata, T., Yoneda, M., Haghipour, N., Eglinton, T. I., and Ohkouchi, N. Improved method for isolation and purification of underivatized amino acids for radiocarbon analysis. *Anal. Chem.* **90**, 12035-12041, 2018.

Ishikawa, N. F., Butman, D., and Raymond, P. A. Radiocarbon age of different photoreactive fractions of freshwater dissolved organic matter. *Org. Geochem.* **135**, 11-15, 2019.

Ishikawa, N. F., Finlay, J. C., Uno, H., Ogawa, N. O., Ohkouchi, N., Tayasu, I., and Power, M. E. Combined use of radiocarbon and stable carbon isotopes for the source mixing model in a stream food web. *Limnol. Oceanogr.* **65**, 2688-2696, 2020.

Ito, K. Determination of iodide in seawater by ion chromatography. *Anal. Chem.* **69**, 3628-3632, 1997.

Ito, K., Nakajima, N., Yamamura, S., Tomita, M., Suzuki, H., and Amachi, S. Draft genome sequence of *Arenibacter* sp. Strain C-21, an iodine-accumulating bacterium isolated from surface marine sediment. *Genome Announcements* **4**, e01155-01116, 2016.

Ito, M., Ishimoto, S., Ito, K., and Kotake, N. Geometry and lithofacies of coarse-grained injectites and extrudites in a late Pliocene trench-slope basin on the southern Boso Peninsula, Japan. *Sediment. Geol.* **344**, 336-349, 2016.

Ito, T. Preservation potential of seasonal laminated deposits as a useful tool for environmental analysis

in mesotrophic Lake Kizaki, central Japan. *J. Asian Earth Sci.* **73**, 139-148, 2013.

Itoh, M., Kobayashi, Y., Chen, T. Y., Tokida, T., Fukui, M., Kojima, H., Miki, T., Tayasu, I., Shiah, F. K., and Okuda, N. Effect of interannual variation in winter vertical mixing on CH_4 dynamics in a subtropical reservoir. *J. Geophys. Res. Biogeosci.* **120**, 1246-1261, 2015.

Iwata, H., Hirata, R., Takahashi, Y., Miyabara, Y., Itoh, M., and Iizuka, K. Partitioning eddy-covariance methane fluxes from a shallow lake into diffusive and ebullitive fluxes. *Boundary-Layer Meteorol.* **169**, 413-428, 2018.

Iwata, H., Nakazawa, K., Sato, H., Itoh, M., Miyabara, Y., Hirata, R., Takahashi, Y., Tokida, T., and Endo, R. Temporal and spatial variations in methane emissions from the littoral zone of a shallow mid-latitude lake with steady methane bubble emission areas. *Agricul. Forest Meteorol.* **295**, 2020.

Jansson, M., Bergström, A.-K., Blomqvist, P., and Drakare, S. Allochthonous organic carbon and phytoplankton/bacterioplankton production relationships in lakes. *Ecology* **81**, 3250-3255, 2000.

Jones, R. I. and Grey, J. Biogenic methane in freshwater food webs. *Freshw. Biol.* **56**, 213-229, 2011.

Kadota, S. Studies on the limnology of the lakes of Yatsugatake group-I: Observations on the feeding habits of the plankton of Lake Shirakoma. *Bull. Jpn. Soc. Scientif. Fisheries* **26**, 452-461, 1960.

Kaneko, M., Takano, Y., Chikaraishi, Y., Ogawa, N. O., Asakawa, S., Watanabe, T., Shima, S., Krüger, M., Matsushita, M., Kimura, H., and Ohkouchi, N. Quantitative analysis of coenzyme F430 in

environmental samples: a new diagnostic tool for methanogenesis and anaerobic methane oxidation. *Anal. Chem.* **86**, 3633-3638, 2014.

Kaneko, M., Takano, Y., Ogawa, N. O., Sato, Y., Yoshida, N., and Ohkouchi, N. Estimation of methanogenesis by quantification of coenzyme F430 in marine sediments. *Geochem. J.* **50**, 453-460, 2016.

Kaneko, N., Maekawa, T., and Igari, S. Generation of archaeal methane and its accumulation mechanism into interestrial water. *J. Jpn. Pet. Inst.* **67**, 97-110, 2002. (in Japanese with English abstract)

Kankaala, P., Taipale, S., Li, L., and Jones, R. I. Diets of crustacean zooplankton, inferred from stable carbon and nitrogen isotope analyses, in lakes with varying allochthonous dissolved organic carbon content. *Aquat. Ecol.* **44**, 781-795, 2010.

Karlsson, J., Jonsson, A., Meili, M., and Jansson, M. Control of zooplankton dependence on allochthonous organic carbon in humic and clear-water lakes in northern Sweden. *Limnol. Oceanogr.* **48**, 269-276, 2003.

Katayama, T., Yoshioka, H., Muramoto, Y., Usami, J., Fujiwara, K., Yoshida, S., Kamagata, Y., and Sakata, S. Physicochemical impacts associated with natural gas development on methanogenesis in deep sand aquifers. *ISME J.* **9**, 436-446, 2015.

Kate, M. Membrane lipids of archaea *in New Comprehensive Biochemistry Vol. 26* (eds Kate, M., Kushner, D. J., and Matheson, A. T.) Elsevier, 261-295, 1993.

Kawagucci, S., Ueno, Y., Takai, K., Toki, T., Ito, M., Inoue, K., Makabe, A., Yoshida, N., Muramatsu, Y., Takahata, N., Sano, Y., Narita, T., Teranishi, G., Obata, H., Nakagawa, S., Nunoura, T., and Gamo, T. Geochemical origin of hydrothermal fluid methane in sediment-associated fields and its relevance to the geographical distribution of whole hydrothermal circulation. *Chem. Geol.* **339**, 213-225, 2013.

Kawagucci, S., Matsui, Y., and BernasconiGreen, G. Radiocarbon content of dioxide and methane in hydrothermal fluids of Okinawa Trough vents. *Geochem. J.* **54**, 129-138, 2020.

Kelsey, S. A., Grottoli, A. G., Bauer, J. E., Lorenz, K., Lal, R., Matsui, Y., and Huey-Sanders, T. M. Effects of agricultural and tillage practices on isotopic signatures and fluxes of organic and inorganic carbon in headwater streams. *Aquat. Sci.* **82**, 23, 2020.

Kessler, J. D., Reeburgh, W. S., Southon, J., and Varela, R. Fossil methane source dominates Cariaco Basin water column methane geochemistry. *Geophys. Res. Lett.* **32**, L12609, 2005.

Khaing, S. Y., Sugai, Y., and Sasaki, K. Gold dissolution from ore with iodide-oxidising bacteria. *Sci. Rep.* **9**, 4178, 2019.

Khatun, S., Iwata, T., Kojima, H., Fukui, M., Aoki, T., Mochizuki, S., Naito, A., Kobayashi, A., and Uzawa, R. Aerobic methane production by planktonic microbes in lakes. *Sci. Total Environ.* **696**, 133916, 2019.

Killops, S. and Killops, V. *introduction to organic geochemistry 2nd edition*. Blackwell publishing, Oxford, 2005.

Kim, M., Shin, B., Lee, J., Park, H. Y., and Park, W. Culture-independent and culture-dependent analyses of the bacterial community in the phycosphere of cyanobloom-forming *Microcystis aeruginosa. Sci. Rep.* **9**, 20416, 2019.

Koga, Y. and Nakano, M. A dendrogram of archaea based on lipid component parts composition and its relationship to rRNA phylogeny. *Syst. Appl. Microbiol.* **31**, 169-182, 2008.

Kojima, H., Tokizawa, R., Kogure, K., Kobayashi, Y., Itoh, M., Shiah, F.-K., Okuda, N., and Fukui, M. Community structure of planktonic methane-oxidizing bacteria in a subtropical reservoir characterized by dominance of phylotype closely related to nitrite reducer. *Sci. Rep.* **4**, 5728, 2014.

Krüger, M., Meyerdierks, A., Glöckner, F. O., Amann, R., Widdel, F., Kube, M., Reinhardt, R., Kahnt, J., Böcher, R., Thauer, R. K., and Shima, S. A conspicuous nickel protein in microbial mats that oxidize methane anaerobically. *Nature* **426**, 878, 2003.

Kruger, B. R., Werne, J. P., Branstrator, D. K., Hrabik, T. R., Chikaraishi, Y., Ohkouchi, N., and Minor, E. C. Organic matter transfer in Lake Superior's food web: Insights from bulk and molecular stable isotope and radiocarbon analyses. *Limnol. Oceanogr.* **61**, 149-164, 2016.

Kruse, S., Pakhomov, E. A., Hunt, B. P. V., Chikaraishi, Y., Ogawa, N. O., and Bathmann, U. Uncovering the trophic relationship between Themisto gaudichaudii and salpa thompsoni in the antarctic polar frontal zone. *Mar. Ecol. Prog. Ser.* **529**, 63-74, 2015.

Kunisue, S., Mita, I., and Waki, F. Relationship between subsurface geology and productivity of natural

gas and iodine in the Mobara gas field, Boso Peninsula, central Japan. *J. Jpn. Pet. Inst.* **67**, 83-96, 2002. (in Japanese with English abstract)

Larsen, T., Yokoyama, Y., and Fernandes, R. Radiocarbon in ecology: Insights and perspectives from aquatic and terrestrial studies. *Methods Ecol. Evol.* **9**, 181-190, 2018.

Lee, J. Y., Yoshioka, T., and Hanazato, T. Faunal trophic interaction in an oligotrophic-dystrophic lake (Shirakoma-ike, Japan). *Limnology* **3**, 0151-0158, 2002.

Li, M., Nkrumah, P. N., and Xiao, M. Biochemical composition of *Microcystis aeruginosa* related to specific growth rate: insight into the effects of abiotic factors. *Inland Waters* **4**, 357-362, 2014.

Lin, W., Byrne, T. B., Kinoshita, M., McNeill, L. C., Chang, C., Lewis, J. C., Yamamoto, Y., Saffer, D. M., Casey Moore, J., Wu, H. Y., Tsuji, T., Yamada, Y., Conin, M., Saito, S., Ito, T., Tobin, H. J., Kimura, G., Kanagawa, K., Ashi, J., Underwood, M. B., and Kanamatsu, T. Distribution of stress state in the Nankai subduction zone, southwest Japan and a comparison with Japan Trench. *Tectonophysics* **692**, 120-130, 2016.

Lipp, J. S., Morono, Y., Inagaki, F., and Hinrichs, K. U. Significant contribution of Archaea to extant biomass in marine subsurface sediments. *Nature* **454**, 991, 2008.

Liu, X., Li, M., Castelle, C. J., Probst, A. J., Zhou, Z., Pan, J., Liu, Y., Banfield, J. F., and Gu, J. D. Insights into the ecology, evolution, and metabolism of the widespread Woesearchaeotal lineages. *Microbiome* **6**, 102, 2018.

Londry, K. L., Dawson, K. G., Grover, H. D., Summons, R. E., and Bradley, A. S. Stable carbon isotope

fractionation between substrates and products of *Methanosarcina barkeri*. *Org. Geochem.* **39**, 608-621, 2008.

Loveless, J. P. and Meade, B. J. Geodetic imaging of plate motions, slip rates, and partitioning of deformation in Japan. *J.Geophys. Res.* **115**, 2010.

Luton, P., Wayne, J., Sharp, R., and Riley, P. The *mcrA* gene as an alternative to 16S rRNA in the phylogenetic analysis of methanogen populations in landfill. *Microbiology* **148**, 3521-3530, 2002.

Machida, I., Suzuki, Y., and Takeuchi, M. Carbon-14 age and chemical evolution of $Ca(HCO_3)_2$-type groundwater of age less than 8,000 years in a confined sandy and muddy Pleistocene aquifer, Japan. *Hydrogeol. J.* **21**, 1289-1305, 2013.

Magen, C., Lapham, L. L., Pohlman, J. W., Marshall, K., Bosman, S., Casso, M., and Chanton, J. P. A simple headspace equilibration method for measuring dissolved methane. *Limnol.Oceanogr. Methods* **12**, 637-650, 2014.

Malcolm, S. J. and Price, N. B. The behaviour of iodine and bromine in estuarine surface sediments. *Mar. Chem.* **15**, 263-271, 1984.

Mallet, C. R., Lu, Z., and Mazzeo, J. R. A study of ion suppression effects in electrospray ionization from mobile phase additives and solid-phase extracts. *Rapid Commun. Mass Spectrom.* **18**, 49-58, 2004.

Martin, M. Cutadapt removes adapter sequences from high-throughput sequencing reads. *EMB Net J.*

17, 3, 2011.

Maslin, M. A. and Swann, G. E. A. Isotopes in marine sediments in *Isotopes in Palaeoenvironmental Research Developments in Paleoenvironmental Research* (ed Melanie, J. L.) Kluwer Academic Publishers, 227-290, 2006.

Matsushita, M., Ishikawa, S., Nagai, K., Hirata, Y., Ozawa, K., Mitsunobu, S., and Kimura, H. Regional variation of CH_4 and N_2 production processes in the deep aquifers of an accretionary prism. *Microbes Environ.* **31**, 329-338, 2016.

Matsushita, M., Magara, K., Sato, Y., Shinzato, N., and Kimura, H. Geochemical and microbiological evidence for microbial methane production in deep aquifers of the cretaceous accretionary prism. *Microbes Environ.* **33**, 205-213, 2018.

Mayr, S., Latkoczy, C., Krüger, M., Günther, D., Shima, S., Thauer, R. K., Widdel, F., and Jaun, B. Structure of an F430 variant from archaea associated with anaerobic oxidation of methane. *J. Am. Chem. Soc.* **130**, 10758-10767, 2008.

Mayumi, D., Mochimaru, H., Tamaki, H., Yamamoto, K., Yoshioka, H., Suzuki, Y., Kamagata, Y., and Sakata, S. Methane production from coal by a single methanogen. *Science* **354**, 222-225, 2016.

McCallister, S. L., Bauer, J. E., and Canuel, E. A. Bioreactivity of estuarine dissolved organic matter: a combined geochemical and microbiological approach. *Limnol. Oceanogr.* **51**, 94–100, 2006a.

McCallister, S. L., Bauer, J. E., Ducklow, H. W., and Canuel, E. A. Sources of estuarine dissolved and particulate organic matter: A multi-tracer approach. *Org. Geochem.* **37**, 454-468, 2006b.

McCallister, S. L., Ishikawa, N. F., and Kothawala, D. N. Biogeochemical tools for characterizing organic carbon in inland aquatic ecosystems. *Limnol. Oceanogr. Lett.* **3**, 444-457, 2018.

McCarthy, M. D. Major Bacterial contribution to marine dissolved organic nitrogen. *Science* **281**, 231-234, 1998.

McCarthy, M. D., Benner, R., Lee, C., and Fogel, M. L. Amino acid nitrogen isotopic fractionation patterns as indicators of heterotrophy in plankton, particulate, and dissolved organic matter. *Geochim. Cosmochim. Acta* **71**, 4727-4744, 2007.

McDermott, J. M., Seewald, J. S., German, C. R., and Sylva, S. P. Pathways for abiotic organic synthesis at submarine hydrothermal fields. *Proc. Natl. Acad. Sci.,* **112**, 7668-7672, 2015.

McGinnis, D. F., Kirillin, G., Tang, K. W., Flury, S., Bodmer, P., Engelhardt, C., Casper, P., and Grossart, H. P. Enhancing surface methane fluxes from an oligotrophic lake: exploring the microbubble hypothesis. *Environ. Sci. Technol.* **49**, 873-880, 2015.

McMahon, K. W., Thorrold, S. R., Elsdon, T. S., and McCarthy, M. D. Trophic discrimination of nitrogen stable isotopes in amino acids varies with diet quality in a marine fish. *Limnol. Oceanogr.* **60**, 1076-1087, 2015.

McMahon, K. W. and McCarthy, M. D. Embracing variability in amino acid $\delta^{15}N$ fractionation: mechanisms, implications, and applications for trophic ecology. *Ecosphere* **7**, e01511, 2016.

Minagawa, M. and Wada, E. Stepwise enrichment of ^{15}N along food chains: Further evidence and the relation between $\delta^{15}N$ and animal age. *Geochim. Cosmochim. Acta* **48**, 1135-1140, 1984.

Miyata, Y., Minami, M., and Nakamura, T. Environmental analysis by apparent radiocarbon age difference: molluscan shells and bone samples from Lake Biwa., *Summaries of Researches using AMS at Nagoya University* 49-54, 2011.

Mochimaru, H., Uchiyama, H., Yoshioka, H., Imachi, H., Hoaki, T., Tamaki, H., Nakamura, K., Sekiguchi, Y., and Kamagata, Y. Methanogen diversity in deep subsurface gas-associated water at the Minami-kanto gas field in Japan. *Geomicrobiol. J.* **24**, 93-100, 2007.

Mostofa, K. M. G., Liu, C. Q., Mottaleb, M. A., Wan, G., Ogawa, H., Vione, D., Yoshioka, T., and Wu, F. *Dissolved organic matter in natural waters*. Springer, Berlin Heidelberg, 2013.

Motojima, K., Shinada, Y., and Maki, S. Natural gas depoits on the Lake Suwa, Nagano prefecture. *Rep. Geol. Survey Jpn.* **4**, 31-38, 1953. (in Japanese with English abstract)

Muramatsu, Y., Fehn, U., and Yoshida, S. Recycling of iodine in fore-arc areas: evidence from the iodine brines in Chiba, Japan. *Earth Planet. Sci.Lett.* **192**, 583-593, 2001.

Naito, Y. I., Chikaraishi, Y., Ohkouchi, N., Mukai, H., Shibata, Y., Honch, N. V., Dodo, Y., Ishida, H., Amano, T., Ono, H., and Yoneda, M. Dietary Reconstruction of the Okhotsk culture of Hokkaido, Japan, based on nitrogen composition of amino acids: Implications for correction of ^{14}C marine reservoir effects on human bones. *Radiocarbon* **52**, 671-681, 2010.

Naito, Y. I., Bocherens, H., Chikaraishi, Y., Drucker, D. G., Wißing, C., Yoneda, M., and Ohkouchi, N. An overview of methods used for the detection of aquatic resource consumption by humans: Compound-specific delta N-15 analysis of amino acids in archaeological materials. *J. Archaeol.*

Sci. Rep. **6**, 720-732, 2016.

Nakahara, N., Nobu, M. K., Takaki, Y., Miyazaki, M., Tasumi, E., Sakai, S., Ogawara, M., Yoshida, N., Tamaki, H., Yamanaka, Y., Katayama, A., Yamaguchi, T., Takai, K., and Imachi, H. *Aggregatilinea lenta* gen. nov., sp. nov., a slow-growing, facultatively anaerobic bacterium isolated from subseafloor sediment, and proposal of the new order *Aggregatilineales* ord. nov. within the class *Anaerolineae* of the phylum *Chloroflexi*. *Int. J. Syst. Evol. Microbiol.* **69**, 1185-1194, 2019.

Nakai, N., Yoshida, Y., and Ando, N. Isotopic studies on oil and natural gas fields in Japan. *Chikyukagaku* **7.8**, 87-98, 1974.(in Japanese with English abstract)

Nakazato, R., Hirabayashi, K., and Okino, T. Abundance and seasonal trend of dominant chironomid adults and horizontal distribution of larvae in eutrophic Lake Suwa, Japan. *Jpn. J. Limnol.* **59**, 443-455, 1998.

Nebbioso, A. and Piccolo, A. Molecular characterization of dissolved organic matter (DOM): a critical review. *Anal. Bioanal. Chem.* **405**, 109-124, 2013.

Nishida, K., Chew, Y. C., Miyairi, Y., Hirabayashi, S., Suzuki, A., Hayashi, M., Yamamoto, Y., Sato, M., Nojiri, Y., and Yokoyama, Y. Novel reverse radioisotope labelling experiment reveals carbon assimilation of marine calcifiers under ocean acidification conditions. *Methods Ecol. Evol.* **11**, 739-750, 2020.

Nishiyama, T., Ueki, A., Kaku, N., and Ueki, K. *Clostridium sufflavum* sp. nov., isolated from a

methanogenic reactor treating cattle waste. *Int. J. Syst. Evol. Microbiol.* **59**, 981-986, 2009.

Nomaki, H., Uejima, Y., Ogawa, N. O., Yamane, M., Watanabe, H. K., Senokuchi, R., Bernhard, J. M., Kitahashi, T., Miyairi, Y., Yokoyama, Y., Ohkouchi, N., and Shimanaga, M. Nutritional sources of meio- and macrofauna at hydrothermal vents and adjacent areas: natural-abundance radiocarbon and stable isotope analyses. *Mar. Ecol. Prog. Ser.*, **622**, 49-65, 2019.

Nunoura, T., Takaki, Y., Kazama, H., Hirai, M., Ashi, J., Imachi, H., and Takai, K. Microbial diversity in deep-sea methane seep sediments presented by SSU rRNA gene tag sequencing. *Microbes Environ.* **27**, 382-390, 2012.

Ogawa, N. O., Nagata, T., Kitazato, H., and Ohkouchi, N. Ultra-sensitive elemental analyzer/isotope ratio mass spectrometer for stable nitrogen and carbon isotope analyses. In *Earth, Life and Isotopes* (Eds Ohkouchi, N., Tayasu, I., and Koba, K.), Kyoto University Press: Kyoto, 339-353, 2010.

Ohkouchi, N., Ogawa, N. O., Chikaraishi, Y., Tanaka, H., and Wada, E. Biochemical and physiological bases for the use of carbon and nitrogen isotopes in environmental and ecological studies. *Prog. Earth Planet. Sci.* **2**, 2015.

Ohkouchi, N., Chikaraishi, Y., Close, H. G., Fry, B., Larsen, T., Madigan, D. J., McCarthy, M. D., McMahon, K. W., Nagata, T., Naito, Y. I., Ogawa, N. O., Popp, B. N., Steffan, S., Takano, Y., Tayasu, I., Wyatt, A. S. J., Yamaguchi, Y. T., and Yokoyama, Y. Advances in the application of amino acid nitrogen isotopic analysis in ecological and biogeochemical studies. *Org. Geochem.*

113, 150-174, 2017.

Orcutt, B., LaRowe, D., Biddle, J., Colwell, F., Glazer, B., Reese, B., Kirkpatrick, J., Lapham, L., Mills, H., Sylvan, J., Wankel, S., and Wheat, C. Microbial activity in the marine deep biosphere: progress and prospects. *Front. Microbiol.* **4**, 1-15, 2013.

Oremland, R. S. Methanogenic activity in plankton samples and fish intestines A mechanism for in situ methanogenesis in oceanic surface waters. *Limnol. Oceanogr.* **24**, 1136-1141, 1979.

Ortiz-Alvarez, R. and Casamayor, E. O. High occurrence of *Pacearchaeota* and *Woesearchaeota* (Archaea superphylum DPANN) in the surface waters of oligotrophic high-altitude lakes. *Environ. Microbiol. Rep.* **8**, 210-217, 2016.

Park, H. D. and Hayashi, H. Role of encystment and excystment of Peridinium bipes *F. occulatum* (Dinophyceae) in freshwater red tides in Lake Kizali, Japan. *J. Phycol.*, **29**, 435–441, 1993.

Park, H. D., Watanabe, M. F., Harada, K. I., Suzuki, M., Hayashi, H., and Okino, T. Seasonal-Variations of *Microcystis* Species and Toxic Heptapeptide Microcystins in Lake Suwa. *Environ. Toxicol. Water Qual.* **8**, 425-435, 1993.

Park, H. D., Iwami, C., Watanabe, M. F., Harada, K. I., Okino, T., and Hayashi, H. Temporal variabilities of the concentrations of intra- and extracellular microcystin and toxic *Microcystis* species in a hypertrophic lake, Lake Suwa, Japan (1991–1994). *Environ. Toxicol. Water Qual.* **13**, 61-72, 1998.

Passaris, I., Van Gaelen, P., Cornelissen, R., Simoens, K., Grauwels, D., Vanhaecke, L., Springael, D.,

and Smets, I. Cofactor F430 as a biomarker for methanogenic activity: Application to an anaerobic bioreactor system. *Appl. Microbiol. Biotechnol.* **102**, 1191-1201, 2018.

Pearson, A., McNichol, A. P., Schneider, R. J., Von Reden, K. F., and Zheng, Y. Microscale AMS ^{14}C measurement at NOSAMS. *Radiocarbon* **40**, 61-75, 1998.

Pearson, A., Eglinton, T. I., and McNichol, A. P. An organic tracer for surface ocean radiocarbon. *Paleoceanography* **15**, 541-550, 2000.

Peterson, B. J. and Fry, B. Stable isotopes in ecosystem studies. *Annu. Rev. Ecol. Syst.* **18**, 293-320, 1987.

Ploug, H. Cyanobacterial surface blooms formed by *Aphanizomenon* sp. and *Nodularia spumigena* in the Baltic Sea: Small-scale fluxes, pH, and oxygen microenvironments. *Limnol.Oceanogr.* **53**, 914-921, 2008.

Popp, B. N., Graham, B. S., Olson, R. J., Hannides, C. C. S., Lott, M. J., López-Ibarra, G. A., Galván-Magaña, F., and Fry, B. Insight into the trophic ecology of yellowfin tuna, thunnus albacares, from compound-specific nitrogen isotope analysis of proteinaceous amino acids. in *Terrestrial Ecology Vol. 1* (eds Dawson, T.E. and Siegwolf, R.T.W.), Elsevier, 173-190, 2007.

Proskurowski, G., Lilley, M. D., Seewald, J. S., Früh-Green, G. L., Olson, E. J., Lupton, J. E., Sylva, S. P., and Kelley, D. S. Abiogenic hydrocarbon production at Lost City Hydrothermal Field. *Science* **319**, 604-607, 2008.

Quast, C., Pruesse, E., Yilmaz, P., Gerken, J., Schweer, T., Yarza, P., Peplies, J., and Glöckner, F. O.

The SILVA ribosomal RNA gene database project: improved data processing and web-based tools. *Nucleic Acids Res.* **41**, D590-D596, 2012.

Quay, P., Stutsman, J., Wilbur, D., Snover, A., Dlugokencky, E., and Brown, T. The isotopic composition of atmospheric methane. *Global Biogeochem.l Cycles* **13**, 445-461, 1999.

Repeta, D. J. Chemical characterization and cycling of dissolved organic matter. in *Chemical characterization and cycling of dissolved organic matter*. 2nd edn (Eds Hansell. D. A. and Carlson, C. A.). Elsevier, 21-63, 2015.

Repeta, D. J., Ferrón, S., Sosa, O. A., Johnson, C. G., Repeta, L. D., Acker, M., DeLong, E. F., and Karl, D. M. Marine methane paradox explained by bacterial degradation of dissolved organic matter. *Nat. Geosci.* **9**, 884-887, 2016.

Reynolds, C. S. Cyanobacterial water-blooms in *Advances in Botanical Research Vol. 13* (ed Callow, J. A.). Academic Press, Oxford, 67-143, 1987.

Román, S., Ortiz-Álvarez, R., Romano, C., Casamayor, E. O., and Martin, D. Microbial community structure and functionality in the deep sea floor: Evaluating the causes of spatial heterogeneity in a submarine canyon system (NW Mediterranean, Spain). *Front Mar. Sci.* **6**, 2019.

Sagiya, T., Nishimura, T., Iio, Y. and Tada, T. Crustal deformation around the northern and central Itoigawa-Shizuoka Tectonic Line. *Earth, Planets and Space* **54**, 1059-1063, 2002.

Sakai, S., Ehara, M., Tseng, I. C., Yamaguchi, T., Bräuer, S. L., Cadillo-Quiroz, H., Zinder, S. H., and Imachi, H. *Methanolinea mesophila* sp. nov., a hydrogenotrophic methanogen isolated from

rice field soil, and proposal of the archaeal family *Methanoregulaceae fam*. nov. within the order *Methanomicrobiales*. *Int. J. Syst. Evol. Microbiol.* **62**, 1389-1395, 2012.

Sano, Y., Kinoshita, N., Kagoshima, T., Takahata, N., Sakata, S., Toki, T., Kawagucci, S., Waseda, A., Lan, T., Wen, H., Chen, A. T., Lee, H., Yang, T. F., Zheng, G., Tomonaga, Y., Roulleau, E., and Pinti, D. L. Origin of methane-rich natural gas at the West Pacific convergent plate boundary. *Sci. Rep.* **7**, 15646, 2017.

Sarvala, J. and Halsinaho, S. Crustacean zooplankton of finnish forest lakes in relation to acidity and other environmental factors. in Acidification in Finland (eds Kauppi, P., Anttilla, P., and Kenttamies, K.). Springer, Berlin Heidelberg, 1009-1027, 1990.

Sass, H., Parkes, R. J. and Webster, G. Marine deep biosphere. in *Encyclopedia of Microbiology 4th Edition* (ed Schmidt, T. M.) Academic Press, Oxford, 18-27, 2019.

Sato, R., Kawanishi, H., Schimmelmann, A., Suzuki, Y., and Chikaraishi, Y. New amino acid reference materials for stable nitrogen isotope analysis. *Bunseki Kagaku* **63**, 399-403, 2014. (in Japanese with English abstract)

Satoh, N., Fukuda, H., Miyairi, Y., Yokoyama, Y., and Nagata, T. Position-dependent radiocarbon content of the macroalgae Undaria pinnatifida as an indicator of oceanographic conditions during algal growth. *J. Oceanogr.* **75**, 349-358, 2019.

Sawaki, T., Kaneko, N., Maekawa, T., and Igari, S. Fuel resource map "Kanto Region". Deological Survey of Japan, Tsukuba, Japan, 2015.

Schirmack, J., Mangelsdorf, K., Ganzert, L., Sand, W., Hillebrand-Voiculescu, A., and Wagner, D. *Methanobacterium movilense* sp. nov., a hydrogenotrophic, secondary-alcohol-utilizing methanogen from the anoxic sediment of a subsurface lake. *Int. J. Syst. Evol. Microbiol.* **64**, 522-527, 2014.

Schmale, O., Wäge, J., Mohrholz, V., Wasmund, N., Gräwe, U., Rehder, G., Labrenz, M., and Loick-Wilde, N. The contribution of zooplankton to methane supersaturation in the oxygenated upper waters of the central Baltic Sea. *Limno. Oceanogr.* **63**, 412-430, 2018.

Schwab, V. F., Nowak, M. E., Elder, C. D., Trumbore, S. E., Xu, X., Gleixner, G., Lehmann, R., Pohnert, G., Muhr, J., Küsel, K., and Totsche, K. U. ^{14}C-free carbon is a major contributor to cellular biomass in geochemically distinct groundwater of shallow sedimentary bedrock aquifers. *Water Resour. Res.* **55**, 2104-2121, 2019.

Scott, A. R., Kaiser, W. R., and Ayers, W. B., Jr. Thermogenic and secondary biogenic gases, San Juan Basin, Colorado and New Mexico—Implications for coalbed gas producibility1. *AAPG Bulletin* **78**, 1186-1209, 1994.

Sheppard, M. I. and Hawkins, J. L. Iodine and microbial interactions in an organic soil. *J. Environ. Radioact.* **29**, 91-109, 1995.

Sherwood Lollar, B., Lacrampe-Couloume, G., Slater, G. F., Ward, J., Moser, D. P., Gihring, T. M., Lin, L. H., and Onstott, T. C. Unravelling abiogenic and biogenic sources of methane in the Earth's deep subsurface. *Chem. Geol.* **226**, 328-339, 2006.

Shima, S., Krueger, M., Weinert, T., Demmer, U., Kahnt, J., Thauer, R. K., and Ermler, U. Structure of a methyl-coenzyme M reductase from Black Sea mats that oxidize methane anaerobically. *Nature* **481**, 98, 2011.

Simkus, D. N., Slater, G. F., Lollar, B. S., Wilkie, K., Kieft, T. L., Magnabosco, C., Lau, M. C. Y., Pullin, M. J., Hendrickson, S. B., Wommack, K. E., Sakowski, E. G., Heerden, E. v., Kuloyo, O., Linage, B., Borgonie, G., and Onstott, T. C. Variations in microbial carbon sources and cycling in the deep continental subsurface. *Geochim. Cosmochim. Acta* **173**, 264-283, 2016.

Slater, G. F., Lippmann-Pipke, J., Moser, D. P., Reddy, C. M., Onstott, T. C., Lacrampe-Couloume, G., and Lollar, B. S. ^{14}C in methane and DIC in the deep terrestrial subsurface: Implications for microbial methanogenesis. *Geomicrobiol. J.* **23**, 453-462, 2006.

Snelgrove, P. V. R., Soetaert, K., Solan, M., Thrush, S., Wei, C. L., Danovaro, R., Fulweiler, R. W., Kitazato, H., Ingole, B., Norkko, A., Parkes, R. J., and Volkenborn, N. Global carbon cycling on a heterogeneous seafloor. *Trends Ecol. Evol.* **33**, 96-105, 2018.

Sohlenkamp, C. and Geiger, O. Bacterial membrane lipids: diversity in structures and pathways. *FEMS Microbiol. Rev.* **40**, 133-159.

Sommer, U. *Plankton Ecology: Succession in Plankton Communities*. Springer Berlin Heidelberg, 1989.

Sommer, U., Sommer, F., Santer, B., Zöllner, E., Jürgens, K., Jamieson, C., Boersma, M., and Gocke, K. Daphnia versus copepod impact on summer phytoplankton: functional compensation at both

trophic levels. *Oecologia* **135**, 639-647, 2003.

Sørensen, K., Řeháková, K., Zapomělová, E., and Oren, A. Distribution of benthic phototrophs, sulfate reducers, and methanogens in two adjacent saltern evaporation ponds in Eilat, Israel. *Aquat. Microb. Ecol.* **56**, 275-284, 2009.

Springer, E., Sachs, M. S., Woese, C. R., and Boone, D. R. Partial gene sequences for the A subunit of methyl-coenzyme M reductase (*mcrI*) as a phylogenetic tool for the family *Methanosarcinaceae*. *Int. J. Syst. Bacteriol.* **45**, 554-559, 1995.

Steffan, S. A., Chikaraishi, Y., Currie, C. R., Horn, H., Gaines-Day, H. R., Pauli, J. N., Zalapa, J. E., and Ohkouchi, N. Microbes are trophic analogs of animals. *Proc. Natl. Acad. Sci.,* **112**, 15119-15124, 2015.

Steinberg, D. K. and Landry, M. R. Zooplankton and the Ocean Carbon Cycle. *Ann. Rev. Mar. Sci.* **9**, 413-444, 2017.

Steinberg, L. M. and Regan, J. M. Phylogenetic comparison of the methanogenic communities from an acidic, oligotrophic fen and an anaerobic digester treating municipal wastewater sludge. *Appl. Environ. Microbiol.* **74**, 6663-6671, 2008.

Suda, K., Ueno, Y., Yoshizaki, M., Nakamura, H., Kurokawa, K., Nishiyama, E., Yoshino, K., Hongoh, Y., Kawachi, K., Omori, S., Yamada, K., Yoshida, N., and Maruyama, S. Origin of methane in serpentinite-hosted hydrothermal systems: The CH_4–H_2–H_2O hydrogen isotope systematics of the Hakuba Happo hot spring. *Earth Planet. Sci. Lett.* **386**, 112-125, 2014.

Suda, K., Gilbert, A., Yamada, K., Yoshida, N., and Ueno, Y. Compound- and position-specific carbon isotopic signatures of abiogenic hydrocarbons from on–land serpentinite–hosted Hakuba Happo hot spring in Japan. *Geochim. Cosmochim. Acta* **206**, 201-215, 2017.

Suganuma, Y., Haneda, Y., Kameo, K., Kubota, Y., Hayashi, H., Itaki, T., Okuda, M., Head, M. J., Sugaya, M., Nakazato, H., Igarashi, A., Shikoku, K., Hongo, M., Watanabe, M., Satoguchi, Y., Takeshita, Y., Nishida, N., Izumi, K., Kawamura, K., Kawamata, M., Okuno, J. i., Yoshida, T., Ogitsu, I., Yabusaki, H., and Okada, M. Paleoclimatic and paleoceanographic records through Marine Isotope Stage 19 at the Chiba composite section, central Japan: A key reference for the Early–Middle Pleistocene Subseries boundary. *Quarter. Sc. Rev.* **191**, 406-430, 2018.

Suwa Construction Office, *Lake bottom survey of Lake Suwa*, Nagano Pref. Office, 2019.

Takano, Y., Chikaraishi, Y., Ogawa, N. O., Kitazato, H., and Ohkouchi, N. Compound-specific nitrogen isotope analysis of d-alanine, l-alanine, and valine: application of diastereomer separation to $\delta^{15}N$ and microbial peptidoglycan studies. *Anal. Chem.* **81**, 394-399, 2009.

Takano, Y., Kaneko, M., Kahnt, J., Imachi, H., Shima, S., and Ohkouchi, N. Detection of coenzyme F430 in deep sea sediments: A key molecule for biological methanogenesis. *Org. Geochem.* **58**, 137-140, 2013.

Takano, Y., Chikaraishi, Y., Imachi, H., Miyairi, Y., Ogawa, N. O., Kaneko, M., Yokoyama, Y., Krüger, M., and Ohkouchi, N. Insight into anaerobic methanotrophy from $^{13}C/^{12}C$-amino acids and $^{14}C/^{12}C$-ANME cells in seafloor microbial ecology. *Sci. Rep.* **8**, 14070, 2018.

Takizawa, Y., Dharampal, P. S., Steffan, S. A., Takano, Y., Ohkouchi, N., and Chikaraishi, Y. Intra-trophic isotopic discrimination of $^{15}N/^{14}N$ for amino acids in autotrophs: Implications for nitrogen dynamics in ecological studies. *Ecol. Evol.* **7**, 2916-2924, 2017.

Tang, K. W., McGinnis, D. F., Ionescu, D., and Grossart, H. P. Methane production in oxic lake waters potentially increases aquatic methane flux to air. *Environ. Sci. Technol. Lett.* **3**, 227-233, 2016.

Tarnovetskii, I. Y., Merkel, A. Y., Kanapatskiy, T. A., Ivanova, E. A., Gulin, M. B., Toshchakov, S., and Pimenov, N. V. Decoupling between sulfate reduction and the anaerobic oxidation of methane in the shallow methane seep of the Black sea. *FEMS Microbiol. Lett.* **365**, 2018.

Tayasu, I., Hirasawa, R., Ogawa, N. O., Ohkouchi, N., and Yamada, K. New organic reference materials for carbon- and nitrogen-stable isotope ratio measurements provided by Center for Ecological Research, Kyoto University, and Institute of Biogeosciences, Japan Agency for Marine-Earth Science and Technology. *Limnology* **12**, 261-266, 2011.

Taylor, P. J. Matrix effects: the Achilles heel of quantitative high-performance liquid chromatography–electrospray–tandem mass spectrometry. *Clin. Biochem.* **38**, 328-334, 2005.

Teske, A. and Sorensen, K. Uncultured Archaea in deep marine subsurface sediments: have we caught them all? *ISME j.* **2**, 3-18, 2008.

Thauer, R. K. and Bonacker, L. G. Biosynthesis of Coenzyme F430, a nickel porphinoid involved in methanogenesis. in *Ciba Foundation Symposium 180 - The Biosynthesis of the Tetrapyrrole Pigments* (eds Derek J. C. and Kate, A.). Wiley, Baffins Lane, Chichester, England, 210-227,

1994.

Thauer, R. K. Biochemistry of methanogenesis: a tribute to Marjory Stephenson. *Microbiology* **144**, 2377-2406, 1998.

Thauer, R. K., Kaster, A. K., Seedorf, H., Buckel, W., and Hedderich, R. Methanogenic archaea: ecologically relevant differences in energy conservation. *Nat.e Rev. Microbiol.* **6**, 579-591, 2008.

Thauer, R. K. Methyl (alkyl)-coenzyme M reductases: Nickel F-430-containing enzymes involved in anaerobic methane formation and in anaerobic oxidation of methane or of short chain alkanes. *Biochemistry* **58**, 5198-5220, 2019.

Thurman, E. M. Organic Geochemistry of Natural Water. Springer Netherlands, 1985.

Tranvik, L. J., Downing, J. A., Cotner, J. B., Loiselle, S. A., Striegl, R. G., Ballatore, T. J., Dillon, P., Finlay, K., Fortino, K., Knoll, L. B., Kortelainen, P. L., Kutser, T., Larsen, S., Laurion, I., Leech, D. M., McCallister, S. L., McKnight, D. M., Melack, J. M., Overholt, E., Porter, J. A., Prairie, Y., Renwick, W. H., Roland, F., Sherman, B. S., Schindler, D. W., Sobek, S., Tremblay, A., Vanni, M. J., Verschoor, A. M., von Wachenfeldt, E., and Weyhenmeyer, G. A. Lakes and reservoirs as regulators of carbon cycling and climate. *Limnol.Oceanogr.* **54**, 2298-2314, 2009.

Ueno, M., Shiina, K., Homma, T., Shinada, Y., and Higuchi, Y. Recent Development of mobara gas field with special reference to its production performance. *Jpn. Pet. Inst.* **29**, 39-47, 1964. (in Japanese with English abctract)

Umeda, K., Asamori, K., and Kusano, T. Release of mantle and crustal helium from a fault following an inland earthquake. *Applied Geochemistry* **37**, 134-141, 2013.

Unosawa, A., Oka, S., Sakamoto, T., and Komazawa, M. Geological map of Chiba 1:200,000. Geological Survey of Japan, Tsukuba, 1983.

Valentine, D. L. Emerging topics in marine methane biogeochemistry. *Ann. Rev. Mar. Sci.* **3**, 147-171, 2011.

Vogel, T. M., Oremland, R. S., and Kvenvolden, K. A. Low-temperature formation of hydrocarbon gases in San Francisco Bay sediment (California, U.S.A.). *Chem. Geol.* **37**, 289-298, 1982.

Volkman, J. K., Barrett, S. M., Blackburn, S. I., Mansour, M. P., Sikes, E. L., and Gelin, F. Microalgal biomarkers: A review of recent research developments. *Org. Geochem.* **29**, 1163-1179, 1998.

Volkman, J. K. Sterols in microorganisms. *Appl. Microbiol. Biotechnol.* **60**, 495-506, 2003.

Vu, H. T. L., Yukphan, P., Bui, V. T. T., Charoenyingcharoen, P., Malimas, S., Nguyen, L. K., Muramatsu, Y., Tanaka, N., Tanasupawat, S., Le, B. T., Nakagawa, Y., and Yamada, Y. *Acetobacter sacchari* sp. nov., for a plant growth-promoting acetic acid bacterium isolated in Vietnam. *Ann. Microbiol.* **69**, 1155-1163, 2019.

Wada, E. Stable $\delta^{15}N$ and $\delta^{13}C$ isotope ratios in aquatic ecosystems. *Proc.Jpn. Acad. Series B* **85**, 98-107, 2009.

Wang, H., Lu, J., Wang, W., Yang, L., and Yin, C. Methane fluxes from the littoral zone of hypereutrophic Taihu Lake, China. *J, Geophys. Res. Atmosph.* **111**, 2006.

Wang, Q., Dore, J. E., and McDermott, T. R. Methylphosphonate metabolism by *Pseudomonas* sp. populations contributes to the methane oversaturation paradox in an oxic freshwater lake. *Environ. Microbiol.* **19**, 2366-2378, 2017.

Watanabe, K., Park, H. D., and Kumon, F. Historical change of phytoplankton in a eutrophic lake in Japan as determined by analysis of photosynthetic pigments in a lakebed sediment core. *Env. Earth Sci.* **66**, 2293-2300, 2012.

Watanabe, T., Miura, A., Iwata, T., Kojima, H., and Fukui, M. Dominance of Sulfuritalea species in nitrate-depleted water of a stratified freshwater lake and arsenate respiration ability within the genus. *Environ. Microbiol. Rep.* **9**, 522-527, 2017.

Wetzel, R. G. Planktonic communities: zooplankton and their interactions with fish. in *Limnology 3rd Edition* (ed Wetzel, R. G.). Academic Press, Oxford, 395-488, 2001.

Whiticar, M. J., Faber, E., and Schoell, M. Biogenic methane formation in marine and freshwater environments: CO_2 reduction vs. acetate fermentation—Isotope evidence. *Geochim. Cosmochim. Acta* **50**, 693-709, 1986.

Whiticar, M. J. Carbon and hydrogen isotope systematics of bacterial formation and oxidation of methane. *Chem. Geol.* **161**, 291-314, 1999.

Whitman, W. B., Coleman, D. C., and Wiebe, W. J. Prokaryotes: The unseen majority. *Proc. Natl. Acad. Sci.,* **5**, 6578-6583, 1998.

Williamson, C. E. Invertebrate predation on planktonic rotifers. *Hydrobiologia* **104**, 385-396, 1983.

Williamson, C. E. The swimming and feeding behavior of Mesocyclops. *Hydrobiologia* **134**, 11-19, 1986.

Wolf, H. G. and Carvalho, G. R. Resting eggs of lake-Daphania II. In situ observations on the hatching of eggs and their contribution to population and community structure. *Freshwater Biol.* **22**, 471-478, 1989.

Wyatt, A. S. J., Matsumoto, R., Chikaraishi, Y., Miyairi, Y., Yokoyama, Y., Sato, K., Ohkouchi, N., and Nagata, T. Enhancing insights into foraging specialization in the world's largest fish using a multi-tissue, multi-isotope approach. *Ecol. Monogr.*, **89**, e01339, 2019.

Xu, S., Sun, Q., Zhou, X., Tan, X., Xiao, M., Zhu, W., and Li, M. Polysaccharide biosynthesis-related genes explain phenotype-genotype correlation of *Microcystis* colonies in Meiliang Bay of Lake Taihu, China. *Sci. Rep.* **6**, 35551, 2016.

Yamada, T., Sekiguchi, Y., Hanada, S., Imachi, H., Ohashi, A., Harada, H., and Kamagata, Y. *Anaerolinea thermolimosa* sp. nov., *Levilinea saccharolytica* gen. nov., sp. nov. and *Leptolinea tardivitalis* gen. nov., sp. nov., novel filamentous anaerobes, and description of the new classes *Anaerolineae* classis nov. and *Caldilineae* classis nov. in the bacterial phylum *Chloroflexi*. *Int. J. Syst. Evol. Microbiol.* **56**, 1331-1340, 2006.

Yamaguchi, Y. T., Chikaraishi, Y., Takano, Y., Ogawa, N. O., Imachi, H., Yokoyama, Y., and Ohkouchi, N. Fractionation of nitrogen isotopes during amino acid metabolism in heterotrophic and chemolithoautotrophic microbes across Eukarya, Bacteria, and Archaea: Effects of nitrogen

sources and metabolic pathways. *Org. Geochem.* **111**, 101-112, 2017.

Yamamoto, S., Miyairi, Y., Yokoyama, Y., Suga, H., Ogawa, N. O., and Ohkouchi, N. Compound-Specific Radiocarbon Analysis of Organic Compounds from Mount Fuji Proximal Lake (Lake Kawaguchi) Sediment, Central Japan. *Radiocarbon* **62**, 439-451, 2020.

Yamane, M., Yokoyama, Y., Hirabayashi, S., Miyairi, Y., Ohkouchi, N., and Aze, T. Small- to ultra-small-scale radiocarbon measurements using newly installed single-stage AMS at the University of Tokyo. *Nuclear Instruments and Methods in Physics Res. B* **455**, 238-243, 2019.

Yan, X., Xu, X., Wang, M., Wang, G., Wu, S., Li, Z., Sun, H., Shi, A., and Yang, Y. Climate warming and cyanobacteria blooms: Looks at their relationships from a new perspective. *Water Res.* **125**, 449-457, 2017.

Yasuno, N., Shikano, S., Shimada, T., Shindo, K., and Kikuchi, E. Comparison of the exploitation of methane-derived carbon by tubicolous and non-tubicolous chironomid larvae in a temperate eutrophic lake. *Limnology* **14**, 239-246, 2013.

Yokoyama, Y., Koizumi, M., Matsuzaki, H., Miyairi, Y., and Ohkouchi, N. Developing Ultra Small-Scale Radiocarbon Sample Measurement at the University of Tokyo. *Radiocarbon* **52**, 310-318, 2010.

Yokoyama, Y., Miyairi, Y., Aze, T., Yamane, M., Sawada, C., Ando, Y., de Natris, M., Hirabayashi, S., Ishiwa, T., Sato, N., and Fukuyo, N. A single stage accelerator mass spectrometry at the Atmosphere and Ocean Research Institute, The University of Tokyo. *Nuclear Inst. Methods in*

Physics Res. B **455**, 311-316, 2019.

Yoshida, T., Yuki, Y., Lei, S., Chinen, H., Yoshida, M., Kondo, R., and Hiroishi, S. Quantitative detection of toxic strains of the cyanobacterial genus *Microcystis* by competitive PCR. *Microbes Environ.* **18**, 16-23, 2003.

Yoshida, Y. and Muramatsu, S. Effects of microorganisms on the fate of Iodine in the soil environment. *Geomicrobiol. J.* **16**, 85-93, 1999.

Yoshioka, T., Wada, E., and Saijo, Y. Isotopic characterization of lake Kizaki and lake Suwa. *Jpn J. Limnology* **49**, 119-128, 1988.

Yoshioka, T., Wada, E., and Hayashi, H. A Stable isotope study on seasonal food web dynamics in a eutrophic lake. *Ecology* **75**, 835-846, 1994.

Yoshiyama, Y., Koda, H., and Fukushima, K. Concentration, isolation and characterization of high molecular weight organic matter dissolved in lake waters using a tangential flow ultrafiltration. *Res. Org. Geochem.* **18**, 37-45, 2003.

Zepp Falz, K., Holliger, C., Großkopf, R., Liesack, W., Nozhevnikova, A. N., Müller, B., Wehrli, B., and Hahn, D. Vertical distribution of methanogens in the anoxic sediment of rotsee (Switzerland). *Appl. Environ. Microbiol.* **65**, 2402-2408, 1999.

Zhou, Z., Pan, J., Wang, F., Gu, J. D., and Li, M. Bathyarchaeota: globally distributed metabolic generalists in anoxic environments. *FEMS Microbiol. Rev.* **42**, 639-655, 2018.

Zhou, Z., Liu, Y., Lloyd, K. G., Pan, J., Yang, Y., Gu, J. D., and Li, M. Genomic and transcriptomic

insights into the ecology and metabolism of benthic archaeal cosmopolitan, Thermoprofundales (MBG-D archaea). *ISME J.* **13**, 885-901, 2019.

Ziegler, S. E. and Fogel, M. L. Seasonal and diel relationships between the isotopic compositions of dissolved and particulate organic matter in freshwater ecosystems. *Biogeochemistry* **64**, 25-52, 2003.